Intestinal Helminth Infection Modulates the Immune Response to Airway Allergens

Doctoral thesis

to obtain a doctorate (PhD)

from the Faculty of Medicine

of the University of Bonn

Maria Martina Doverman

from Gravesend, Kent, England

2026

Written with the authorization of
the Faculty of Medicine of the University of Bonn

First reviewer: Prof. Dr. Christoph Wilhelm

Second reviewer: Prof. Dr. Irmgard Förster

Day of oral examination: 23.04.2026

From the Institute of Clinical Chemistry and Clinical Pharmacology

Table of Contents

List of abbreviations

ACC1	Acetyl-CoA Carboxylase 1
ANOVA	Analysis of Variance
APC	Antigen-Presenting Cell
Areg	Amphiregulin
Arg1	Arginase 1
ATP	Adenosine Triphosphate
DC	Dendritic Cell
ETC	Electron Transport Chain
ECAR	Extracellular Acidifcation Rate
$FADH_2$	Flavin Adenine Dinucleotide
FAO	Fatty Acid Oxidation
GSH	Glutathione
HDM	House Dust Mite
3,4-HPPA	3-(4-hydroxyphenyl)propionic acid
3,3-HPPA	3-(3-hydroxyphenyl)propionic acid
3-HPPA SO_4	3-(3-hydroxyphenyl)propionic acid sulphate
IC	Inhaled Corticosteroids
ILC1	Innate Lymphoid Cell 1
ILC2	Innate Lymphoid Cell 2
ILC3	Innate Lymphoid Cell 3
MHC	Major Histocompatibility Complex
NAC	N-acetyl-cysteine
NADH	Nicotinamide Adenine Dinucleotide (Reduced)
NK	Natural Killer
NLR	NOD-Like Receptor
OCR	Oxygen Consumption Rate

OXPHOS	Oxidative Phosphorylation
PAMP	Pathogen-Associated Molecular Pattern
PPAR	Peroxisome Proliferator-Activated Receptors
ROS	Reactive Oxygen Species
SCFA	Short-Chain Fatty Acids
SEM	Standard Error of the Mean
TCA	Tricarboxylic Acid
TCR	T Cell Receptor
Th1	T helper 1
Th2	T helper 2
Th17	T helper 17
TLR	Toll-Like Receptor
TSLP	Thymic Stromal Lymphopoietin
TXNIP	Thioredoxin-Interacting Protein
VAT	Visceral Adipose Tissue

1. Introduction

1.1 Basic Overview of the Immune System

The immune system is a complex network of immune cells and proteins, such as antibodies and effector molecules known as cytokines, that protect a host from harmful toxins and pathogens. The majority of immune cells in the body develop in the bone marrow before entering tissues where they mature and reside at barrier sites such as the skin, lungs, and gastrointestinal tract (Murphy and Weaver, 2017). Immune cells can also circulate through the bloodstream and enter the lymphatic system (Murphy and Weaver, 2017). The lymphatic system carries immune cells to the site of infection, prevents fluid buildup, and carries antigens to specialized organs of the lymphatic system, known as lymph nodes, and the spleen (Ozdowski and Gupta, 2023). These organs act as immune filters and can trap harmful pathogens such as bacteria, as well as being the site of activation for immune cells such as T cells and B cells (Bujoreanu and Gupta, 2025). Based on the type of antigen an immune cell encounters, there are three types of responses that can then be generated (Murphy and Weaver, 2017):

Type 1 for viruses and intracellular pathogens.

Type 2 for allergies and parasites.

Type 3 for fungi and extracellular pathogens.

1.1.1 Initiation of an Immune Response

As mentioned, barrier sites include the skin and mucosal sites such as the lungs and the gastrointestinal tract. These barrier sites act as the first line of defense by creating a physical barrier in the form of the epidermis layer of the skin or mucous membranes and tight junctions at mucosal sites (Belkaid and Artis, 2013). Epithelial cells make up these barriers and have the capacity to sense changes in the environment and contribute to the first line of defense (Hammad and Lambrecht, 2015; Larsen et al., 2020). Beyond the epithelial cells, the immune response is divided into the innate and adaptive immune responses. The innate immune response is the body's more primitive immune response. It is a fast-acting and short-term response encompassing effector molecules and phagocytic cells such as neutrophils and macrophages, which engulf harmful pathogens and neutralise them (Wang et al., 2024). Furthermore, granulocytes, including eosinophils, mast cells, and basophils, as well as neutrophils, release effector proteins that kill parasites or bacteria (Wang et al., 2024). In addition,

specialised cells of the innate immune system known as Antigen-Presenting Cells (APCs), which include Dendritic Cells (DCs) and macrophages, patrol and survey below the submucosa by elongating specialised structures known as dendrites (Fan et al., 2025; Steinman and Cohn, 1973). Dendritic Cells recognise Pathogen-Associated Molecular Patterns (PAMPs) such as peptides on the surface of pathogens. PAMPs are sensed by Toll-Like Receptors (TLRs) on the DC cell surface or endosome and NOD-Like Receptors (NLRs), which are capable of cytoplasmic pathogen sensing (Krishnaswamy et al., 2013; Pradeu et al., 2024). Both TLRs and NLRs can trigger a signalling cascade, which causes APCs to internalise the target antigen and degrade it into peptides that can be presented on Major Histocompatibility Complex (MHC), specifically, MHCI or MHCII molecules (Thery and Amigorena, 2001). The gap between the innate and adaptive immune responses is bridged once dendritic cells migrate to lymph nodes, where they can present antigens on MHCII to naive $CD4^+$ T cells for further differentiation, thereby generating adaptive T cells (Förster et al., 1999). Naive $CD4^+$T cells can be differentiated into T helper 1 (Th1), T helper 2 (Th2), or T helper 17 (Th17) cells. This process requires three signals (Jain and Pasare, 2017):

1. Recognition of the presented antigen on APC MHC molecules via T Cell Receptor (TCR).
2. Engagement of activation receptor CD28 on T cells and CD80/CD86 on DCs.
3. Environmental cytokines drive the type of response.

Environmental cytokines, such as IL-12 and IL-4, drive Th1 differentiation through Tbet expression and Th2 differentiation through GATA3 expression, respectively (Yamane and Paul, 1999). While secretion of IL-6 and IL-23 by DCs promotes Th17 differentiation through $ROR\gamma t$ expression (Huang et al., 2012; Kaiko et al., 2008; Yamane and Paul, 1999). The differentiation of naive CD4 T cells into adaptive Th1, Th2, and Th17 is initiated by the three major classes of immune responses outlined earlier: Type 1, Type 2, and Type 3 immunity, respectively. The adaptive immune response is longer lasting, generating memory T cells, which can recognise previously seen antigens, leading to faster immune responses upon reencounter with said antigens (Murphy and Weaver, 2017). Although it should be noted that in recent years there is new evidence suggesting innate immune cells can display memory-like phenotypes (Sherwood et al., 2022). While CD4 T cells perform the general adaptive immune responses, CD8 T cells perform more targeted responses (Koh et al., 2023). The generation of activated CD8 involves cross-presentation of antigen on MHCI molecules from DCs to naive CD8 T cells. Activated CD8 T cells are also known as cytotoxic T cells, as they release perforin and granzyme B, which directly target infected cells and kill them (Koh et al.,

2023). Notably, cytotoxic T cells are primarily important during viral infections but also play a role in immunotherapeutic strategies in cancer (Koh et al., 2023; MacNabb et al., 2022). As well as the generation of CD4 and CD8 T cells, the adaptive immune response also includes activation of B cells through interaction of CD4 T cells. Once activated, B cells become plasma cells that secrete immunoglobulin proteins known as antibodies. Antibodies can neutralise pathogens by coating their surface as well as activating granulocytes expressing Fc receptors to induce degranulation (Murphy and Weaver, 2017).

1.1.2 Generation of Type 2 Immunity

Type 2 immunity plays an essential evolutionary role in wound healing, helminth clearance, and maintaining metabolic homeostasis (Kopp et al., 2023). However, type 2 immune responses can also lead to significant pathology when activated by completely unrelated antigens such as allergens (Kopp et al., 2023). When helminths or allergens enter the host, they can create damage to the epithelial barrier, which causes the release of Thymic Stromal Lymphopoietin (TSLP), IL-33, and IL-25 (Hammad and Lambrecht, 2015). The release of these cytokines, or “alarmins”, activates and recruits a network of innate cells, including DCs, group 2 ILC2s, eosinophils, basophils, mast cells, and macrophages, to the site of inflammation (Hammad and Lambrecht, 2015). Importantly, alarmins such as IL-33 drive immune responses by acting on tissue-resident immune cells such as ILC2s and T cells independent of TCR engagement (Humphreys et al., 2008; Kondo et al., 2008; Schmitz et al., 2005). Compared to Th1 and Th17 cells, the generation of adaptive Th2 cells in vivo remains somewhat elusive, however, in the absence of the DC subset cDC2, mice fail to mount an effective Th2 response to *H. polygyrus* infection, which suggests a significant role of cDC2 in Th2 differentiation (Liu et al., 2022). However, the exact mechanisms of Th2 generation remain to be defined (Kopp et al., 2023). As mentioned above, IL-4 is necessary to drive GATA3 transcription factor expression, but it is also necessary for the class switching of B cells to produce IgE (Mandler et al., 1993). The evolutionary role of IgE is debated to be in response to venom and toxins rather than anti-helminth immunity, however, various helminth infections induce IgE secretion in the blood (Fitzsimmons et al., 2014; Pritchard et al., 2021). IgE cross-linking on FcεRI expressed on mast cells, basophils, and eosinophils causes degranulation and release of proteins known as histamine (Gomez, 2019). Histamine plays a significant role during allergic reactions and contributes to mucous production, itching, swelling, and smooth muscle contraction (White, 1990). During parasitic infections, histamine has a more complex role, which can both support parasite persistence in the case of Filariae, but contributes to the expulsion of *Nippostrongylus brasiliensis* (*N. brasiliensis*) (Fox et al., 2015; Murray et al.,

1971). Additionally, the secretion of type 2 cytokine IL-13 promotes goblet cell hyperplasia and mucous secretion, contributing to the “weep and sweep” response in expelling helminths (von Moltke et al., 2016). However, during allergic asthma, the activation of goblet cells and mucous production contributes to significant pathology (Ordoñez et al., 2001). This highlights the duality of the type 2 immune response that walks a thin line between protective and pathogenic.

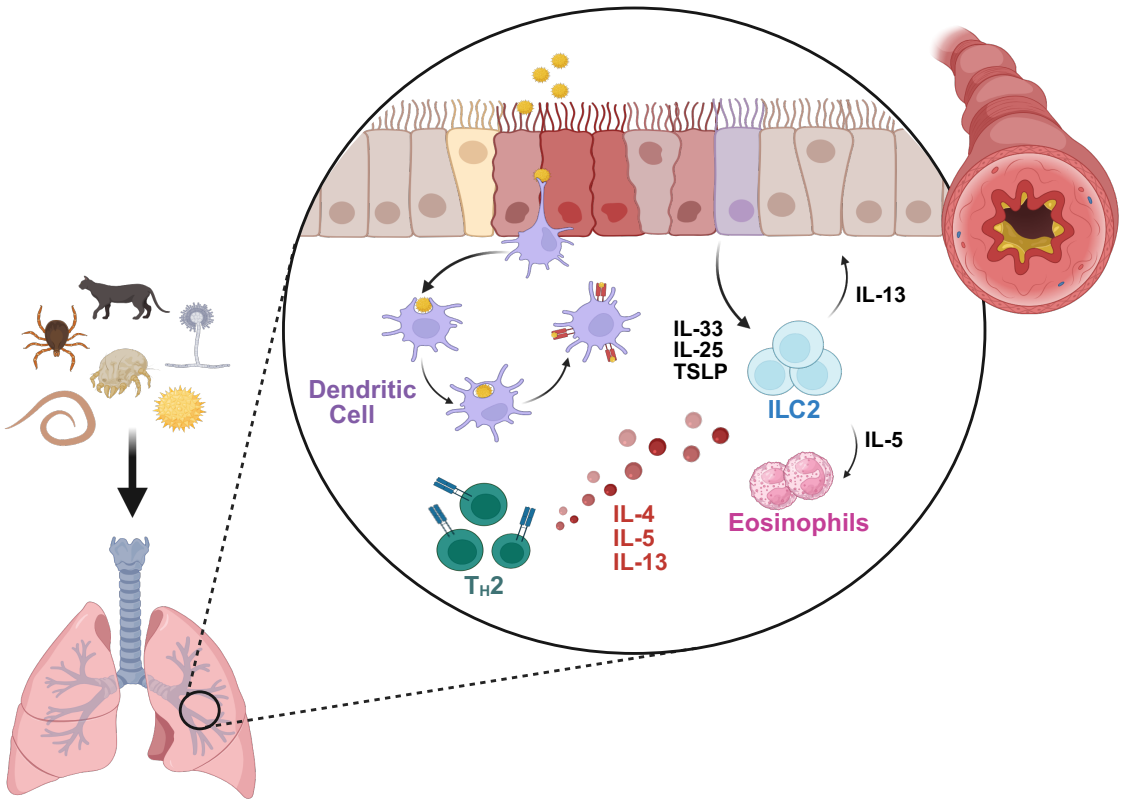

Figure 1.1: Generation of type 2 immune response. Allergen antigens from house dust mite, animal dander, pollen or helminths enter the airways. Dendritic cells sample the lumen and process the antigen and present it to T cells on MHCII to generate Th2 cells. Damage to the epithelial cells releases alarmins IL-33, IL-25, and TSLP, which activate ILC2. ILC2s secrete IL-13, which induces goblet cell hyperplasia and mucus secretion, leading to narrowing of airways. IL-5 from ILC2 promotes eosinophil maturation. Th2 cells also produce IL-4, IL-5, and IL-13. Production of IL-13 leads to goblet cell hyperplasia and excessive mucous secretion.

1.1.3 Type 2 Immunity and Asthma—Clinical Disease Relevance

As mentioned above, the generation of an effective type 2 immune response is vital for the expulsion of parasitic helminth infections. However, in the case of allergies and asthma, the initiation of type 2 immunity becomes pathological. Statistics carried out by the World Health Organisation estimate that approximately 262 million people worldwide suffer from asthma.

The data has been extrapolated to predict that this figure will increase by 100 million in 2025 (Kuruvilla et al., 2019). Severe asthma attacks can be fatal, and since 2019, a recorded 455,000 people have died from asthma, with deaths occurring mainly in low- and lower-middle-income countries (Kuruvilla et al., 2019). In the early to mid-20th century, asthma was considered a rare disease; as such, existing literature on asthma was scarce. However, from the late 20th century, the reporting of asthma in scientific journals increased dramatically. While diagnostics have improved, leading to higher incidence rates, it is clear that the prevalence of asthma since the latter half of the 21st century has also increased. Asthma is well described as a chronic lung disease associated with narrowing of the airways, persistent wheezing, and coughing. The underlying inflammation drives mucous hypersecretion, structural airway remodelling, and bronchial hyperresponsiveness, all of which contribute to disease pathology (Hammad and Lambrecht, 2021). The previous classification of asthma outlined just two forms of the disease: allergic and non-allergic. This ideology has evolved to describe asthma as eosinophilic asthma (type 2 high or ultra-high) and non-eosinophilic (type 2 low) asthma (Hammad and Lambrecht, 2021). The asthma endotypes have different mechanisms underpinning the disease pathology; as such, disease treatments differ in their effectiveness depending on the endotype (Hammad and Lambrecht, 2021). Although Inhaled Corticosteroids (IC) have improved eosinophilic asthma management, the disease remains incurable, and the mortality and treatment inequities remain high in low-income countries (Howell et al., 2023). Additionally, a small percentage of adults and children are nonresponsive to ICs and have severe asthma, highlighting the continued need to investigate alternative biological therapeutics against asthma (Howell et al., 2023). The results of this thesis investigated type 2 airway inflammation; thus, the cell types driving eosinophilic asthma will be the focus of this review.

1.1.4 ILC2 Drive Allergic Airway Inflammation

Type 2 driven asthma is strongly characterised by an overall increase in eosinophilia in the lungs of patients, as well as an increase in neutrophils, ILC2s and mast cells (Howell et al., 2023). Such an influx of immune cells leads to the characteristic pathology of asthma, such as airway mucous, airway remodelling, narrowing of the airways, and airway hyperresponsiveness. IL-33 is an important driver of type 2 immune responses and can even elicit acute allergic asthma responses in the absence of T and B cells (Oboki et al., 2010). While this inflammation fails to become chronic in the absence of an adaptive response, this finding suggested that the initiation of allergic asthma can be driven by an innate cell population, and such inflammation would later be attributed to ILC2s, (Kim et al., 2012; Klein Wolterink et al.,

2012; Neill et al., 2010; Wilhelm et al., 2011). Innate lymphocytes (ILCs), including ILC2, are defined by their transcription factors and cytokine profiles. Analogous to Th1, Th2, and Th17 cells, ILCs can be grouped into Innate Lymphoid Cell 1 (ILC1), ILC2, and Innate Lymphoid Cell 3 (ILC3) based on expression of T-bet, GATA3, and RORγt, respectively (Colonna, 2018). Unlike their adaptive Th2 counterparts, ILC2s lack antigen-specific receptors and instead respond to epithelial-derived alarmins such as IL-33, IL-25, and TSLP. Upon activation, ILC2s produce large quantities of IL-5 and IL-13 as well as IL-9 and Amphiregulin (Areg) (Kobayashi et al., 2021).

The role of Th2 immune cells in allergic asthma is not redundant, as ILC2 and Th2 cells display a close relationship. Together they coordinate their responses during type 2 airway inflammation to drive pathogenesis. In particular, by producing IL-2, Th2 cells promote ILC2 survival and IL-13 production (Salter et al., 2019; Wilhelm et al., 2011). ILC2-derived IL-5 is essential for eosinophil maturation, proliferation, and survival in an antigen-independent manner (Nussbaum et al., 2013; Van Gool et al., 2014). In addition, ILC2 produce small amounts of the eosinophil eotaxin, CCL11 in vitro (Moro et al., 2016). While this has not been validated in vivo, it highlights the close regulation of eosinophilia through ILC2 activation. ILC2s also secrete IL-9 in an autocrine manner, supporting their survival during *N. brasiliensis* infection and promoting IL-5, IL-13, and Areg production (Turner et al., 2013; Wilhelm et al., 2011). In allergic asthma, however, IL-9 supports the persistence of pathogenic ILC2s, and its absence reduces ILC2, Th2, and mast cells and confers protection (Bick et al., 2024; Li et al., 2022). Areg secretion by ILC2s is required for tissue repair following viral infection, yet elevated Areg levels in blood, saliva, and sputum correlate with asthma severity in humans (Hachim et al., 2020; Monticelli et al., 2011). Overall, these findings highlight that although ILC2s have protective functions, their aberrant activation during asthma and allergy drives pathological type 2 inflammation. Uniquely, lung ILC2s have the highest expression of the IL-33 receptor (ST2) compared with ILC2s in other tissues (Matsuyama et al., 2023). Indeed, the importance of IL-33 in the lung is reflected in the first breath drawn in newborn mice, which triggers an IL-33 response causing an expansion of ILC2 (Saluzzo et al., 2017). In the naive mouse lung, ILC2s position themselves in adventitial regions around large vessels and airways (Cautivo et al., 2022; Dahlgren et al., 2019). When activated by IL-33, ILC2s accumulate in adventitial niches, where under half of the cells occupy parenchymal sites in close proximity to alveoli (Dahlgren et al., 2019). The positioning of ILC2 in close proximity to epithelial cells, patrolling cells, and blood supply allows for a direct network of communication between immune cells, circulating nutrients, and oxygen. While this further highlights the

important role of ILC2 during homeostasis, expressing high amounts of ST2 and their unique position within the tissue ensures a fast response to IL-33 released from damaged epithelial cells in allergic airway inflammation (Matsuyama et al., 2023).

1.2 Metabolic Regulation of Type 2 Immunity

While it is an established fact that cells require fuel to generate energy during steady-state and especially during activation, the concept of immunometabolism is relatively new. The generation of an immune response is a metabolically demanding process on surrounding immune cells as cells rapidly increase cytokine production and proliferation (Frauwirth et al., 2002; Newsholme et al., 1985; Pearce and Pearce, 2018; Pearce et al., 2008). Thus, understanding how immune cells, such as ILC2 and Th2 in allergic airway inflammation, utilise different metabolic pathways or nutrients can also inform how we treat diseases.

1.2.1 A Brief Introduction to Metabolism

The energy source for all cellular activities is Adenosine Triphosphate (ATP). Metabolic pathways generate ATP and include glycolysis, the Tricarboxylic Acid (TCA) cycle, Oxidative Phosphorylation (OXPHOS), beta-oxidation, and fermentation (O'Neill et al., 2016). The main fuel sources of such pathways include glucose, lipids, and amino acids. When glucose enters the cell, it can fuel two major pathways, glycolysis and the TCA cycle. Glycolysis converts glucose to pyruvate for the rapid generation of ATP. The Warburg effect is a unique metabolic feature in tumour cells as well as immune cells following proinflammatory signals (Warburg, 1925). It is a process whereby cells will ferment pyruvate to lactate rather than enter oxidation in the mitochondria despite adequate oxygen availability (Warburg, 1925). The end result is less energy, or ATP, but produced at a much faster rate, which allows for rapid proliferation of cells (Kornberg, 2020). Under normal conditions and healthy mitochondria, pyruvate can enter the TCA cycle, which produces Nicotinamide Adenine Dinucleotide (Reduced) (NADH) and Flavin Adenine Dinucleotide ($FADH_2$). NADH and $FADH_2$ are reducing agents that donate their electrons to the electron transport chain (ETC) to fuel OXPHOS within the mitochondria. OXPHOS is a more fuel-efficient pathway that generates greater ATP output compared with glycolysis, albeit at a much slower rate. Cells may also use amino acids such as glutamine in glutaminolysis or fatty acids in beta oxidation to fuel OXPHOS (O'Neill et al., 2016).

Importantly, inflammation shapes the nutrient landscape. For example, during inflammation the body sequesters certain micronutrients such as minerals and vitamins as a mechanism to

prevent the pathogen from accessing these valuable nutrients (Roth-Walter et al., 2024). On the other hand, macronutrients such as glucose, lipids, and amino acids are often increased at the sites of inflammation, likely due to increased vascular permeability (Roth-Walter et al., 2024). Airway inflammation can also create a hypoxic environment, and oxygen availability can also program how an immune cell will use nutrients to fuel metabolic pathways (Missiaen et al., 2023). While increased nutrient availability during inflammation can support rapid ATP generation, immune cells must compete for these resources. This competition, in turn, influences which metabolic pathways different immune cell types can engage.

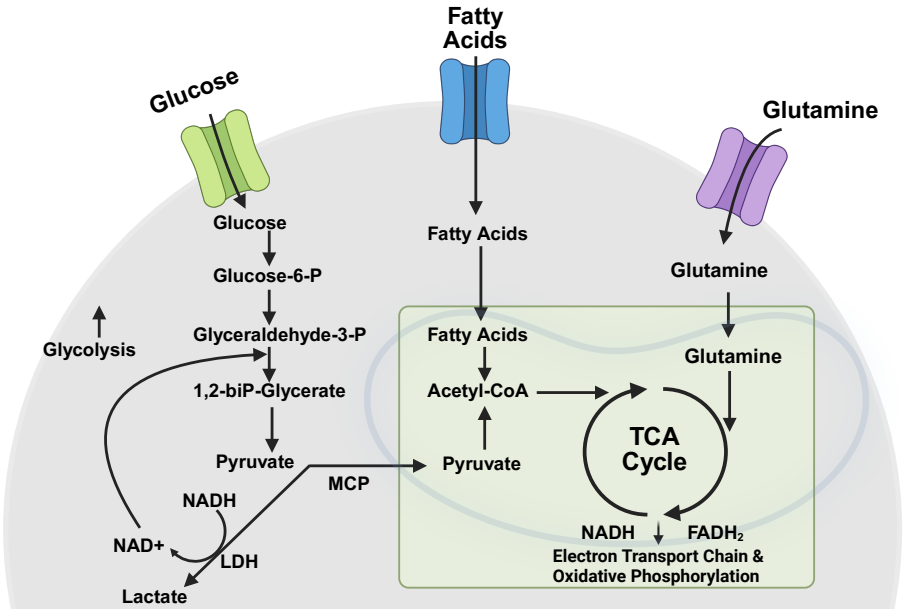

Figure 1.2: Cells use glucose, fatty acids, and amino acids to fuel metabolism. Glycolysis involves the intracellular breakdown of glucose to pyruvate. Under anaerobic and Warburg metabolism, pyruvate is fermented to lactate under the oxidation of NADH to NAD^+. During aerobic glycolysis, pyruvate can be converted to acetyl-CoA and further enter the TCA cycle within the mitochondria. Fatty acids can also enter the TCA cycle by undergoing fatty acid oxidation Fatty Acid Oxidation (FAO) to produce acetyl-CoA, which enters the TCA cycle. Amino acids such as glutamine can undergo glutaminolysis which produces a TCA cycle intermediate. High-energy NADH and $FADH_2$ are generated by the TCA cycle and enter the electron transport chain Electron Transport Chain (ETC) in OXPHOS.

1.2.1.1 Th2 Metabolism

Preliminary papers from the beginning of the millennium investigated glycolytic pathways involved in T cell activation and differentiation of T cell subsets. Th2, Th1, and Th17 were found to express higher Glut1 (Slc2a1) and glycolytic profiles than Tregs, which are more reliant on lipid oxidation (Frauwirth et al., 2002; Michalek et al., 2011). In addition to glycolytic pathways in Th2 differentiation, lipid metabolism plays a distinct role in pathogenic and protective Th2 responses through regulation of Peroxisome Proliferator-Activated Receptors (PPAR).

In particular, PPARγ facilitates exogenous lipid uptake in immune cells and is important for metabolic reprogramming (Daynes and Jones, 2002). Early studies, not centered on T cells, examined whether targeting PPARγ and PPARα could reduce type 2 airway inflammation, revealing a connection between PPARs and type 2 immune responses (Banno et al., 2018). Following this, Angela et al. (2016) revealed a link between mTOR signalling and PPARγ in the early activation of CD4 T cell subsets, including Th2. Interestingly, Th2 cells express higher levels of PPARγ than other T cell subsets, and while PPARγ has only a modest role in Th2 differentiation, it is critical for IL-5 production and for enhancing sensitivity to IL-33 signalling during allergic airway inflammation (Nobs et al., 2017). The importance of lipid metabolism in Th2 is further highlighted by mice with a T cell-specific deletion of PPARγ failing to mount protective responses during infection with *Heligmosomoides polygyrus*(*H. polygyrus*) as well as pathogenic responses in House Dust Mite (HDM)-induced asthma (Chen et al., 2017). This data indicates a direct regulation of lipid metabolism in the generation of both protective and pathogenic Th2 responses. In addition to external lipid uptake, anabolic lipid metabolism via Acetyl-CoA Carboxylase 1 (ACC1) is crucial for the in vitro activation and proliferation of CD4 T cells (Angela et al., 2016). ACC1 is a rate-limiting enzyme involved in de novo fatty acid biosynthesis and is tightly linked to overall cell energy metabolism (Lee et al., 2014). In particular, ACC1 was found to be most highly expressed in IL33R$^+$ IL-5$^+$ lymphocytes in the naive mouse lung, which significantly increased upon IL-33 stimulation (Angela et al., 2016). Knocking out ACC1 in CD4 T cells was sufficient to abrogate airway inflammation in a papain model of allergic asthma (Nakajima et al., 2021). Overall, the data appears to suggest that glycolytic programming is important for early activation and differentiation of Th2 cells, but lipid metabolism dominates to regulate Th2 cells during inflammation Lin et al. (2023).

While most studies have focused on glycolysis and lipid metabolism, very little is known about how Th2 cells use amino acids to fuel their immune response. A new study, however, has found that SLC7A8 (LAT2) is upregulated on Th2 more than any other T cell subset and is important for the generation of effective type 2 immune response in the context of helminth and allergic asthma (Panda et al., 2023). SLC7A8 transports a range of large and small neutral amino acids such as leucine and arginine which support mTOR activation. As mTOR is an important regulator of glucose and lipid metabolism in Th2 cells, it is not surprising that activated Th2 cells will increase their transport of such amino acids (Wolfson and Sabatini, 2017). However, the specific role of certain amino acids through SLC7A8 transport in specific metabolic pathways in Th2 has not yet been elucidated. Overall, the literature on Th2-specific

immunometabolism during type 2 inflammation requires further investigation. Nevertheless, it is evident that the mTOR-lipid-glycolysis axis is crucial for effective Th2 responses during type 2 inflammation.

1.2.1.2 ILC2 Metabolism

While ILC2 share transcriptional and functional similarities to their adaptive Th2 counterparts, ILC2 in disease contexts display enhanced metabolic flexibility (Wientjens et al., 2025). As ILC2s reside in tissue niches that have very different nutrient landscapes, such as skin, liver, lung, and adipose tissue, ILC2s must adapt their metabolism to the nutrient and cytokine environment in which they reside (Yu et al., 2022). While more extensively explored than Th2 metabolism, research into ILC2 metabolism is also relatively recent, with the first seminal papers on ILC2 metabolism emerging approximately 9 years ago. Monticelli et al. (2016) demonstrated that precursor and mature ILC2 express Arginase 1 (Arg1), an enzyme necessary to transform arginine into urea and ornithine in the urea cycle, which is necessary for fueling pathways that support proliferation. Upon activation in allergic airway inflammation or with *N. brasiliensis*, ILC2s increase their expression of Arg1. The deletion of which reduced ILC2 numbers in allergic airways (pathogenic) and during *N. brasiliensis* infection (protective). Importantly, during Arg1 inhibition, activated ILC2 were unable to utilise glycolysis, linking arginine uptake and glycolytic capacity of ILC2 (Monticelli et al., 2016). Surace et al. (2021) conducted metabolomics on ILC2 supporting the importance of arginine in ILC2, as it was one of the most abundant amino acids in human circulating ILC2. In addition to arginine, however, leucine and valine were significantly upregulated in human ILC2, both of which support the mTOR pathway (Wolfson and Sabatini, 2017). Leucine is transported by SLC7A5 (LAT1) and steady-state ILC2 expressed high levels of CD98, the co-transporter of SLC7A5 (Surace et al., 2021). The authors demonstrated that resting circulating ILC2 imported amino acids such as leucine and valine to support OXPHOS and to sustain functionality and proliferation rather than engaging in glycolytic pathways. When activated by IL-33, however, human ILC2 further increase OXPHOS as well as increase their glycolytic capacity to support IL-13 and IL-5 production (Surace et al., 2021). While the authors observed that CD98 expression did not increase in ILC2 upon IL-33 activation, which they suggest means that activated ILC2 do not depend on external uptake of amino acids, their control group contained IL-2 in the cell culture, which also can contribute to ILC2 activation, leading to IL-5 and IL-13 production and masking the differences by also increasing CD98 expression (Roediger et al., 2015; Surace et al., 2021).

Hodge et al. (2023) validated the findings of increased valine and leucine in murine ILC2 following IL-33 activation and also observed that murine ILC2 express more CD98 and its binding partners SLC7A5 and SLC7A8 than ILC3, CD4 T cells, and B cells. In addition, upon activation, ILC2 increases kynurenine uptake, which is transported by SLC7A5. This suggests that activated ILC2s do increase their import of external amino acids rather than relying solely on intracellular sources (Hodge et al., 2023). Expression of both SLC7A5 and SLC7A8 was crucial on ILC2 for proliferation and function during helminth infection, although in the absence of either one, functionality in ILC2 is preserved, suggesting a compensatory role (Hodge et al., 2023). Surace et al. (2021) highlighted that ILC2 use amino acids to support their mitochondria, and Hodge et al. (2023) further support this idea, as inhibition of LAT1 or LAT2 impacted mitochondrial function. In addition, SLC7A8 expression on ILC2 is not only important in protective ILC2 contexts but also during allergic airway inflammation (Panda et al., 2022). Both Hodge et al. (2023) and Panda et al. (2022) indicate that amino acid signalling through SLC7A5 and SLC7A8 is important in the mTOR pathway and mitochondrial function. In addition, Ye et al. (2020) identified a critical role for c-Myc in ILC2 biology. c-Myc belongs to a family of oncogenes and plays a significant role in controlling cellular metabolism (including amino acid metabolism) and proliferation, and its activity is tightly linked to mTOR signalling (Lin et al., 2025). However, Ye et al. (2020) did not directly connect c-Myc deficiency in ILC2s to metabolic dysfunction. This link was later clarified by Panda et al. (2022), who showed that loss of the amino acid transporter SLC7A8 disrupts both mTOR activity and c-Myc expression in ILC2s, highlighting the integrated roles of amino acid availability, mTOR signalling, and c-Myc in supporting ILC2 metabolic programming. While amino acid metabolism is vital for ILC2 mitochondrial metabolism, like Th2, ILC2s rely more heavily on uptake of external fatty acids than other ILC subsets, as well as CD4 T cells (Wilhelm et al., 2016). During helminth infection, ILC2 increase their uptake of external fatty acids to fuel FAO (Wilhelm et al., 2016). The increase in fatty acids was also observed in the context of vitamin A deficiency and hints at evolutionary adaptation of ILC2 during times of nutrient scarcity and parasite infections to ensure barrier protection and compensate for a weaker adaptive immune response (Wilhelm et al., 2016). However, external lipid uptake is not unique to the protective function of ILC2, as it is also observed in the context of allergic inflammation (Karagiannis et al., 2020).

Like Th2, ILC2 expresses high levels of PPARγ, and its expression is important for the import of fatty acids. To handle the increase in lipids and prevent lipotoxicity, ILC2 upregulates Diacylglycerol O-acyltransferase 1 (DGAT1), an enzyme that converts diacylglycerols into tri-

acylglycerols, incorporating them into lipid droplets (Karagiannis et al., 2020). Surace et al. (2021) observed that IL-33 activated ILC2 increase their expression of GLUT1, for glucose import, and Karagiannis et al. (2020) also observed that airway ILC2s increase glucose uptake during allergic airway inflammation. In particular, glucose availability was important for the uptake of lipids and storage into lipid droplets as well as mTOR signalling (Karagiannis et al., 2020). In contrast to this, blocking glucose availability to protective ILC2 during helminth infection did not alter ILC2 function, whereas blocking lipid availability did impair expulsion (Wilhelm et al., 2016). This suggests subtle metabolic programming during protective and pathogenic functions of ILC2. Karagiannis et al. (2020) further highlighted the importance of mTOR regulation in ILC2 as inhibiting mTOR prevented ILC2 function and proliferation. This work preceded the discovery of amino acid–dependent signalling and mTOR regulation in ILC2s, with current knowledge from Hodge et al. (2023); Panda et al. (2022); Surace et al. (2021), it is likely that mTOR inhibition would also impair amino acid uptake, thereby contributing to the defective proliferative response. It would also be valuable to determine if glucose deprivation affects the expression of CD98, SLC7A5, and SLC7A8 during pathogenic ILC2 activation, given their roles in nutrient sensing and transport. While the importance of glucose, lipids, and amino acids is unraveling in ILC2 and Th2 metabolism, more recently, a role for iron uptake has been revealed. In particular, Hurrell et al. (2024) demonstrated that activated ILC2s increase their iron uptake during allergic asthma through CD71 or transferrin receptor 1. Iron is an important cofactor for a large number of enzymes governing cellular metabolism, and its uptake is also regulated by mTOR activation (Bayeva et al., 2012). Collectively, these metabolic studies position mTOR as a central regulator of ILC2 function, with glucose playing a more context-dependent role, whereas amino acid and lipid metabolism serve as key determinants of both steady-state and activated ILC2 biology. However, whether protective and pathogenic ILC2s rely on distinct metabolic programmes remains an open and unresolved question.

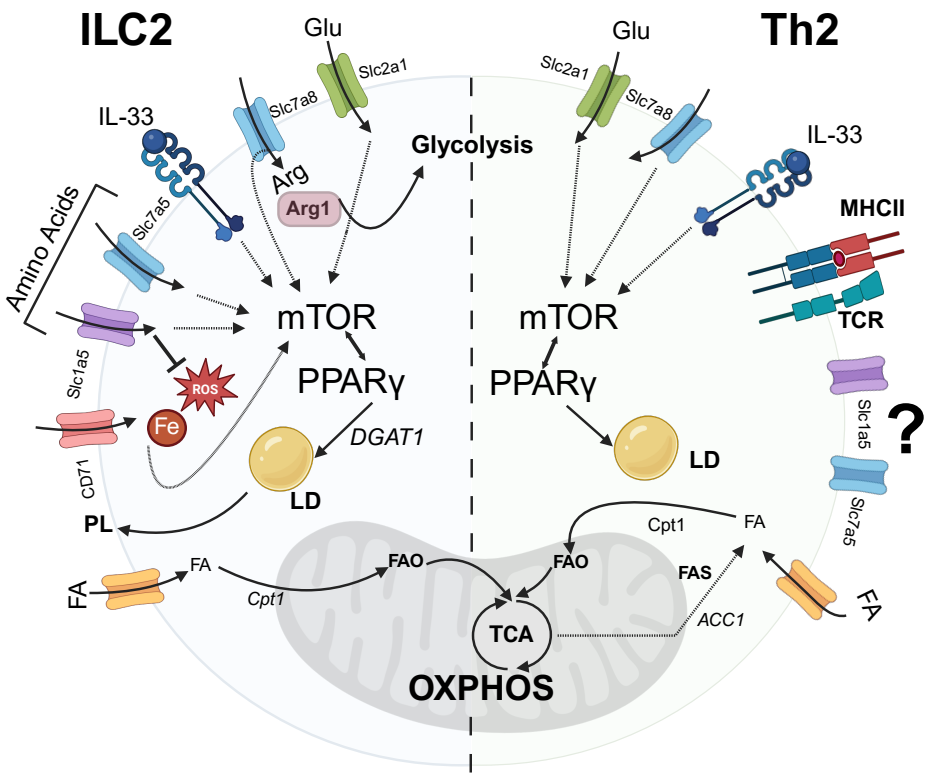

Figure 1.3: Features of ILC2 and Th2 metabolism. Upon activation with IL-33, ILC2 and Th2 upregulate Glut1 on their surface to increase the uptake of glucose, supporting glycolysis. ILC2 also rely on arginine and the enzyme Arg1 to support glycolysis. In pathogenic ILC2 and Th2, glucose uptake supports mTOR regulation and the transcription of PPARγ, which supports the acquisition of external fatty acids. The enzyme DGAT1 converts excess fatty acids to lipid droplets (LD) and fatty acids are also funnelled to phospholipid (PL) membranes to support proliferation. Activated ILC2 upregulate iron receptor CD71 and amino acid transporters Slc1a5, Slc7a5, and Slc7a8, which support mTOR regulation and redox balancing. Th2 also increase their expression of Slc7a8 likely to support mTOR function. Th2 rely on the upregulation of ACC1 to promote fatty acid synthesis and support proliferation and function. Both ILC2 and Th2 rely on fatty acid oxidation to support their function during activation.

1.2.1.3 The role of ROS in ILC2 and Th2

As cells such as ILC2 and Th2 rely heavily on FAO, a significant amount of Reactive Oxygen Species (ROS) is generated in the process. Therefore, it is important to consider ROS pathways in the metabolic regulation of type 2 immunity. ROS is a general term to describe O_2 radical species such as superoxide anions species like superoxide ($O_2^{\bullet -}$), hydroxyl radical ($OH^{\bullet}$), peroxyl radical ($LOO^{\bullet}$), alkoxyl radical ($LO^{\bullet}$) or non radical species like hydrogen peroxide (H_2O_2), singlet oxygen ($^1O_2$), lipid hydroperoxide (LOOH), peroxynitrite ($ONOO^-$), hypochlorous acid (HOCl), or ozone (O_3) (Circu and Aw, 2010). The role of ROS is two-fold, where physiological levels serve as messengers for intracellular signalling, whereas excess ROS can cause DNA damage within a cell and trigger apoptotic pathways (Circu and Aw,

2010). Lungs are a highly vascularised tissue with high oxygen exposure, making them susceptible to ROS. In particular, allergic asthma is associated with increased endogenous ROS, which contributes to the pathogenesis of asthma (Jiang et al., 2014). Sources of ROS during allergic asthma include epithelial cells, macrophages, eosinophils, and neutrophils (Jiang et al., 2014). Thus, understanding how ILC2 and Th2 regulate their redox systems in response to extracellular ROS and intracellular ROS can inform us how these cells are protected from damage and contribute to pathogenicity.

Zheng et al. (2020) demonstrated that BALF ILC2 following acute IL-33 exposure has increased cellular ROS compared to naive. When pretreated in vitro with N-acetyl-cysteine (NAC) prior to activation with IL-33, ILC2 had reduced ROS and reduced cytokine production. This suggests that initial activation of ILC2 requires a boost in ROS to promote functionality. Moreover, early ROS generation in ILC2 was important for metabolic programming, as both mTOR signalling and CD98 expression were reduced in NAC-pretreated ILC2 (Zheng et al., 2020). Similarly, Th2 cells appear to rely on early ROS generation post-activation during allergic asthma in mice and support their metabolic pathways (Choi et al., 2024). While intracellular ROS appears to be important for initial priming of activated ILC2, Zheng et al. (2020) show in a follow-up study that extracellular ROS is harmful to ILC2, suppressing proliferation but not impacting functionality. On the contrary, Wientjens et al. (2025) has shown that ILC2s are heavily reliant on cystine uptake to support their antioxidant systems during allergic airway inflammation, which supports their lipid metabolic pathways. Cells can balance ROS in several ways, including the Glutathione (GSH) redox system and the thioredoxin system, both of which are tightly coupled to each other (Circu and Aw, 2010). Wientjens et al. (2025) showed that targeting the thioredoxin system was detrimental to ILC2 in vitro and could be rescued using GSH. In addition, blocking the thioredoxin system during allergic airway inflammation led to reduced ILC2 numbers and protected the lung from excessive damage (Wientjens et al., 2025). A similar reduction was observed in Th2, suggesting that while ROS in both ILC2 and Th2 cells is important for early activation, they rely on their antioxidant systems to prevent excessive ROS accumulation for the maintenance of allergic airway inflammation.

Thioredoxin-Interacting Protein (TXNIP) is an important negative regulator of the thioredoxin system. It directly binds to thioredoxin and inhibits its antioxidant function (Choi and Park, 2023). The upregulation of TXNIP is associated with several chronic diseases, including type 2 diabetes and kidney disease (Choi and Park, 2023). However, whether it has a role

in ILC2 allergic asthma is unclear. Paradoxically, Kokubo et al. (2023) demonstrated that TXNIP upregulation in Th2 cells is important for ROS scavenging and generation of memory Th2 cells. TXNIP was increased upon the contraction phase during memory T cell formation, and deficiency of TXNIP led to enhanced apoptosis and decreased numbers of memory Th2 cells (Kokubo et al., 2023). Memory T cells switch their metabolic programming from anabolic to catabolic metabolism, thus, the upregulation of TXNIP during the contraction phase may also reflect this change in metabolism. In addition, memory T cells divide more slowly and remain in a dormant phase, and increased TXNIP expression is associated with slowed cell division (Singh, 2013; Whitmire et al., 2008). Nevertheless, the exact role of TXNIP in ILC2 and Th2 redox balancing during protective and pathogenic inflammation remains an open question.

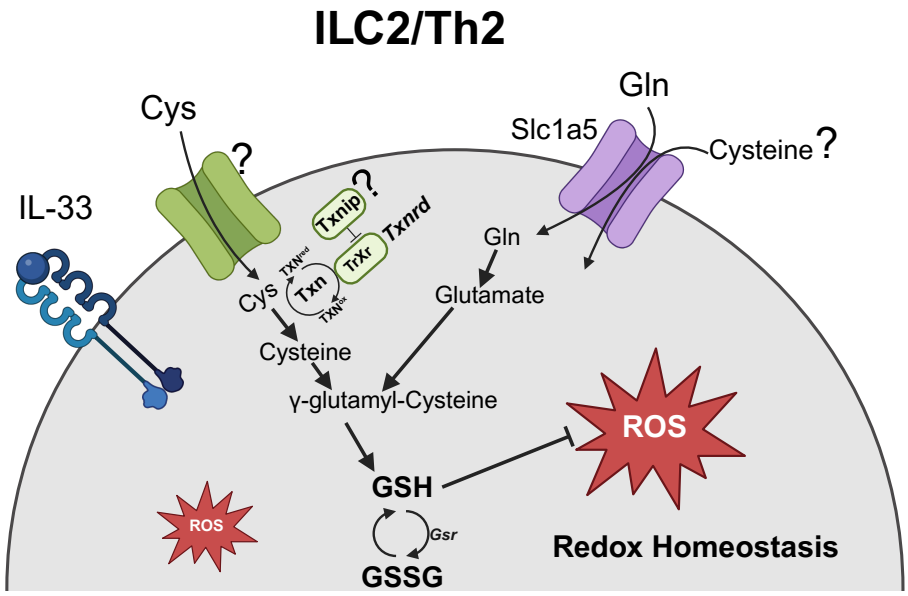

Figure 1.4: ROS balancing is a key feature of activated ILC2 and Th2. Both cystine and cysteine availability in ILC2 is important for their maintenance during allergic inflammation and activation by IL-33. Cysteine is the rate-limiting substrate for the synthesis of GSH which acts as an important ROS scavenger in cells to ensure redox balancing. ILC2 increase their expression of SlC1A5, which can transport glutamine and possibly regulated by cysteine. The main cystine transporter in ILC2 and Th2 has not yet been determined during allergic inflammation. ILC2s and Th2s rely thioredoxin system to support ROS balancing capacities. TXNIP is a negative regulator of thioredoxin, however its exact role in Th2s and ILC2s during allergic inflammation remains unclear.

1.3 Modulators of Type 2 Inflammation—Cytokines, Diet, and Helminths

As outlined earlier, the evolutionary role of type 2 immunity was to protect the host against parasitic helminth infections, venom, and toxins, as well as metabolic homeostasis. However, in high-income countries, type 2 immunity is now commonly associated with allergies and asthma, where aberrant activation of type 2 immune cells can have detrimental outcomes such as anaphylaxis in severe allergic responses and morbidity in uncontrolled asthmatic attacks. Given this duality between protective and pathological outcomes, type 2 immunity must be tightly regulated. Therefore, a central question is how type 2 effector cells, such as ILC2, integrate environmental and tissue-derived signals to regulate their activation, proliferation, and survival.

1.3.1 Cytokine Modulators of ILC2

As described, ILC2s are activated by epithelial-derived cytokines IL-33, IL-25, and TSLP. In addition, IL-7 is important for the survival of ILC2 at steady-state and is mainly produced by thymic epithelial cells (Sheikh et al., 2022). Also stated above, upon activation, IL-2 and IL-9 become important for the maintenance of activated ILC2 (Bick et al., 2024; Roediger et al., 2015; Salter et al., 2019). Karagiannis et al. (2020) demonstrated that IL-33 alone is sufficient for proliferation but is enhanced upon the addition of IL-7 in airway ILC2s compared to IL-25 and IL-7 or TSLP and IL-7. In addition, IL-33 + IL-7 drove glucose uptake, lipid uptake, and lipid droplet formation compared to IL-25 or TSLP. This suggests that IL-33 activation of airway ILC2s drives the metabolic rewiring during airway inflammation. In more recent years, ILC2s have been divided into subsets whereby the population of airway ILC2 activated by IL-33 are described as natural ILC2 or nILC2 (Huang and Paul, 2016; Huang et al., 2015). A second population known as inflammatory ILC2 or iILC2 has been described (Huang and Paul, 2016; Huang et al., 2015). iILC2s do not respond to IL-33, as they do not express the ST2 receptor; rather, they respond to IL-25 and are commonly associated with helminth infections (Huang and Paul, 2016; Huang et al., 2015) . In addition, they are a transient population, capable of migrating between tissues. While this population has been characterised during helminth infection, common inducers of allergic airway inflammation in mice, such as papain and HDM, also promote IL-25 release from epithelial cells; thus, it is possible this population arises during allergic asthma as well (Jang et al., 2017; Yu et al., 2010). However, the ontogeny of iILC2 remains poorly defined, and it is unclear whether metabolic differences exist between nILC2 and iILC2. Clarifying how these ILC2 subsets can be selectively targeted may be important for mitigating allergic airway inflammation in specific disease settings. This question is particularly relevant given the identification of a

$CD45RO^+$ ILC2 population in humans, thought to be analogous to mouse iILC2. Notably, $CD45RO^+$ ILC2 are increased in the blood and mucosal tissues of asthma patients and correlate with steroid resistance (van der Ploeg et al., 2021). This makes it relevant to revisit how the immune response typically restrains type 2 immune responses, which historically has been type 1 immunity suppressing type 2 immune responses.

Preliminary papers showed how IFNγ, a classic type 1-associated interferon, can suppress class switching of IgE antibodies (Billiau and Matthys, 2009). In the late 90s, Cohn et al. (1999) showed that Th1 cells have the potential to suppress allergic airway inflammation and that IFNγ can suppress mucous production and eosinophilia. Early papers also showed that IFNγ can suppress Th2 differentiation by suppressing the IL-4-STAT6 axis and that inducing Tbet expression in T cells through IFNγ suppresses GATA3 and Th2 differentiation (Hu and Ivashkiv, 2009). However, it is only in the last 10 years that it has been uncovered that IFNγ can counter-regulate ILC2. Molofsky et al. (2015) showed that steady-state ILC2 preferentially express IFNγ receptor rather than IFNα or IFNβ (IFNAR) receptor, and in vivo ILC2 and Th2 were suppressed in the lung during simultaneous exposure to IFNγ and IL-33 (Molofsky et al., 2015). VAT ILC2 and Th2 were also suppressed by IFNγ, albeit to a lesser extent (Molofsky et al., 2015). One year later, Moro et al. (2016) showed that IFNγ and IL-27 suppress ILC2 through a STAT1-dependent pathway. The authors also reported that iILC2 are less responsive to IFNγ suppression than nILC2, pointing to subset-specific regulatory control. They additionally note that endogenous IFNγ rises in the late stages of *N. brasiliensis* infection, pointing to an evolutionary function of type 1 immunity in curbing type 2 responses to prevent tissue pathology (Moro et al., 2016). Cautivo et al. (2022) reported that under mixed type 1/type 2 inflammatory conditions, IFNγ acts to confine ILC2 within the adventitial niche, thereby blocking their extravasation. While Moro et al. (2016) claim that IFNγ does not cause apoptosis of ILC2, as ILC2 are vital in tissue repair following influenza infection, Cautivo et al. (2022) demonstrate that when cultured with just survival factor IL-7, IFNγ can induce cell death. An important difference in these models is that Moro et al. (2016) cultured ILC2s with IL-2 and IFNγ. As IL-2 is a potent activator (or reactivator) of previously activated ILC2, this may have prevented their apoptosis. In addition to these findings, while ILC2s express receptors for IL-10 and IFNβ, only IFNβ, like IFNγ, suppressed their proliferation and function in vitro, IL-10 had no effect (Moro et al., 2016). While Moro et al. (2016) demonstrate that STAT1 mediates IFNγ and IL-27-dependent suppression of ILC2, the underlying mechanisms remain undefined. Moreover, whether IFNγ universally drives ILC2 death under specific disease contexts is still speculative. Importantly, it also re-

mains unknown whether IFNγ imposes metabolic constraints on ILC2 that could contribute to their reduced proliferation and function.

1.3.2 Dietary Regulation of Asthma

Although cytokine-mediated pathways constrain ILC2, they represent only part of the regulatory landscape. As cellular metabolism and nutrient availability play a significant role in immune responses, it is becoming more widely recognised that diet can influence our immune system (Munteanu and Schwartz, 2022). Pathogenic ILC2 rely on glucose uptake to regulate lipid metabolism and Karagiannis et al. (2020) influenced such properties by weaning mice onto a ketogenic diet for 3 weeks prior to exposure to papain. The ketogenic diet is high in fats, with adequate protein, and very low in carbohydrates (Zhu et al., 2022). The authors showed that mice weaned on a ketogenic diet are protected from excessive airway inflammation and ILC2s were reduced. Moreover, lipid uptake and droplet formation were impaired in the ILC2 (Karagiannis et al., 2020). A ketogenic diet increases ketone bodies in circulation, and recent literature has suggested that the ketone body beta-hydroxybutyrate may indirectly suppress ILC2 proliferation during allergic airway inflammation through modulation of mast cells (Thio et al., 2022). However, the exact mechanism of suppression remains unknown. Moreover, the beneficial effects of the ketogenic diet on asthma in humans are lacking in depth and clarity. However, a high sucrose diet in mice exacerbated allergic airway inflammation, which may link how obesity and diets high in sugar and carbohydrates worsen asthma and why the ketogenic diet is protective (Everaere et al., 2016; Musiol et al., 2023).

In another study, a high-fiber diet protected mice from allergic asthma by reducing ILC2. Interestingly, a diet high in pectin induced the most production of Short-Chain Fatty Acids (SCFA) and was associated with increased IFNγ during allergic airway inflammation (Lewis et al., 2019). In particular, the SCFA butyrate, but not acetate or propionate, was found to protect mice from allergic asthma by suppressing ILC2. Butyrate was capable of down-regulating GATA3 and impairing OXPHOS in ILC2 (Lewis et al., 2019). As the production of SCFA relies on microbiota, this data could suggest a link between microbiota and dietary metabolites in shaping immune responses during airway inflammation. Finally, there is some evidence that fasting may reduce asthma, as a period of fasting protected mice from OVA and IL-33-induced allergic airway inflammation by reducing ILC2 and eosinophils (Suzuki et al., 2021). Like the ketogenic diet, fasting reduces circulating glucose as well as increasing ketone bodies (Longo and Mattson, 2014). Overall, these studies suggest that increased

availability of dietary glucose in Western diets may support pathogenic ILC2 during asthma, and focusing on nutrition may be an additional support to current therapeutic strategies in asthma treatment.

1.3.3 Helminths as Modulators of Allergic Disease

Epidemiological data suggests the presence of a chronic helminth infection is associated with a lower incidence of asthma. However, the species of helminth plays a role, where hookworms seem to demonstrate the most correlation of protection (Bohnacker et al., 2020). While effective type 2 immune responses are important for expulsion of parasites, helminths have evolved strategies for dampening type 2 inflammation to promote chronicity of infection. For example, the murine intestinal nematode *H. polygyrus* establishes a chronic infection that can suppress IL-33 secretion from epithelial cells (Osbourn et al., 2017). It was discovered that *H. polygyrus* secretes a protein known as HpARI, and this protein can protect from allergic asthma in murine models (Osbourn et al., 2017). Several studies have shown that chronic infection with *Schistosoma mansoni* or *Schistosoma japonicum* is often associated with atopy in humans but also protects from induction of allergic asthma. The literature suggests this is an IL-10-dependent mechanism and a switch to the generation of regulatory T cells, which contributes to the dampening of general immune responses (Resende et al., 2019; Smits et al., 2007).

Trichuris muris (*T. muris*) is a natural gut-dwelling parasite of mice and is closely linked to the human *T. trichuria* and porcine *T. suis*. Heavy worm burden of *T. trichuria* in children was associated with reduced skin allergy, however, allergic rhinitis was not tested in this cohort (Rodrigues et al., 2008). Administration of *T. suis* has shown promising protection against Th1-driven colitis, however, protection against allergic rhinitis in humans is not evident (Bager et al., 2010). Nevertheless, *T. muris* provided scientists with a unique opportunity to study the induction of type 1 and type 2 immune responses, as *T. muris* induces a heterogeneous immune response (Else and Grencis, 1991). A high dose of *T. muris* ova leads to the induction of an effective type 2 immune response and expulsion, whereas a low dose induces a chronic and persistent infection associated with the generation of a type 1 immune response (Klementowicz et al., 2012). The mechanism by which *T. muris* induces a type 1 immune response is still unknown, however, there is evidence that burrowing of *T. muris* into the epithelium of the cecum induces bacterial translocation and lipopolysaccharide (LPS) signalling, which may contribute to the induction of a systemic switch to type 1 immunity (Hayes and Grencis, 2021). The switching of the immune response to type 1 allows enables a chronic

infection, and indeed, a high-dose acute infection can be switched to a chronic infection by administering IL-12 (Bancroft et al., 1997). Equally, a chronic infection can be prevented by blocking IL-12 (Blackwell and KJ, 2001).

While human studies are inconclusive on the protection of *T. trichuria* against allergic asthma, in mice, chronic *T. muris* has been shown to be protective against murine models of asthma (Chenery et al., 2016). Mice lacking T or B cells were still able to generate a chronic infection, which could suggest an innate immune cell, such as Natural Killer (NK) cells or ILC1, which produce significant IFNγ, is driving the chronicity. Depleting NK cells during acute infection did not impact expulsion, suggesting NK cells are not necessary for induction of Th2 response during resistant infection (Koyama, 2002). However, depleting NK cells during chronic *T. muris* has not been performed. While IL-10 from a myeloid-derived source appears to increase during chronic *T. muris* infection, depleting IL-10 did not reverse protection against allergic asthma (Chenery et al., 2016). Consequently, the mechanism of protection against allergic asthma in mice during chronic *T. muris* infection remains unclear, as well as the immune cells driving the IFNγ response. In addition to its ability to modulate the cytokine response, *T. muris* also secretes a protein known as p43 which binds to IL-13, thus inhibiting its function and preventing expulsion (Bancroft and Grencis, 2021). Much like HpARI from *H. polygyrus* blocks IL-33, p43 may protect against IL-13 during allergic airway inflammation, however, no such studies have been conducted yet on the therapeutic potential of p43 in such contexts. Furthermore, in humans, chronic *T. trichuria* is associated with malnutrition, including protein malnutrition in children (Papier et al., 2014). In mice with *T. muris*, amino acids are found in the feces compared to unaffected mice, suggesting poor absorption (Houlden et al., 2015). As ILC2 rely heavily on amino acids, this could impact the generation of effective ILC2 responses. Additionally, *T. muris* requires significant glucose uptake from the host (Hansen et al., 2016), and as pathogenic ILC2 appear to thrive on excess glucose availability, reduced glucose in the environment may be contributing to impaired ILC2 function. In addition to changes in nutrient availability, the presence of IFNγ may contribute to the suppression of ILC2 and Th2 during allergic asthma. However, the contribution of intestinal chronic *T. muris* infection to host and cellular metabolism during allergy has not yet been explored.

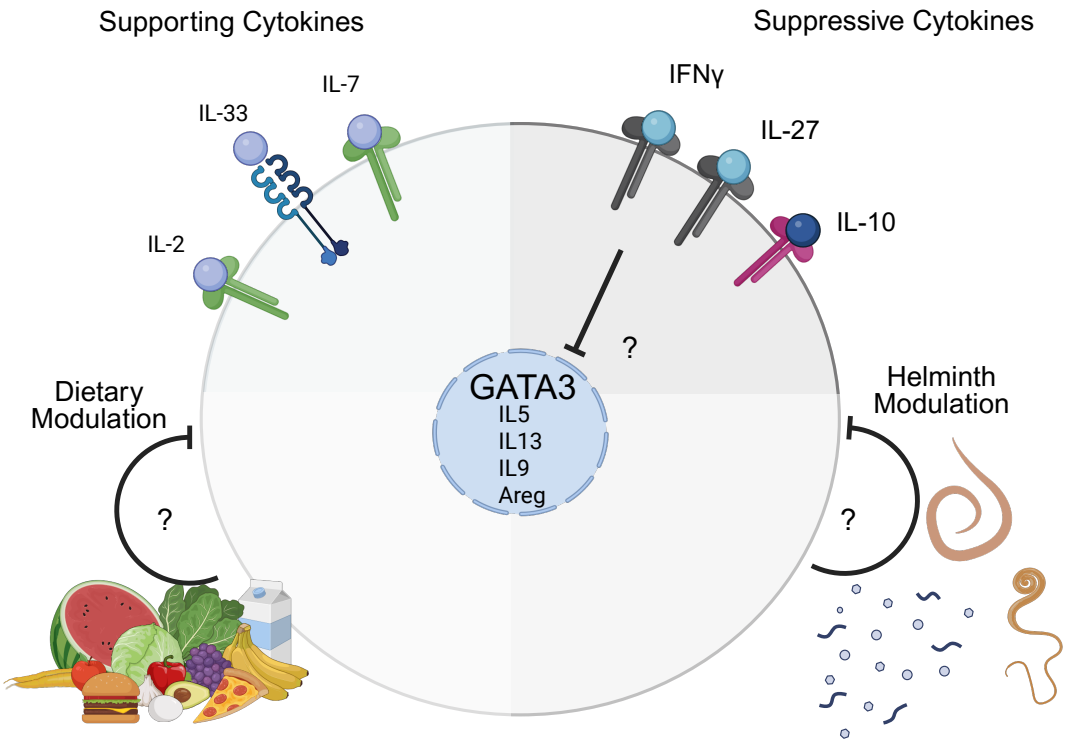

Figure 1.5: A basic overview of the regulatory landscape of ILC2. ILC2 are supported by activating cytokines IL-33 and IL-2 as well as survival cytokine IL-7. Suppression of ILC2 can occur transcriptionally by IFNγ and IL-27. While the receptor for IL-10 exists on the surface of ILC2, it is unclear whether IL-10 suppresses ILC2 in vitro or in vivo. Dietary modulation can impact the outcome of allergic asthma, including suppressing ILC2, although the exact mechanisms are not fully understood. Additionally, helminth infections are correlated with reduced incidences of allergic asthma, yet the direct suppression of ILC2 has not always been determined.

1.4 Thesis Aims and Objectives

Humans have co-evolved with multicellular organisms such as helminths, which are thought to modulate the immune system and dampen excessive type 2 responses. In high-income countries lacking exposure to helminth infections, dysregulated type 2 immunity may contribute to allergic diseases. Chronic *T. muris* infection protects mice from ILC2-driven allergic airway inflammation, however, the underlying mechanisms remain poorly defined. While chronic *T. muris* significantly alters host nutrient availability, how these changes influence ILC2 biology during allergic inflammation has not been investigated.

Aim 1: Determine whether helminth-driven changes in the nutrient environment contribute to protection from ILC2 mediated airway inflammation. Using metabolomic data generated in our laboratory, we investigate whether alterations in tissue metabolites during chronic *T. muris* infection influence the development of allergic airway inflammation

and suppress ILC2 activation.

Aim 2: As nutrient availability and metabolic competition shape immune cell function, we investigate how chronic *T. muris* infection alters ILC2 cellular metabolism during allergic airway inflammation.

Aim 3: A cell's ability to balance ROS is an important but often underinvestigated aspect of cell metabolism. We investigate the role of redox balancing in the suppression of ILC2s during chronic *T. muris* infection and allergy.

Aim 4: Define the role of IFNγ in regulating ILC2 metabolism and function during helminth-induced protection. Chronic *T. muris* infection leads to increased IFNγ, yet its impact on ILC2 metabolism and allergic inflammation remains unclear. Using the chronic *T. muris* + papain model, we investigate how IFNγ shapes the mixed type 1/ type 2 immune environment and whether it contributes to reduced ILC2-mediated airway inflammation.

2. Materials and Methods

2.1 Materials

2.1.1 Consumables

Table 2.1: Consumables

Category	Description	Supplier
Strainers	LABSOLUTE®Cell Strainer 70 µM (Ref. 7.696768)	TH Geyer
	LABSOLUTE®Cell Strainer 40 µM (Ref. 7.696767)	TH Geyer
Dishes	Petri Dishes, PS, 35/10 MM (Ref. 627161)	Greiner Bio-One
Serological Pipettes	5 mL costar®STRIPETTE (Ref. 4487)	Corning
	10 mL costar®STRIPETTE (Ref. 4488)	Corning
	25 mL costar®STRIPETTE (Ref. 4489)	Corning
Pipette Tips	Pipette Tips 1000 µL (Cat#06-379-2018)	nerbe plus
	Pipette Tips 200 µL (Cat#70.3030.100)	Sarstedt
	Pipette Tips 10 µL (Cat#TXL-10)	Corning
96-well plates	96 Well Cell Culture U-bottom Plate (Cat#TPP92697)	TPP
Tubes	Falcon®Centrifuge Tubes 50 mL (Cat#352070)	Corning
	Falcon®Centrifuge Tubes 15 mL (Cat#352096)	Corning
	Cluster Tubes (Cat#732-5554)	732-5554
	Microcentrifuge Tube 1.5 mL (Cat#5615000)	Ratiolab
	Microcentrifuge Tube 2.0 ml (Cat#BCT4T-4653763)	Ratiolab
Syringes	Non-sterile 3 ml syringes (Cat#4616025V)	BRAUN
Columns	LS Columns (Cat#130-042-401)	Miltenyi Biotec

2.1.1.1 Metabolic Dyes

Table 2.2: Metabolic Dyes

Dye	Supplier	Description
BioTracker Cystine-FITC (Cat#SCT047)	Sigma-Aldrich	Cystine uptake probe
BODIPY™493/503 (Cat#D3922)	ThermoFisher	Lipid droplet stain
BODIPY™FL C_{16} (Cat#D3821)	ThermoFisher	Lipid uptake probe
DCFDA (2',7'-Dichlorofluorescein diacetate) (Cat#CAY20656-500)	Cayman	Reactive oxygen species
Image-iT™ Lipid Peroxidation Kit (Cat#C10445)	ThermoFisher	Lipidperoxidation

2.1.1.2 Devices

Table 2.3: Devices

Device	Name	Supplier
Centrifuges	Centrifuge (5417R)	Eppendorf AG
	Centifuge (5430)	Eppendorf AG
	Centifuge (5810R)	Eppendorf AG
Incubators	Heracell™ 150 CO_2	Heraeus
Pipettes	Eppendorf Research® plus Pipette (10, 20, 200, 1000)	Eppendorf AG
Multi-channel pipettes	Finnpipette™ (10, 300)	ThermoFisher
Vortexing	Vortex Mixer	Bender & Hobein
Thermocyler	Thermocycler	Eppendorf AG
	Quantstudio 6 RT-PCR	ThermoFisher
Flow Cytometers	BD LSRFortessa™ Cell Analyzer	BD Biosciences

2.1.1.3 Liquids and Buffers

Table 2.4: Liquids and Buffers

Liquid/Buffer	Supplier/Composition
ACK Lysis Buffer Cat#E-CK-A105)	Elabscience
β-mercaptoethanol (Cat#P07-05020)	PAN Biotech
DPBS, no calcium, no magnesium, pH 7.2 (Cat#14190169)	Thermo Scientific
Fetal Bovine Serum (FBS) (Cat#10270106)	ThermoFisher
Dimethylsulfoxide (Cat#4720.4)	Carl Roth
HEPES (Cat#P05-01100)	PAN Biotech
MEM NEAA (Cat#11140-035)	ThermoFisher
Percoll® (Cat#GE17-0891-01)	Sigma-Aldrich
Sodium pyruvate (Cat#11360-039)	ThermoFisher

2.1.1.4 Drugs and Treatments

Table 2.5: Drugs and Treatments

Category	Description	Supplier
Anesthesia	Isoflurane Baxter vet (Cat#HDG9623V)	Baxter
Infection	*T. muris* eggs	in house propagation
Allergens	House Dustmite Extract (Cat#XPB82D3A2.5)	Greer
	Papain (Cat#8933.1)	Carl Roth
Redox Modulators	L-Glutathione (Cat#G4251)	Sigma-Aldrich
	N-Acetyl-L-cysteine (Cat#A9165)	Sigma-Aldrich
Metabolic Modulators	2-Deoxy-D-glucose (2-DG) (Cat#D8375)	Sigma Aldrich
	Oligomycin A (Cat#S1478)	Selleckchem
Cytokines	Recombinant Mouse IL-2 (Cat#575404)	Biolegend
	Recombinant Mouse IL-7 (Cat#577804)	Biolegend
	Recombinant Mouse IL-33 (Cat#580506)	Biolegend
	Recombinant Mouse IFNγ (Cat#315-05-100UG)	PeproTech
	Invivo Mab anti-mouse IFNγ (Cat#BE0055)	Bio X Cell
	Ultra-LEAF™ Purified Rat IgG1, isotype control (Cat#400457)	Biolegendl
Antibiotics	Gibco™ Penicillin-Streptomycin (Cat#15140122)	ThermoFisher
Phenolic Acids	3-(3-Hydroxyphenyl)propionic Acid (Cat#H940090)	Toronto Research Chemicals
	3-(3-Hydroxyphenyl)propionic sulphate (Cat#cay9004103-5)	Cayman Chemical Company

2.1.1.5 Chemicals, Reagents, Enzymes and Kits

Table 2.6: Chemicals, Reagents, Enzymes and Kits

Reagent/Kit	Supplier
2 amino ethanol (Cat#A5611)	Sigma-Aldrich
Aminoguanidine (Cat#CAYM81530)	Cayman
AZDye647-Azide (Cat#CLK-1299-AZ)	Jena Bioscience
Bovine Serum Albumin (BSA) (Cat#A3803)	Sigma-Aldrich
Click-iT™Plus Alexa Fluor™647 Picolyl Azide Toolkit (Cat#C10643)	ThermoFisher
Copper(II) Sulfate pentahydrate (Cat#10038389)	Sigma-Aldrich
DAPI (4′,6-diamidino-2-phenylindole) (Cat#6843.1)	Carl Roth
Deoxyribonuclease I (DNase I) (Cat#DN25)	Sigma Aldrich
Formaldehyde (Cat#F8775-4X25ML)	Sigma-Aldrich
Formalin (Cat#F5554)	Sigma-Aldrich
FOXP3/Transcription staining set (Cat#00-5523-00)	ThermoFisher
GolgiPlug (Cat#51-2301KZ)	BD Bioscience
Ionomycin calcium salt (Cat#I0634)	Sigma-Aldrich
LEGENDplex™MU Anti-Virus Panel (Cat#740621)	Biolegend
LEGENDplex™MU Th Panel Detection Antibodies V03 (Cat#741045)	Biolegend
LEGENDplex™Mouse Th Panel Standard V03 (Cat#741046)	Biolegend
LEGENDplex™Mouse IL-5 Capture bead A5 (Cat#740056)	Biolegend
LEGENDplex™Mouse IL-13 Capture Bead B9 (Cat#740739)	Biolegend
LEGENDplex™Mouse IL-9 Capture Bead B9 (Cat#740739)	Biolegend
LEGENDplex™Mouse IFNγ Capture Bead A4 (Cat#740065)	Biolegend
LEGENDplex™Mouse IL-6 Capture Bead A8 (Cat#740057)	Biolegend
LEGENDplex™Mouse IL-22 Capture Bead B7 (Cat#740738)	Biolegend
LEGENDplex™Mouse IL-17A Capture Bead B4 (Cat#740061)	Biolegend
LEGENDplex™Mouse IL-10 Capture Bead B2 (Cat#740059)	Biolegend
Liberase™ TL Research Grade (Cat#5401020001)	Sigma Aldrich
MojoSort™ Streptavidin Nanobeads (Cat#480016)	Biolegend
NP-40 (Cat#JM-2111-100)	MBL
Phorbol 12-myristate 13-acetate (Cat#1652981)	PeproTech
Protease/phosphatase Inhibitor Cocktail (100X) (Cat# 5872S)	Cell Signaling Technology
Puromycin-dihydrochlorid (Cat#P8833)	Sigma-Aldrich
Revertaid RT Reverse Transcription Kit (Cat#K1691)	ThermoFisher
RNAeasy micro kit (Cat#74004)	Qiagen
Streptavidin, Pacific Blue™ conjugate (Cat#S11222)	ThermoFisher
Trizol (Cat#15596018)	ThermoFisher
SRI-3770 (Cat#HY-141623)	MedChemExpress
Zombie UV™ Fixable Viability Kit (Cat#423108)	Biolegend

2.1.1.6 Oligonucleotides

Table 2.7: Oligonucleotides

Gene	Supplier	Identifier
Txnip	IDT	Mm.PT.58.28669539
Gclc	IDT	Mm.PT.58.30656560
Slc1a5	IDT	Mm.PT.58.33492914
Nampt	IDT	Mm.PT.58.32381457
Slc7a5	IDT	Mm.PT.58.10563809
Slc7a8	IDT	Mm.PT.58.9941934
Slc27a6	IDT	Mm.PT.58.9548097
Slc27a4	IDT	Mm.PT.58.7213593
Slc38a1	IDT	Mm.PT.58.9661143
Slc43a2	IDT	Mm.PT.58.15973616
Fasn	IDT	Mm.PT.58.14276063
IFN$_\gamma$	IDT	Mm.PT.58.41769240
Il33	IDT	Mm.PT.58.45987473
Tbx21	IDT	Mm.PT.58.5261453
Insr	IDT	Mm.PT.58.31759585
Got1	IDT	Mm.PT.58.10848799
Cpt1a	IDT	Mm.PT.58.10147164
Gsr	IDT	Mm.PT.58.13488384
Nfe2l2	IDT	Mm.PT.58.29108649
Hk1	IDT	Mm.PT.58.9947184
Slc2a1	IDT	Mm.PT.58.7590689
Arg1	IDT	Mm.PT.58.8651372
Irf1	IDT	Mm.PT.58.9199490
Cxcl10	IDT	Mm.PT.58.43575827
GATA3	IDT	Mm.PT.58.29935080
STAT1	IDT	Mm.PT.58.23792152
Ido1	IDT	Mm.PT.58.29540170
Myc	IDT	Mm.PT.58.28494642
Vdr	IDT	Mm.PT.58.13445739
Retn	IDT	Mm.PT.58.10147164
Lpl	IDT	Mm.PT.58.46006099
Dgat1	IDT	Mm.PT.58.32759507
Pparg	IDT	Mm.PT.58.31161924
Pnpla2	IDT	Mm.PT.56a.13424398.g
Col3a1	IDT	Mm.PT.58.13848686
Fn1	IDT	Mm.PT.58.8135568
Ccl11	IDT	Mm.PT.58.28587819
Hprt	IDT	Mm.PT.39a.22214828(1)

2.1.2 Cell Culture Media

Table 2.8: Cell Culture Media

Description	Medium	Supplements
Complete Medium	RPMI 1640 GlutaMAX™	100 U/mL penicillin/streptomycin 1 mM sodium pyruvate Nonessential amino acids (1:100)
0 %	RPMI 1640 GlutaMAX™	-
10 %	RPMI 1640 GlutaMAX™	10 % FBS 100 U/mL penicillin/streptomycin 1 mM sodium pyruvate Nonessential amino acids (1:100)

2.1.2.1 Antibodies

Table 2.9: Antibodies

Specification	Source	Identifier
CD3ε Mouse	BioXCell	Cat# BE0001-1; RRID: AB_1107634
CD3 Mouse	Biolegend	Cat# 100304; RRID: AB_312669
CD11b Mouse/human	Biolegend	Cat# 101204; RRID: AB_312787
CD11c Mouse	Biolegend	Cat# 117304; RRID: AB_313772
CD19 Mouse	Biolegend	Cat# 152407; RRID: AB_2629816
CD19 Mouse	Biolegend	Cat# 115504; RRID: AB_313638
CD4 Mouse	Biolegend	Cat# 100546; RRID: AB_11126142
CD4 Mouse	Biolegend	Cat# 100430; RRID: AB_493698
CD4 Mouse	Biolegend	Cat# 100552; RRID: AB_2563053
CD45 Mouse	Biolegend	Cat# 103154; RRID: AB_2572115
CD90.2 (Thy-1.2) Mouse	Biolegend	Cat# 140318; RRID: AB_11203724
Foxp3	ThermoFisher	Cat# 45-5773-82; RRID: AB_914351
IFNγ Mouse	Biolegend	Cat# 505826; RRID: AB_2295770
IL-5 Mouse/human	Biolegend	Cat# 504306; RRID: AB_315329
IL-13 Mouse/human	ThermoFisher	Cat# 53-7133-82; RRID: AB_2016708
IL-33Rα Mouse	Biolegend	Cat# 145304; RRID: AB_2561914
IL-33Rα Mouse	Biolegend	Cat# 145312; RRID: AB_2565635
GATA3 Mouse	Biolegend	Cat# 653810; RRID: AB_2563216
Gr-1 Mouse	Biolegend	Cat# 108404; RRID: AB_313369
Tbet Mouse	Biolegend	Cat# 644810; RRID: AB_2200542
CD71 Mouse	Biolegend	Cat# 113818; RRID: AB_2749884
CD98 Mouse	Biolegend	Cat# 128212 ; RRID: AB_2750545
MHCII	Biolegend	Cat# 107622; RRID: AB_493727
Ly6C Mouse	Biolegend	Cat# 128044; RRID: AB_2566577
Ly6G Mouse	Biolegend	Cat# 127606; RRID: AB_1236494
Ly6G Mouse	Biolegend	Cat# 127643; RRID: AB_2565971
Sca-1 Mouse	Biolegend	Cat# 108112; RRID: AB_313349
Sca-1 Mouse	Invitrogen	Cat# 45-5981-82; RRID: AB_914372
B220 Mouse/Human	Biolegend	Cat# 103236; RRID: AB_893354
pS6 Mouse	eBioscience	Cat# 25-9007-42; RRID: AB_2637099
pMTOR Mouse	eBioscience	Cat# 48-9718-42; RRID: AB_AB_2574127
Ki-67	eBioscience	Cat# 25-5698-82; RRID: AB_AB_11220070
NK1.1 Mouse	Biolegend	Cat# 108730; RRID: AB_2074426
Puromycin	Biolegend	Cat# 381506; RRID: AB_2927825
Siglec-F Mouse	Biolegend	Cat# 155527; RRID: AB_2890715
TCRβ chain Mouse	Biolegend	Cat# 109206; RRID: AB_313428
TCRβ chain Mouse	Biolegend	Cat# 109222; RRID: AB_893627
Ter119 Mouse	Biolegend	Cat# 116204; RRID: AB_313704
Eomes Mouse	eBioscience	Cat# 61-4875-82; RRID: AB_2574614
Eomes Mouse	BD	Cat# 567171; RRID: AB_2916488
LPAM-1 Mouse	Biolegend	Cat# 120607; RRID: AB_10719833

2.1.2.2 Software

Table 2.10: Software

Software	Supplier	Reference
FlowJo™ Software V10.10.0	Becton, Dickinson and Company; 2023	https://www.flowjo.com/
LEGENDplex™ Analysis Software	Biolegend	https://legendplex.qognit.com
Prism Graphpad 10	GraphPad Software	https://www.graphpad.com
Seahorse Analytics Software 10	Agilent Technologies	https://seahorseanalytics.agilent.com/
R environment		https://rstudio-education.github.io/hopr/starting.html

2.2 Animals

Female C57Bl/6 mice were bred in-house or purchased from Charles River Labs and maintained under specific pathogen-free (SPF) conditions. Red5 animals (kindly provided by Dr. Richard Locksley, University of California, San Francisco) (Nussbaum et al. (2013)) were crossed to Txnip$^{fl/fl}$ (#018313) (Yoshioka et al. (2007)) (purchased from Jackson Laboratory) and maintained at in-house facilities. All procedures were performed according to ethical protocols approved by the local and regional ethical committees. All mice used in the study were between 6-12 weeks of age.

2.3 Maintenance and Oral Infection with *T. muris*

For the generation of *T. muris* eggs, RAG2$^{-/-}$ mice are infected with approximately 150 to 200 eggs per mouse, and eggs were prepared and maintained according to the protocol established by (Antignano et al., 2011). For the induction of chronic infection, C57BL/6 mice were orally infected with approximately 25 eggs via oral gavage in 200 µL of deionised water. At 21 days post oral infection, mice received either papain or house dust mite. For acute infection, C57BL/6 mice were orally infected with approximately 150 eggs via oral gavage in 200 µL deionised water. Mice were sacrificed at d21, d24, or d28 post infection.

2.4 Induction of Type 2 Inflammation with Papain or House Dust Mite

C57BL/6 mice were intranasally administered 10 µg papain in 50 µL PBS under isoflurane anesthesia on d0, d3, d6, and d13. Mice were anaylsed on d7 or on d14. For induction of type 2 inflammation using HDM, C57BL/6 mice were intranasally administered 10 µg HDM in 50 µL PBS under isoflurane on d0, d5, d6, d7, d8, d9, and d10. Analysis was performed on d14.

2.5 In vivo Treatment with anti-IFNγ

C57BL/6 mice were intranasally administered 20 µg anti-mouse IFNγ antibody (InVivoMab, Clone:XMG1.2) in 50 µL PBS under isoflurane anesthesia on d18 post *T. muris muris* infection and again on d0, d3, and d6 of papain exposure. Mice were anaylsed on d7.

2.6 In vivo Treatment with 3-(3-Hydroxyphenyl)propanoic acid (3HPPA)

C57BL/6 mice were administered 166 mg/Kg in autoclaved tap water daily via oral gavage for two weeks during papain exposure. C57BL/6 mice were intranasally administered 10 µg papain in 50 µL PBS under isoflurane anesthesia on d0, d3, d6, and d13. Mice were anaylsed on d14.

2.7 In vivo Treatment with IFNγ and IL-33

C57BL/6 mice were intranasally administered 1 µg carrier-free recombinant IFNγ in 50 µL PBS under isoflurane anesthesia on two consecutive days prior to simultaneous intranasal administration of carrier-free recombinant IL-33 (50 ng/ 50 µL) for a further two consecutive days. Mice were intranasally administered 1 µg carrier-free recombinant IFNγ in 50 µL on d2 post IL-33 exposure and mice were anaylsed on d3.

2.8 Seahorse Assay

For real-time measurement of Oxygen Consumption Rate (OCR) and Extracellular Acidifcation Rate (ECAR), $2x10^4$ ILC2 were cultured in XF media supplemented with 1 % FCS and 10 mM glucose and analyzed with a Seahorse XF HS Mini Analyzer (Seahorse Bioscience). Four consecutive measurements were obtained under basal conditions, followed by the addition of 1 µM oligomycin, which inhibits the mitochondrial ATP synthase; 1.5 µM FCCP, which uncouples ATP synthesis from oxygen consumption; and a combination of 100 nM rotenone plus 1 µM antimycin A, which inhibit the electron transport chain by blocking complexes I and III, respectively. All chemicals used for these assays were obtained from Sigma-Aldrich.

2.9 Cell Isolation From Tissue for Flow Cytometry

Lungs were isolated and placed in RPMI supplemented with 2 % FCS. The tissue was briefly washed in PBS 1X before being finely minced. For collection of lung homogenate, minced tissue was placed on 40 µM filters atop 50 mL Falcons, and 50 µL of PBS 1X was added directly onto tissue. The samples were centrifuged, and tissue was transferred to 2 mL of enzymatic digestion media containing Liberase TL (0.25 mg/ml, Roche) and DNaseA (1mg/ml ; Sigma-Aldrich) and placed at 37° under continuous rocking for 1 hour. Lung homogenate

was transferred to Eppendorfs containing protease inhibitor. Isolated cell suspension was passed through 70 µM filters and washed three times. The cells were resuspended in a 37.5 % percoll gradient for further purification. The upper layer was discarded, and the pellet was resuspended in Ammonium-Chloride-Potassium (ACK) buffer for the lysis of red blood cells. Lysis was quenched with the addition of media, and the isolated cell suspensions were stained with anti-CD16/32 (BioXcell) and with fluorochrome-conjugated antibodies against any combination of the following surface antigens: CD3, CD11b, CD11c, DX5, CD19, CD45, Ter119, NK1.1, Gr-1, CD45, Thy1.2, and ST2. DAPI or fixable Zombie UV dye (Biolegend) was used to exclude dead cells. For examination of transcription factors and cellular proliferation, cells were subsequently treated with the Foxp3 fixation/permeabilization kit (eBioscience) in accordance with the manufacturer's instructions and stained for 60 min with fluorochrome-conjugated antibodies against GATA3 and Ki67.

2.10 Restimulation of Cells with PMA and Ionomycin

Cells isolated from lung tissues were stimulated for 3 h with Phorbol 12,13-dibutyrate (0.5 µg/ml) (PdBU; Biomol) and ionomycin (0.5 µg/ml) (Sigma) in the presence of brefeldin A (1 µg/ml) (GolgiPlug, BD Biosciences). Stimulated cells were stained for surface markers, followed by fixation with the Foxp3 fixation/permeabilization kit (eBioscience) in accordance with the manufacturer's instructions, and stained with antibodies against GATA3, Tbet, IL-5, IL-13, and IFNγ.

2.11 Metabolic Profiling of Immune Cells by Flow Cytometry using SCENITH™

The protocol to charaterise immune cells via flow cytometry by metabolic profiling on a single-cell level was adapted from the original paper of SCENITH™ protocol developed by R. Argüello (Argüello et al. (2020)). After isolation from the lung tissue, $3x10^5$ cells were plated and rested for 30 min at 37°, 5 % CO_2 in the incubator before treating the cells with vehicle control (DMSO, Carl Roth), 2-DG (100 mM), oligomycin A (1 µM) or both drugs simultaneously. The cells were incubated for 30 min at 37° with Puromycin (10 µg/ml) without washing. Cells were washed and incubated with antibodies against surface markers before fixing and permeabilizing them with the Foxp3 fixation/permeabilization kit. An anti-puro monoclonal antibody (1:500, Clone 2A4) was used in intracelluar staining to stain against puromycin for 60 min at 4°. Metabolic capacities and dependencies were calculated according to the formulas provided in the original publication.

2.12 Staining of Cells with BODIPY FLC16 or BODIPY 493 or Cystine

Isolated lung cells were stained with 200 ng/ml BODIPY 493/503 or 25 ng/ml BODIPY FLC16 (both ThermoFisher) for 30 min at 37°C in FCS-free complete medium, washed, stained with surface markers, fixed with Foxp3 fixation/permeabilization kit (eBioscience), and analysed by flow cytometry. 2.5 µM Cystine-FITC for 30 min at 37°C in FBS-free RPMI 1640 complete medium. Afterwards, cells were washed and stained for surface markers before they were analyzed by flow cytometry.

2.13 Quas-R: Azidohomoalanine (AHA) Uptake Assay and Staining

Amino acid uptake via Slc1a5 uptake was assessed using incubating cells isolated from lung tissue and stained for surface and live/dead markers. Cells were washed and then incubated with 100 µM AHA for 5 min at 37°C and fixed with paraformaldehyde (4 % in FACs buffer) followed by permeabilization with NP-40 (0.1 % in PBS). The click reaction was performed using the Click-iT™ Plus Alexa Fluor™ 647 Picolyl Azide Toolkit according to the manufacturer's instructions or by using copper sulfate ($CuSO_4$, 1 mM), sodium ascorbate (NaAsc, 10 mM), tris-hydroxypropyltriazolylmethylamine (THPTA, 1 mM), aminoguanidine (10 mM), PBS and AZDye647-Azide according to Pelgrom *et al.* (Pelgrom et al. (2023)).

2.14 Staining of Cells with MitoTracker Green and TMRM

To probe the mitochondrial mass and membrane potential, freshly isolated lung cells were plated, stained with 50 nM MitoTracker Green FM (Thermo Fisher) and 25 nM TMRM (Sigma-Aldrich) for 30 minutes at 37°C, surface stained, and analysed by flow cytometry.

2.15 Staining of Cells with DCFDA

To assess general reactive oxygen species in the cell, lung cells were plated, stained with 1 µM DCFDA (Cayman Chemicals) in 1X PBS for 30 minutes at 37°C, surface stained and analysed by flow cytometry.

2.16 Flow Cytometric Determination of Apoptosis

To assess apoptosis on a single-cell level by flow cytometry, cells were stained for surface markers before staining against Annexin V for 15 min in Annexin Binding Buffer. PI was added before analyzing cells by flow cytometry. Live cells were identified as Annexin V^-/PI^-, dead cells as AnnexinV^+/PI^+ and early apoptotic as AnnexinV^+/PI^-.

2.17 Lipid Peroxidation Staining

Freshly isolated lung cells were stained with Image-iT Lipid Peroxidation Sensor BODIPYTM 581/591 C11 (ThermoFisher) for two hours at 37°C in FBS-free RPMI 1640 complete medium. Cells were stained for surface markers, fixed with the Foxp3 fixation/permeabilization kit (ThermoFisher), followed by intracellular staining for transcription factors. Samples were analyzed by flow cytometry, and the ratio of signal from the 510 nm to 590 nm channels was used to quantify lipid peroxidation as BODIPY 581/591 C11 ratios (gMFI Bodipy C11ox/(gMFI Bodipy C11ox + gMFI Bodipy C11red).

2.18 Kynurenine Staining

To assess amino acid uptake, lung cells were plated and first surface stained, followed by staining with 0.1 mM kynurenine for 5 minutes at 37◦C, then fixed with PFA for 20 minutes and analysed by flow cytometry.

2.19 NAD^+/NADH and $NADP^+$/NADPH Assay

ILC2 from papain only or papain + *T. muris*-infected mice were FACS sorted and plated at approximately 10,000 or 20,000 cells per well and rested at 37◦ in 2 % medium for 30 minutes before performing the NAD^+/NADH or $NADP^+$/NADPH (Promega) according to the manufacturer's instructions.

2.20 Phospho mTOR and S6 Staining

Activated ILC2 were FACS sorted and plated at approximately 2000-5000 cells/well and cultured in 100 µL 10 % complete RPMI without beta-mercaptoethanol in the presence of IL-7 (10 ng/ml, Biolegend) alone or with IFNγ (10 ng/ml, Biolegend) for 3 days. Cells were fixed immediately with the FOXP3 fixation/permeabilization kit (ThermoFisher) followed by fixation with 90% ice-cold methanol. After fixation, cells were stained with surface and transcription factor antibodies in permeabilisation buffer for 60 minutes and analysed by flow cytometry.

2.21 In Vitro Activation of Naive ILC2

Naive ILC2 were FACS sorted and plated at approximately 2000-5000 cells/well and cultured in 100 µL 10 % complete RPMI without beta mercaptoethanol in the presence of IL-7 (10 ng/ml, Biolegend) alone or in combination with IL-33 (10 ng/ml,Biolegend) and/or IFNγ (10 ng/ml,Biolegend) for 4 days. To assess the role of ROS in suppressing ILC2 proliferation during culture with IFNγ, 5 mM N-acetylcysteine (NAC) (Sigma-Aldrich) and 2 mM glutathione

(GSH) (Sigma-Aldrich) were added to the culture. To investigate the role of TXNIP in driving IFNγ-induced suppression of ILC2, 0.5-5 μM SRI-37330 (MedChem Express), a TXNIP regulator, was added to the culture.

2.22 In Vitro Culture of in Vivo Activated ILC2

Activated ILC2 were FACS sorted and plated at approximately 2000-5000 cells/well and cultured in 100 μL 10 % complete RPMI without beta mercaptoethanol in the presence of IL-7 (10 ng/ml, Biolegend) alone or with IFNγ (10 ng/ml,Biolegend) for 3 days. To assess the role of ROS in suppressing ILC2 proliferation during culture with IFNγ, 5 mM N-acetylcysteine (NAC) (Sigma-Aldrich) and 2 mM glutathione (GSH) (Sigma-Aldrich) were added to the culture.

2.23 Whole Lung Culture of Naive Lung Cells

Whole lung cells ($3x10^5$ cells/well) from naive or d21 *T. muris*-infected mice were cultured in 200 μL 10 % complete RPMI and an activation mix including IL-7 (10 ng/ml, Biolegend), IL-33 (10 ng/ml, Biolegend). To assess the role of endogenous IFNγ contributing to the suppression of lung ILC2 in d21 *T. muris*-infected mice, 10 μg/mL monoclonal anti-IFNγ antibody (InVivoMab, Clone:XMG1.2) was added in combination with IL-33 and IL-7.

2.24 RT qPCR

RNA from tissue or cells was extracted using Trizol (Thermo Fisher Scientific) or the RNAeasy micro kit (Qiagen) and reverse transcribed with the RevertAid Kit (Thermo Fischer Scientific) in accordance with the manufacturer's instructions. The cDNA served as a template for amplification of the genes of interest. Target-gene expression was calculated using the comparative method for relative quantification upon normalization to *Hprt*.

2.25 Metabolomics on Colon and Lung Tissue

Metabolomics was carried out by Metabolon in 2017. Experimental model and tissue sample collection were carried out by Alexander Kasakov and Jayagopi Surendar. Data was visualised in R by Maria Doverman and Svetosar Nesic.

2.26 Data Analysis

All flow cytometry data was analyzed using FlowJo 10.4.2 software (FlowJo, Ashland, OR). All graphs were generated and all statistical analysis was performed using Prism 9 (V9.1.1) software (GraphPad Software, San Diego, CA).

2.27 Statistical Analysis

Data were analyzed with the Prism software (GraphPad). Graphs are display means as Standard Error of the Mean (SEM). A two-tailed Student's t test or ordinary one-way Analysis of Variance (ANOVA) was used for all statistical analyses: ns: not significant, * p % 0.05, **p % 0.01, *** p % 0.001. Statistical details are indicated in the figure legends.

3. Results

3.1 Chronic *T. muris* Protects from Chronic and Acute Airway Inflammation

While the protective effect of chronic *T. muris* infection during allergic airway inflammation has been described (Chenery et al., 2016), the cellular and mechanistic basis of such protection remains poorly defined. Given the broad systemic effects that accompany a chronic helminth infection, we first established whether the infection robustly modulates allergic airway inflammation in both acute and chronic allergic asthma. To do so, mice were infected with a low dose of *T. muris* ova to induce chronic infection and, 21 days later, exposed intranasally to papain to mimic repeated allergen challenge (Figure 3.1A). Chronic *T. muris* infection markedly reduced total lymphocyte recruitment to the airways, including eosinophilia (Figure 3.1B-C). Lung ILC2 numbers were also decreased (Figure 3.1D), although their proliferative capacity remained intact (Figure 3.1E). In contrast, Th2 cell numbers were relatively unchanged (Figure 3.1F). Correspondingly, IL-5 and IL-13 protein levels in the lung homogenate were reduced 3.1G-H). Complementing this, IL-13 mRNA was reduced in lung tissue, with a trend toward lower IL-5 mRNA expression (Figure 3.1I-J). The eosinophil-recruiting chemokine *Ccl11* was also downregulated, indicating an overall suppression of type 2 cytokine and chemokine responses in the airways of *T. muris*-infected mice (Figure 3.1K).

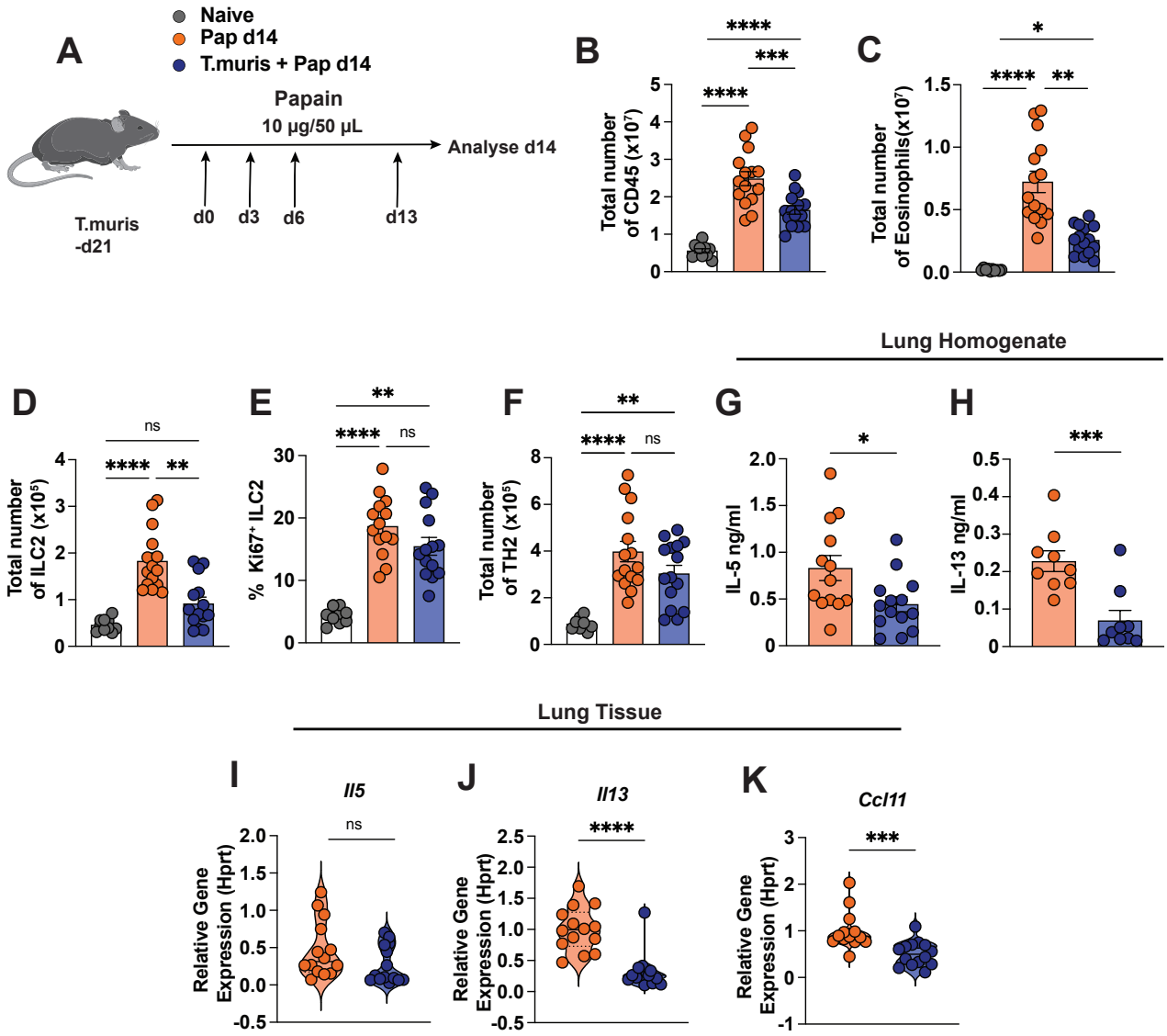

Figure 3.1: Chronic *T. muris* protects from excessive type 2 airway inflammation. (A) Schematic of experimental design where Pap = Papain. (B-C) Total airway lymphocytes and eosinophils in papain and *T. muris* and papain. (D-E) Total number and Ki67$^+$ positive ILC2 in papain and *T. muris* and papain. (F) Total number of Th2 in papain and *T. muris* and papain. (G-H) IL-5 and IL-13 protein quantified by LEGENDplex in papain and *T. muris* and papain. (I-K) Gene expression of *Il5*, *Il13*, and *Ccl11* mRNA in the lung tissue in papain and *T. muris* and papain. ILC2 were gated on CD45$^+$ CD90$^+$ Lin$^-$ GATA3$^+$ (D-E). Th2 were gated on CD45$^+$ CD4$^+$ CD8$^-$ FOXP3$^-$ GATA3$^+$.Results display three independent experiments with three to five mice in each experimental group. All graphs display means ± SEM; ns (not significant) $p > 0.05$, * $p \leq 0.05$, ** $p \leq 0.01$, *** $p \leq 0.001$, **** $p \leq 0.0001$. One-way ANOVA with Tukey's multiple comparisons test and Welch's t-test.

We next employed an acute papain challenge with a reduced duration (Figure 3.2A) to determine whether the protective effect of chronic *T. muris* was reproducible across models of allergic airway inflammation. Chronic *T. muris* infection similarly suppressed type 2 airway

inflammation in the acute model, yielding a more consistent phenotype of protection compared to the chronic airway model across independent experiments. Infected mice exhibited a reduction in airway lymphocyte recruitment, eosinophilia, and Th2 cell infiltration into the lung (Figure 3.2B–D). Lung ILC2 numbers and proliferative capacity were also significantly reduced (Figure 3.2E–G), accompanied by impaired effector function, as evidenced by fewer IL-5^{+}IL-13^{+} double-producing ILC2s (Figure 3.2H–J).

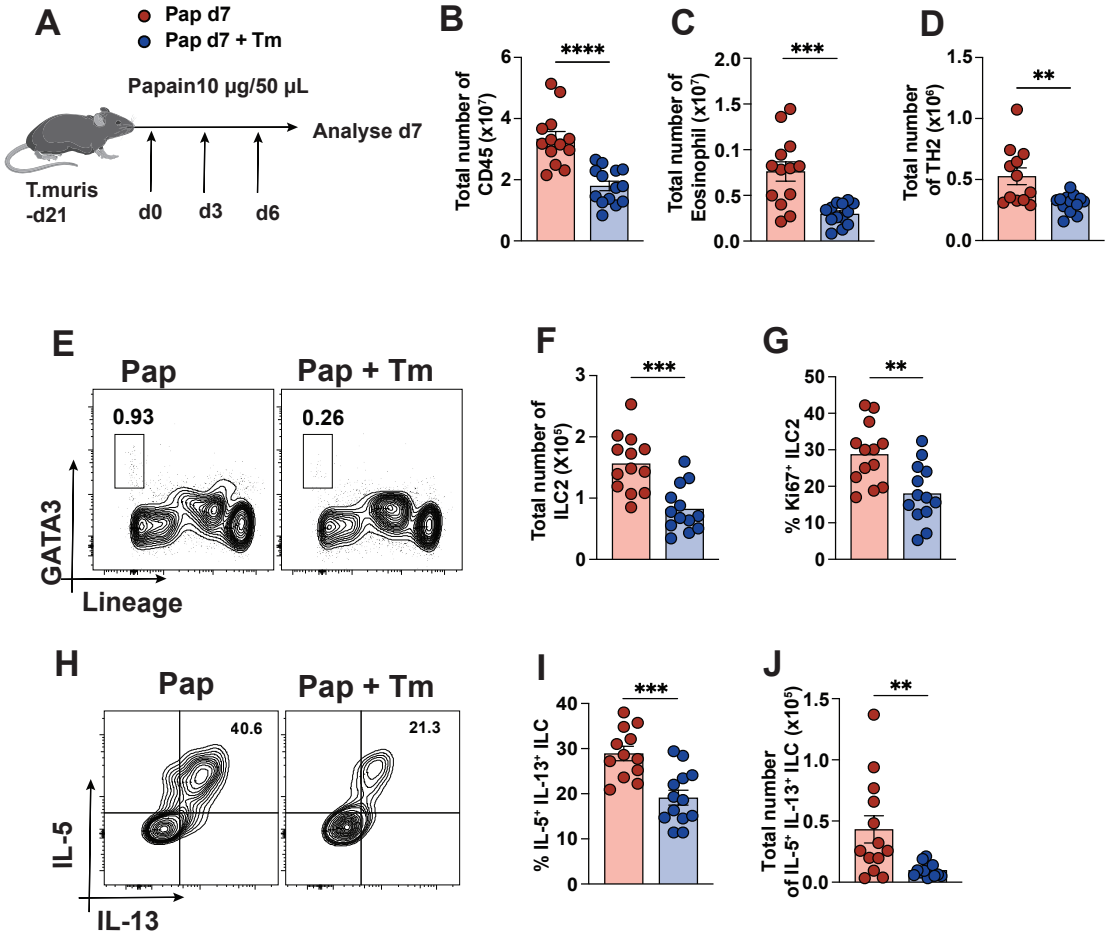

Figure 3.2: Chronic *T. muris* attenuates acute papain-induced airway inflammation. (A) Schematic of experimental design. (B-D) Total airway lymphocytes, eosinophils, and Th2 in papain and *T. muris* and papain. (E) Representative flow cytometric plot of ILC2 gated on CD45^{+} GATA3^{+} Lineage^{-} in papain and *T. muris* and papain mice. (F-G) Total ILC2 and proliferating ILC2 in papain and *T. muris* and papain mice. (H-J) IL-5^{+ve} and IL-13 $^{+ve}$ ILC percentage and total number in papain and *T. muris* and papain. Results display three independent experiments with three to five mice in each experimental group. All graphs display means ± SEM; ns (not significant) $p > 0.05$, * $p \leq 0.05$, ** $p \leq 0.01$, *** $p \leq 0.001$, **** $p \leq 0.0001$. Comparisons between two groups were analyzed by Welch's t-test.

Airway ILC2 from *T. muris*-infected mice had a slight increase in early apoptosis (Figure

3.3A–B). Initiation of apoptosis is strongly linked with inhibition of protein synthesis in a cell, and reduction in such can indicate compromised cellular homeostasis (Jeffrey et al., 2002). Puromycin incorporation is proportional to the rate of protein translation and can be used to assess translational capacity Aviner (2020), thus, we assessed puromycin uptake in ILC2 in our model. However, we observed a comparable puromycin incorporation between control and *T. muris*-infected ILC2 (Figure 3.3C–D) suggesting that the ILC2s retain active protein translation despite reduced proliferation and effector function. Furthermore, as iron uptake in ILC2 is associated with metabolic fitness and is supported by increased expression of the iron transporter CD71 upon activation Hurrell et al. (2024); Wientjens et al. (2025), we examined CD71 expression and observed a comparable increase in both control and *T. muris*-infected ILC2 relative to naive cells (Figure 3.3E).

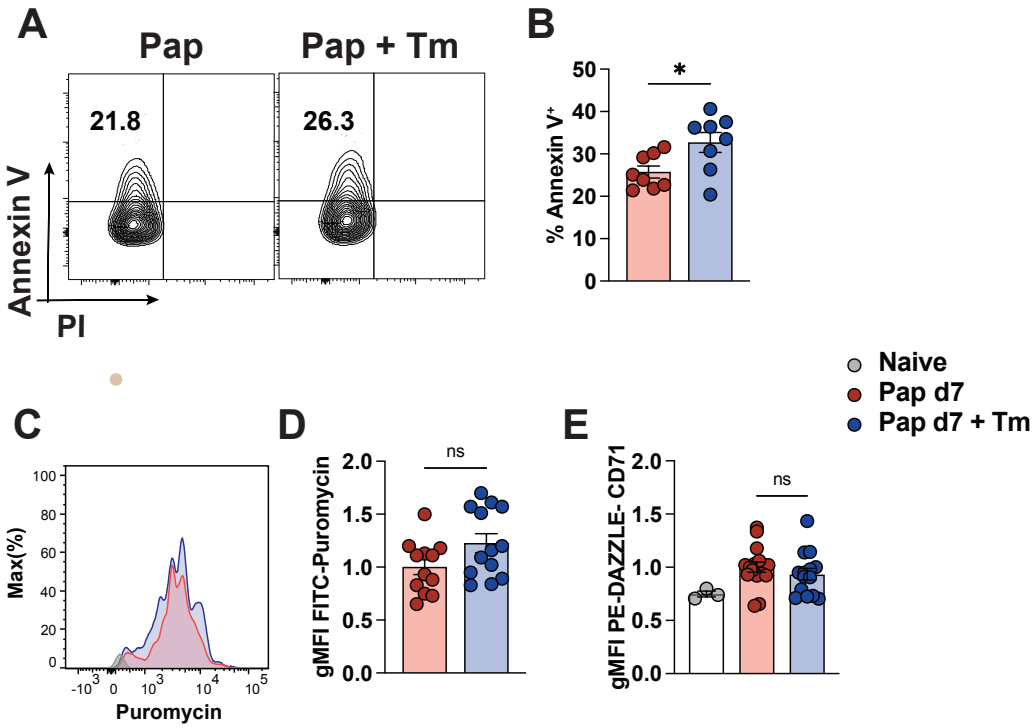

Figure 3.3: ILC2 from Chronic *T. muris* have intact translational capacity. (A) Representative flow histogram of Annexin V^+, PI $^-$ from papain only and *T. muris* and papain mice. (B) Quantitative bar plot of Annexin V^+ ILC2 $^+$ from papain only and *T. muris* and papain mice. (C) Representative histogram of puromycin signal in ILC2 from papain only and *T. muris* and papain mice. (D) gMFI values of puromycin uptake in ILC2 from papain only and *T. muris* and papain mice. (E) gMFI values of CD71 expression on ILC2 from papain only and *T. muris* and papain mice. ILC2 were gated on $CD45^+$ $CD90^+$ Lin^- $IL33R^+$ (A-B) and (E). ILC2 $CD45^+$ $CD90^+$ Lin^- $GATA3^+$ (D). Results display three independent experiments with three to five mice in each experimental group. All graphs display means ± SEM; ns (not significant) $p > 0.05$, * $p \leq 0.05$, ** $p \leq 0.01$, *** $p \leq 0.001$, **** $p \leq 0.0001$. Comparisons between two groups were analyzed by Welch's t-test.

The attenuated type 2 response in the acute model was further supported by reduced IL-5 and

IL-13 protein levels and decreased *Il5* and *Il13* mRNA expression in lung tissue (Figure 3.4A–D). In addition, IL-33 protein levels were reduced in lung homogenates (Figure 3.4H). Expression of the eosinophil-recruiting chemokine *Ccl11*, as well as extracellular matrix–associated genes including *Col3a1* (type III collagen) and *Fn1* (fibronectin), was also decreased (Figure 3.4E–G). Exploratory analyses of lung structural cell populations further supported an ameliorated tissue remodelling response in *T. muris*-infected mice. Papain exposure increased the abundance of alveolar type 2 (AT2) epithelial cells, while no changes were observed in alveolar type 1 (AT1) cells (Figure 3.5A). In contrast, this papain-induced expansion of AT2 cells was not observed in either naive or *T. muris*-infected mice (Figure 3.5A). Similarly, papain challenge increased the frequency of alveolar and peribronchial fibroblasts, whereas these populations were not expanded in *T. muris*-infected mice (Figure 3.5B). In addition, smooth muscle cells and pericytes were reduced in *T. muris*-infected mice compared to papain-only controls, alongside a non-significant reduction in adventitial fibroblasts (Figure 3.5C). Overall this suggests that chronic *T. muris* infection can shape the structural and the immune cell environment during allergic airway inflammation.

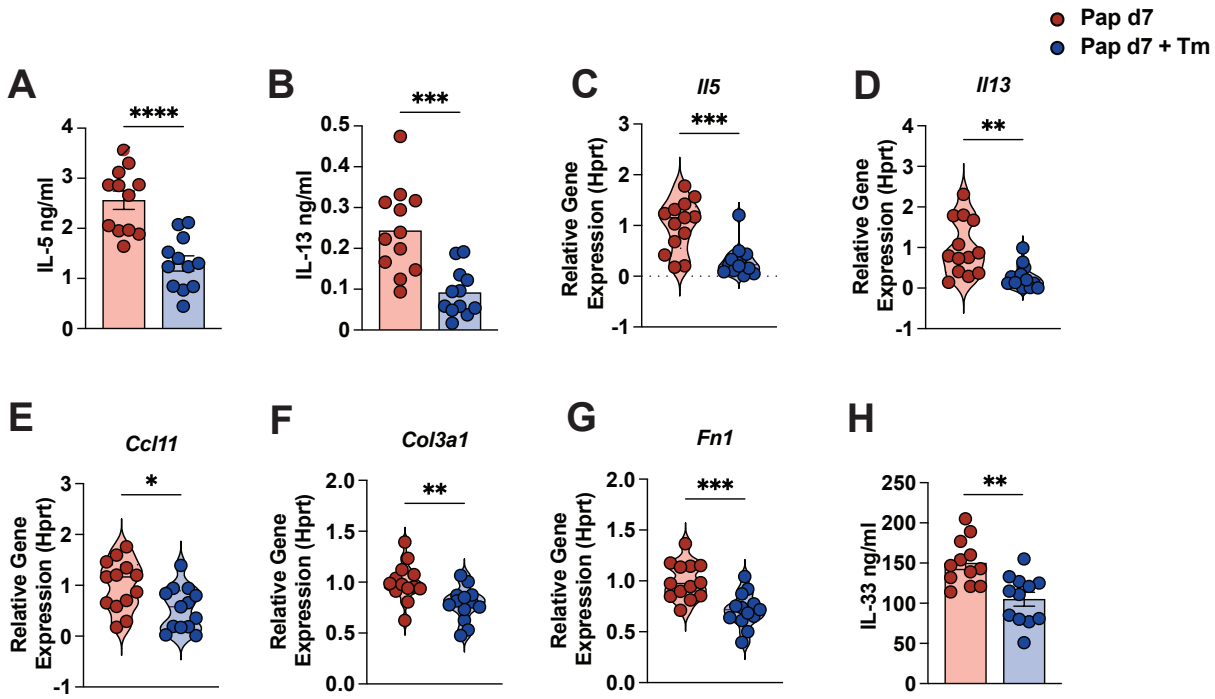

Figure 3.4: Chronic *T. muris* reduces IL-5 and IL-13 as well as fibrosis markers in the lungs of acutely challenged mice. (A-D) IL-5 and IL-13 protein in lung homogenate and gene expression of *Il5* and *Il13* lung tissue from papain only and *T. muris* and papain mice. (E-G) Gene expression of *Ccl11*, *Col3a1*, and *Fn1* in lung tissue from papain only and *T. muris* and papain mice. (H) IL-33 protein measured by LEGENDplex from papain only and *T. muris* and papain mice. Results display three independent experiments with three to five mice in each experimental group. All graphs display means ± SEM; ns (not significant) $p > 0.05$, * $p \leq 0.05$, ** $p \leq 0.01$, *** $p \leq 0.001$, **** $p \leq 0.0001$. Comparisons between two groups were analyzed by Welch's t-test.

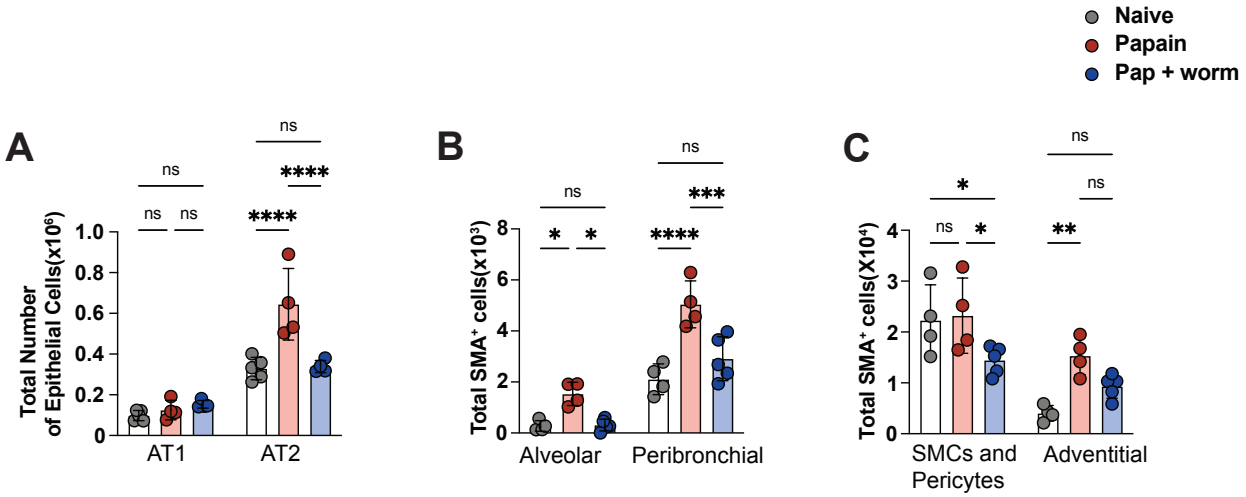

Figure 3.5: Chronic *T. muris* alters structural cell compartments during acute papain exposure. (A) Total number of AT1 and AT2 epithelial cells in papain and *T. muris* and papain mice. (B) Total alveolar and peribronchial fibroblasts in papain and *T. muris* and papain mice. (C) Total smooth muscle cells (SMC) and pericytes and adventitial fibroblasts in papain and *T. muris*-infected and papain mice. AT1 were gated on CD45$^-$ TER119$^-$ EPCAM $^+$ MCHII $^-$(A). AT2 cells were gated on CD45$^-$ TER119$^-$ EPCAM $^+$ MCHII $^+$ (A). Alveolar fibroblasts are characterised by CD45$^-$ CD31$^-$ EPCAM$^-$ TER119$^-$ MCAM$^+$ PDGFRa$^+$(B).Peribronchial fibroblasts are CD45$^-$ CD31$^-$ EPCAM$^-$ TER119$^-$ MCAM$^+$ CD9$^+$. Advential are CD45$^-$ CD31$^-$ EPCAM$^-$ TER119$^-$ MCAM$^+$ PDGFRa$^+$ Sca-1 $^+$. Alveolar, peribronchial, SMCs, and adventitial were also a-SMA$^+$. Results display one independent experiment with four mice in each experimental group. All graphs display means ± SEM; ns (not significant) $p > 0.05$, * $p \leq 0.05$, ** $p \leq 0.01$, *** $p \leq 0.001$, **** $p \leq 0.0001$. Comparisons between two groups were analyzed by Welch's t-test.

3.2 Exploring Nutrient Environment During Chronic *T. muris* Infection

Chronic *T. muris* infection has been reported to alter host nutrient availability and reshape the intestinal microbiome (Holm et al., 2015; Houlden et al., 2015), processes that influence immune responses (Kedia Mehta and Finlay, 2019). Therefore, we explored changes in nutrient availability as a method of protection during allergic airway inflammation. Given that many dietary nutrients are absorbed in the small intestine, we examined the expression of selected nutrient transporters and receptors in small intestinal tissue to assess whether chronic helminth infection was associated with altered nutrient transport capacity. Chronic *T. muris* infection was associated with increased *Tbet* expression in the small intestine (Figure 3.6A), consistent with a type 1–skewed immune environment during chronic infection. In contrast, expression of key nutrient transporters, including the vitamin D receptor (*Vdr*) and fatty acid transporters *Slc27a6* and *Slc27a4*, was unchanged in *T. muris*-infected mice compared with papain-only and naive controls (Figure 3.6B–D). Similarly, expression of most

assessed amino acid transporters was unaltered, with the exception of the glutamine transporter *Slc38a1*, which was significantly reduced in *T. muris*-infected mice (Figure 3.6E–H)

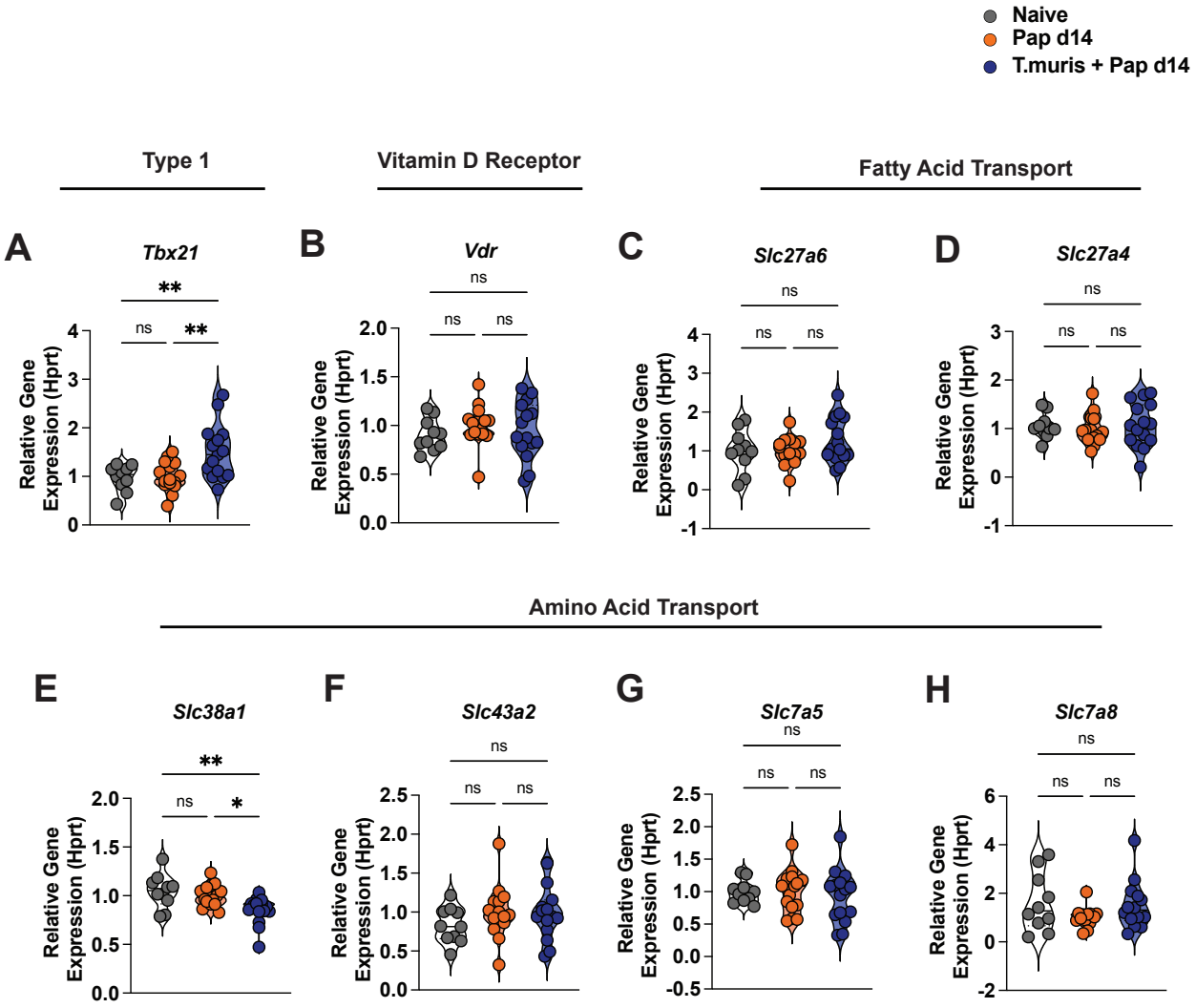

Figure 3.6: Chronic *T. muris* has minimal impact on nutrient transport in the small intestine. (A) Gene expression of *Tbx21* (Tbet) in small intestinal tissue from naive, papain-only, and *T. muris* and papain mice. (B) Vitamin D receptor gene expression *Vdr* in the smalll intestine from naive, papain-only, and *T. muris* and papain mice. (C-D) Gene expression of fatty acid transporters *Slc27a6* and *Slc27a4* in the small intestine from naive, papain-only, and *T. muris* and papain mice. (E-H) Gene expression amino acid transports *Slc38a1*,*Slc43a2*,*Slc7a5* and *Slc7a8* in the small intestine from naive, papain-only, and *T. muris* and papain mice. Results display three independent experiments with three to five mice in each experimental group. All graphs display means ± SEM; ns (not significant) $p > 0.05$, * $p \leq 0.05$, ** $p \leq 0.01$, *** $p \leq 0.001$, **** $p \leq 0.0001$. One-way ANOVA with Tukey's multiple comparisons test.

While nutrient transporter expression in the small intestine remained largely unaltered, this does not fully capture nutrient availability to the host. As adipose tissue is a central metabolic organ, changes in host nutrient availability may be reflected in the adipose tissue (Mısırlıoğlu, 2025). Indeed, beyond the suppression of allergic airway inflammation, we observed that

visceral adipose tissue (VAT) mass was consistently reduced in chronically infected mice (Figure 3.7A). Within the VAT, expression of genes involved in lipid uptake and synthesis, including *Lpl*, *Dgat1*, and *Fasn*, was significantly decreased (Figure 3.7B–D). The adipocytokine *Retn* (resistin) was also downregulated (Figure 3.7E), while expression of the insulin receptor (*Insr*) remained unchanged (Figure 3.7F). In addition, *Ifng* expression was significantly increased in the VAT of chronically infected mice compared to naive and papain-only controls (Figure 3.7G), whereas expression of *Il33* was unaltered (Figure 3.7H). Together, these data indicate that chronic *T. muris* infection is associated with reduced adipose tissue mass and a coordinated shift in metabolic gene expression within the VAT.

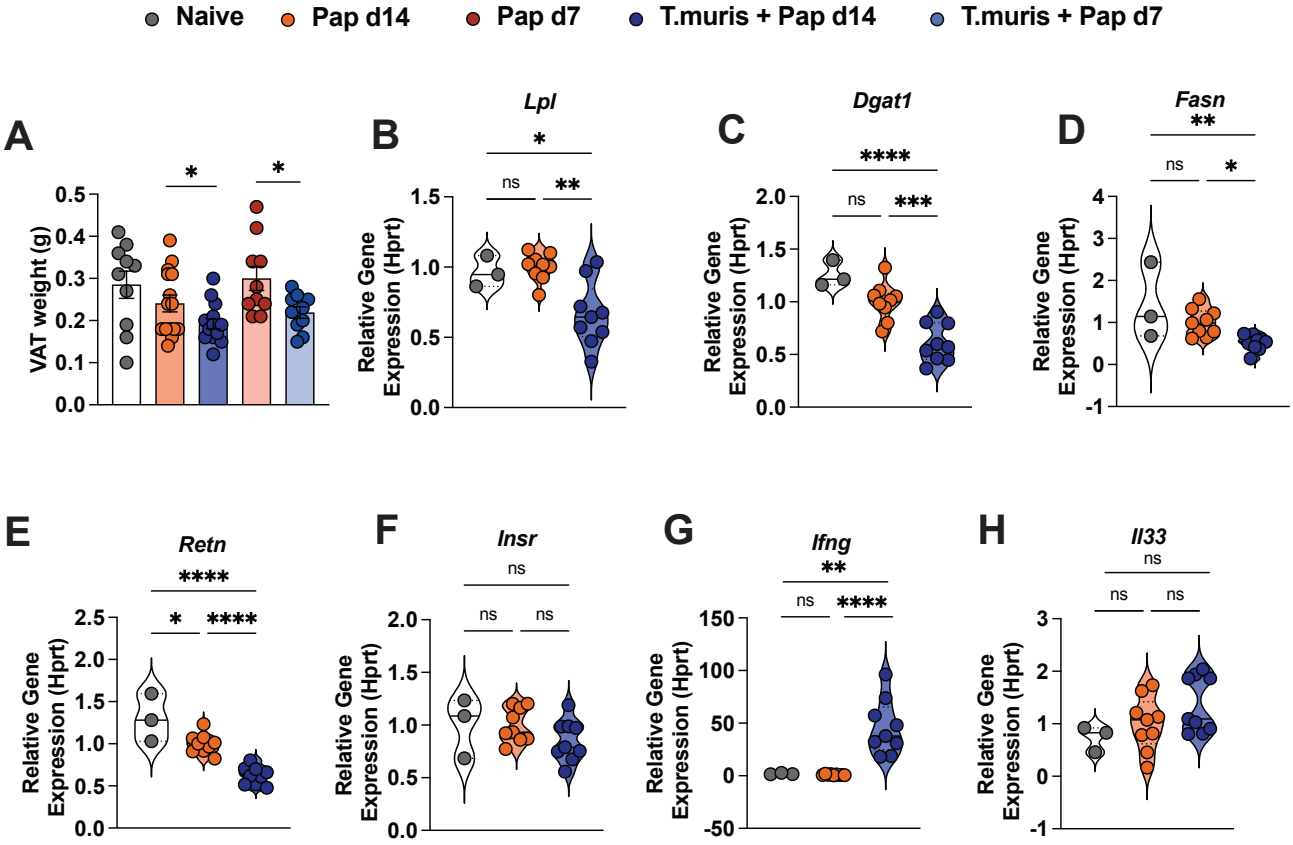

Figure 3.7: Chronic *T. muris* alters the host adipose tissue environment. (A) Visceral adipose tissue Visceral Adipose Tissue (VAT) weight in g from naive, papain-only, and *T. muris* and papain mice. (B-D) Gene expression of *Lpl*, *Dgat1*, and *Fasn* in VAT from naive, papain-only, and *T. muris* and papain mice. (E-F) Gene expression of *Retn* and *Insr* VAT from naive, papain-only, and *T. muris* and papain mice. (G-H) Gene expression of *Ifng* and *Il33* in VAT from naive, papain-only, and *T. muris* and papain mice. Results display two to three independent experiments with three to five mice in each experimental group. All graphs display means ± SEM; ns (not significant) $p > 0.05$, * $p \leq 0.05$, ** $p \leq 0.01$, *** $p \leq 0.001$, **** $p \leq 0.0001$. One-way ANOVA with Tukey's multiple comparisons test.

To assess whether systemic metabolic alterations associated with chronic helminth infection might contribute to the suppression of type 2 airway inflammation, we examined previously

generated untargeted metabolomic datasets comparing colonic and lung tissue from chronically *T. muris*-infected mice at day 14 of papain challenge. As *T. muris* resides within the cecum, chronic infection was associated with widespread alterations in the colonic metabolome, with numerous metabolites significantly increased or decreased compared to papain-only controls (Figure 3.8). In contrast, despite evidence that allergic airway inflammation can remodel the pulmonary nutrient environment, including increased lipid availability (Wientjens et al., 2025), chronic *T. muris* infection was associated with relatively few metabolite changes in the lung during papain challenge compared to papain only controls (Figure 3.8).

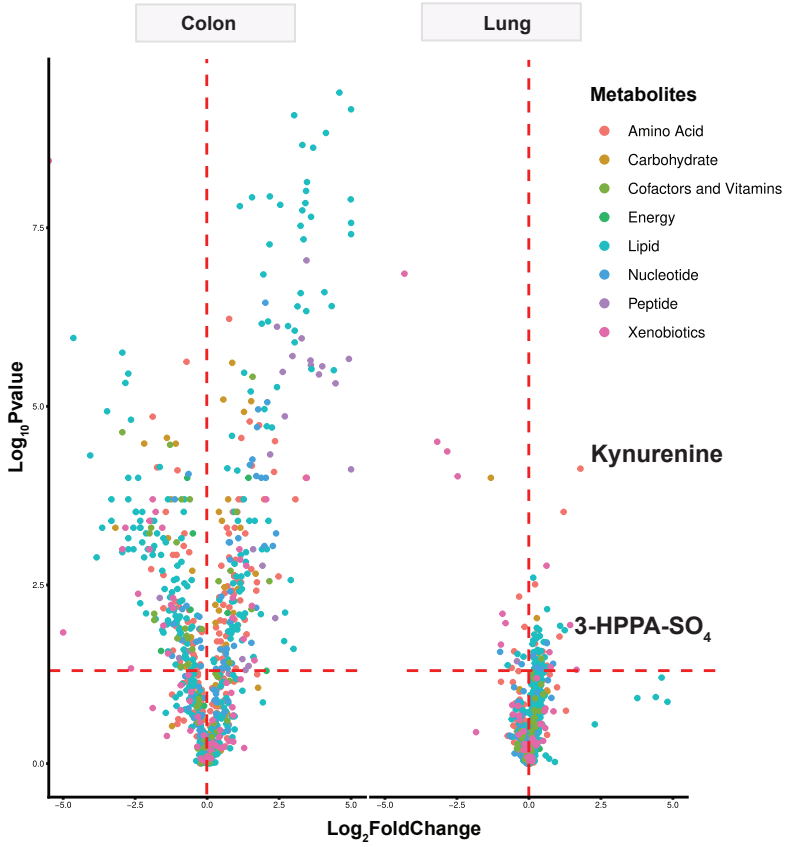

Figure 3.8: Chronic *T. muris* infection alters the colon and lung tissue nutrient environment. Volcano plots of metabolites in colon and lung tissue with $\log_{10}$Pvalue on y-axis and $\log_2$Fold Change on x-axis from chronic *T. muris* and papain compared to papain-only control.

Although metabolite changes in the lung were less extensive overall, both the colon and lung exhibited significant increases in kynurenine and related metabolites during chronic *T. muris* infection (Figure 3.9A). Consistent with elevated kynurenine levels in the lung, expression of *Ido1* was significantly upregulated in infected mice compared with naive and papain-only controls (Figure 3.9B–C). *Ido1* catalyses the conversion of tryptophan to kynurenine and is associated with type 1–skewed immune responses (Taylor and Feng, 1991; Yamamoto and Hayaishi, 1967) . Additionally, its upregulation during chronic helminth infection has been

reported previously in the colon (Bell and Else, 2011; D'Elia et al., 2009; Myhill et al., 2025). In parallel, tryptophan abundance was reduced in lung tissue, consistent with increased conversion through the kynurenine pathway. Kynurenine has been described as an endogenous ligand for the aryl hydrocarbon receptor (AhR) and has been implicated in the regulation of ILC2 responses (Li et al., 2018b). In exploratory whole lung cultures from naive mice, the addition of kynurenine during ILC2 activation was associated with reduced ILC2 numbers (Figure 3.9D), however, this effect was not investigated further. We additionally investigated the expression of the AhR target gene, *Cyp1a1*, but it was not detectable by qPCR in isolated ILC2 from either *T. muris*-infected or papain-only mice. Collectively, these findings indicate that while kynurenine levels are increased in the lung during chronic infection, the contribution of direct AhR-mediated signalling in ILC2 to the suppression of type 2 inflammation remains unclear and was not pursued further in this study.

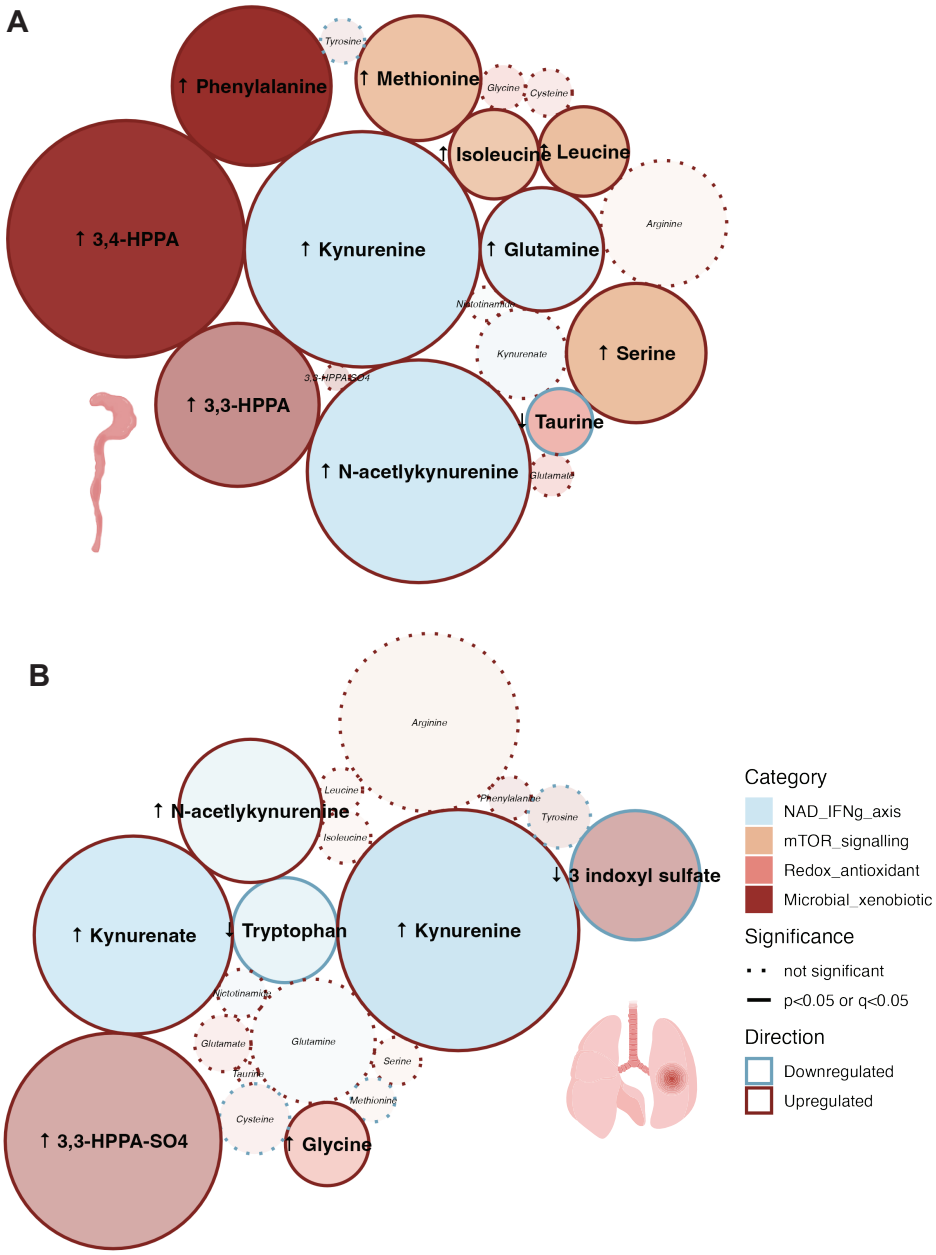

Figure 3.9: Chronic *T. muris* alters kynurenine and xenobiotic metabolites. (A-B) Circular packing plot of select metabolites in colon and lung from chronic *T. muris* and papain compared to papain-only control. Larger circles are more abundant metabolites. The darker the colour, the greater the fold change. Metabolites were selected and colour-coded based on the categories: NAD/IFNγ axis, mTOR signalling, redox pathways, and microbial or xenobiotic derived. Solid lines are significantly changed. Dotted lines are not significantly changed.

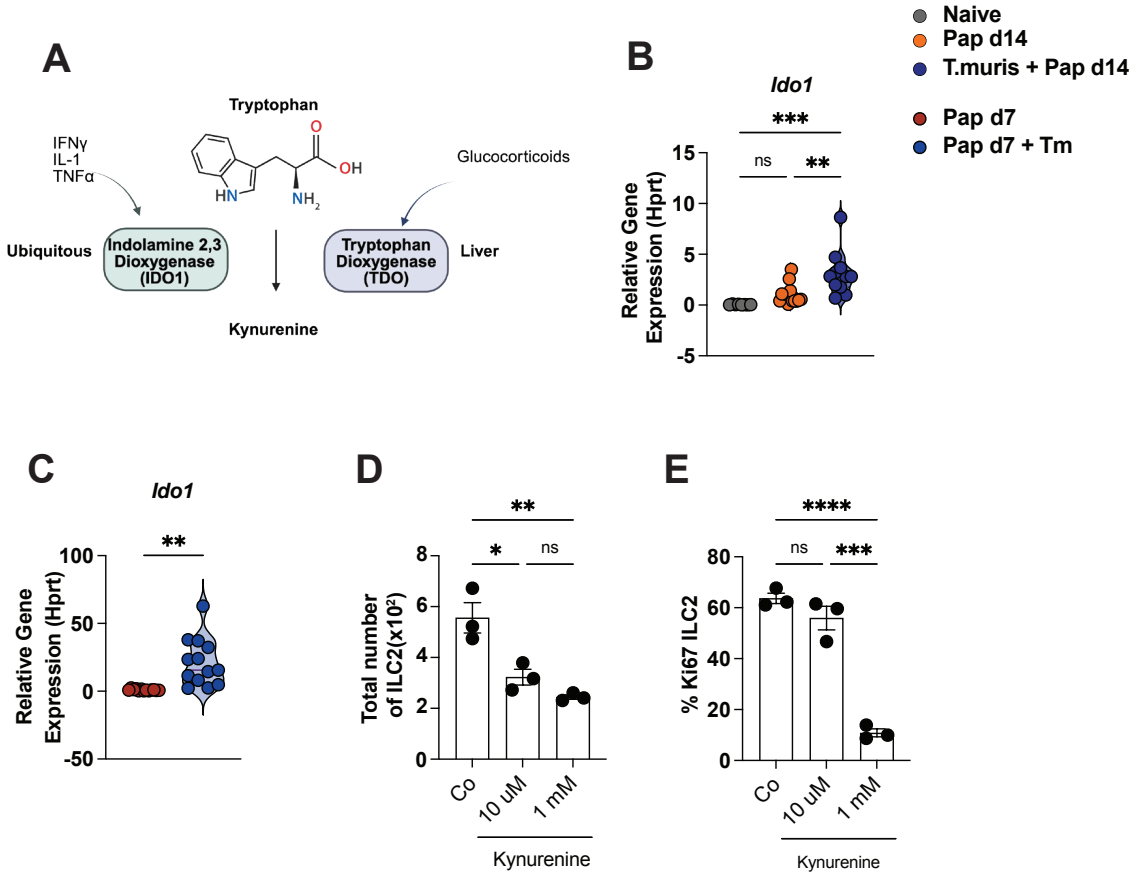

Figure 3.10: Ido1 and kynurenine increase in lung tissue of chronic *T. muris*-infected mice and may suppress ILC2. (A) Schematic demonstrating the simplified conversion of tryptophan to kynurenine via IDO1 or TDO as stimulated by external mediators. (B-C) *Ido1* gene expression in lung tissue from naive, papain-only at day 14 and day 7, and *T. muris*-infected and papain at day 14 and day 7. (D-E) Total ILC2 numbers and Ki67^{+} ILC2s from in vitro activated whole lung culture with kynurenine for 72 hours. Results display (B-C) three and (D-E) one independent experiment with three to five mice in each experimental group. All graphs display means ± SEM; ns (not significant) $p > 0.05$, * $p \leq 0.05$, ** $p \leq 0.01$, *** $p \leq 0.001$, **** $p \leq 0.0001$. One-way ANOVA with Tukey's multiple comparisons test. Comparisons between two groups were analyzed by Welch's t-test.

In addition to increased kynurenine pathway metabolites, several xenobiotic compounds were elevated during chronic *T. muris* infection, including 3-(4-hydroxyphenyl)propionic acid (3,4-HPPA) and 3-(3-hydroxyphenyl)propionic acid (3,3-HPPA) in colonic tissue, as well as 3-(3-hydroxyphenyl)propionic acid sulphate (3-HPPA SO_4) in the lung (Figure 3.9A-B). Phenolic acids have been reported to possess anti-inflammatory and antioxidant properties, including the capacity to scavenge reactive oxygen species (Chen et al., 2020). In particular, 3-HPPA has been described to exert vasodilatory effects and suppress NF-κB signalling in other experimental models (Feng et al., 2022; Najmanová et al., 2016). These observations raised the possibility that alterations in xenobiotic metabolism during chronic *T. muris* infection could contribute to immune modulation, however, the function of these metabolites

during allergic airway inflammation has not been assessed.

As 3,3-HPPA is reported to undergo hepatic sulphation to form 3-HPPA SO_4 (Pimpão et al., 2015), we next assessed whether oral administration of the precursor 3,3-HPPAcould mimic aspects of the xenobiotic metabolic environment observed during chronic infection and modulate allergic airway inflammation during papain challenge (Figure 3.11B). Oral gavage of 3,3-HPPA reduced overall lymphocyte recruitment to the lung, including eosinophils and neutrophils (Figure 3.11C-E). Th2 cell numbers were significantly reduced (Figure 3.11F), while ILC2 numbers showed only a modest, non-significant decrease (Figure 3.11G). Analysis of lung homogenates from 3,3-HPPA–treated mice revealed reduced levels of IFNγ, IL-6, IL-17, and IL-9, whereas levels of the type 2 cytokines IL-5 and IL-13, as well as IL-22, were unchanged (Figure 3.11H). In addition, no impairment in ILC2 effector function was observed (Figure 3.11I-K). Together, these data indicate that although chronic *T. muris* infection is associated with alterations in xenobiotic metabolism, administration of 3,3-HPPAalone is insufficient to suppress ILC2 function in the manner observed during chronic infection. Direct intranasal administration of 3-HPPA SO_4 was also explored, however, these experiments yielded inconsistent results and were not pursued further.

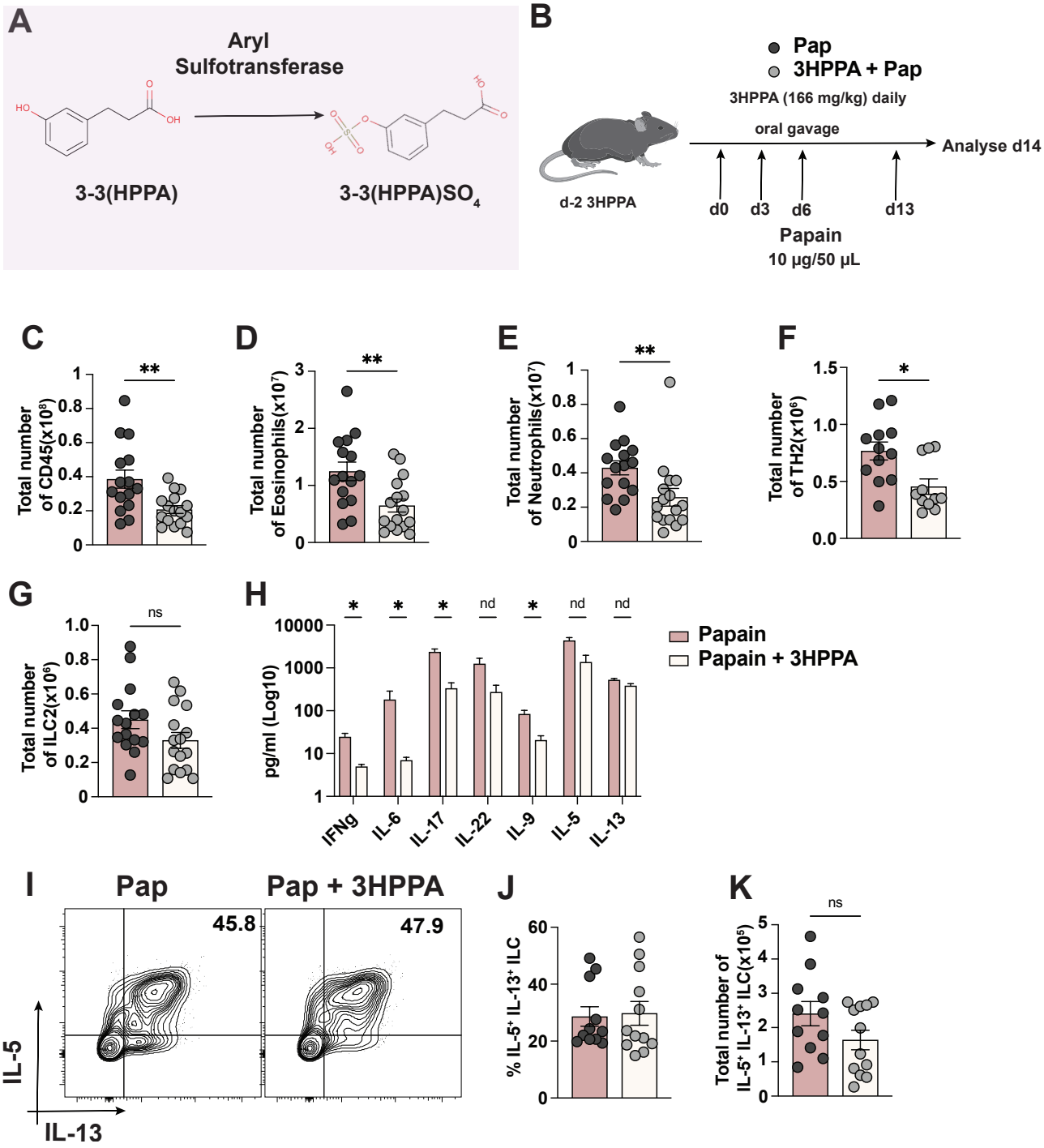

Figure 3.11: Xenobiotic 3,3-HPPA May Contribute To Dampened Airway Inflammation. (A) 3,3-HPPA is likely sulfated by aryl sulfotransferases to 3-HPPA SO_4. (B) Schematic of animal model used in these experiments. Mice received daily administration of 3,3-HPPA prior to papain. (C-E) Total lymphocytes, including eosinophils and neutrophils, in 3,3-HPPA-treated mice compared to papain-only controls. (F) Total Th2 numbers in 3,3-HPPA-treated and papain-only controls. (G) Total ILC2 numbers in 3,3-HPPA-treated and papain-only controls. (H) IFNγ, IL-6, IL-17, IL-9, IL-5, and IL-13 were measured in lung homogenate by LED-GENDplex and displayed as Log_{10}. (I) Representative flow cytometry plot of IL-5$^+$ versus IL-13$^+$ ILC2 in 3HPPA-treated and papain-only controls. (J-K) Percentage and total number of IL-5$^+$ IL-13$^+$ double positive ILC2. ILC2 were gated on CD45$^+$ CD90$^+$ Lin$^-$ GATA3$^+$. Results display three to four independent experiments with three to five mice in each experimental group. All graphs display means ± SEM; ns (not significant) $p > 0.05$, * $p \leq 0.05$, ** $p \leq 0.01$, *** $p \leq 0.001$, **** $p \leq 0.0001$. Comparisons between two groups were analyzed by Welch's t-test or multiple t-tests.

3.3 Chronic *T. muris* Infection Alters Airway ILC2 Metabolism During Allergic Airway Inflammation

While changes in nutrients in the tissue microenvironment were investigated as a mechanism of protection during airway inflammation, we could not conclude that specific metabolites in the tissue were contributing to the reduction in numbers and effector function of ILC2. Thus, we next examined changes in cellular metabolism. ILC2 proliferation and effector function are tightly linked to cellular metabolic state, and both were impaired during chronic *T. muris* infection in the papain model. In addition, ILC2 rely on distinct metabolic pathways that enable their effector function. We therefore examined metabolic features of lung ILC2 during chronic *T. muris* infection and papain. Lipid uptake, assessed using BODIPY FLC16, was reduced in ILC2 from chronically infected mice at day 14 of the papain challenge (Figure 3.12A–B). In contrast, intracellular lipid droplet accumulation, a characteristic feature of activated ILC2, was unchanged, as measured by BODIPY 493/503 staining (Figure 3.12C–D). Mitochondrial integrity is closely linked to immune cell activation, as increased energetic demand is supported through enhanced oxidative phosphorylation (Pearce and Pearce, 2013). Activated ILC2s have been reported to increase mitochondrial mass and membrane polarisation, supporting effector function (Surace et al., 2021). Given the reduced proliferation and cytokine production observed in ILC2 during chronic infection, we next assessed mitochondrial parameters. Lung ILC2 from chronically *T. muris*–infected mice exhibited reduced mitochondrial membrane potential and decreased mitochondrial mass compared to papain-only and naive controls, as measured by tetramethylrhodamine methyl ester (TMRM) and MitoTracker Green fluorescence, respectively (Figure 3.12E–H). In addition, the ratio of TMRM to MitoTracker Green fluorescence was decreased in ILC2 from *T. muris*–infected mice compared to papain-only ILC2, indicating dysfunctional mitochondria.

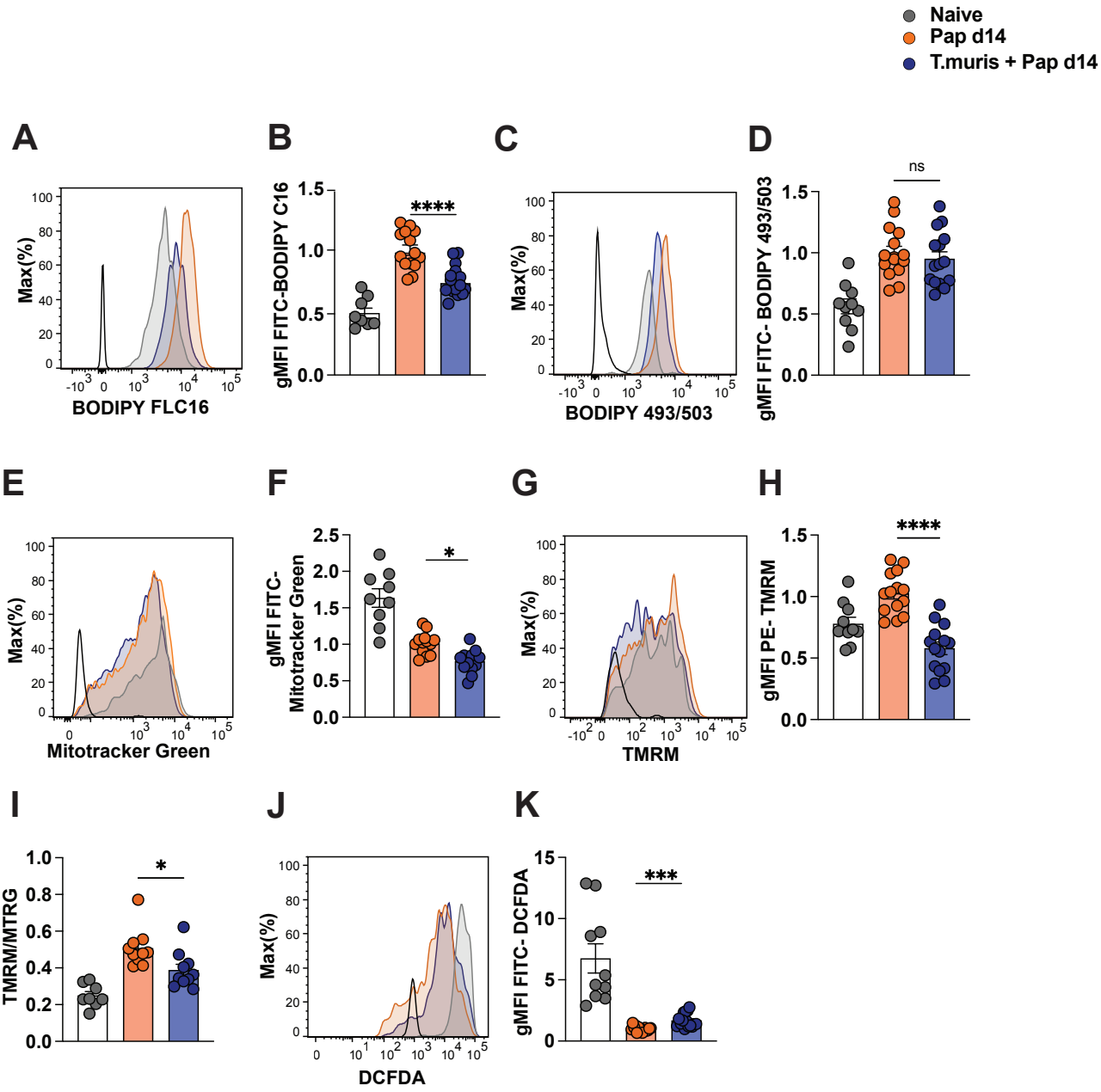

Figure 3.12: Chronic *T. muris* alters ILC2 metabolism during day 14 papain. (A-B) Histogram plot and gMFI values of BODIPY FLC16 uptake in ILC2 from naive, papain-only, and chronic *T. muris*-infected and papain mice. (C-D) Histogram plot and gMFI values of BODIPY 493/503 uptake in ILC2 from naive, papain-only, and chronic *T. muris*-infected and papain mice. (E-F) Histogram plot and gMFI values of MitoTracker Green uptake in ILC2 from naive, papain-only, and chronic *T. muris*-infected and papain mice. (G-H) Histogram plot and gMFI values of TMRM uptake in ILC2 from naive, papain-only, and chronic *T. muris*-infected and papain mice. (I) Ratio of TMRM to MitoTracker Green in ILC2 from naive, papain-only, and chronic *T. muris*-infected and papain mice. (J-K) Histogram plot and gMFI vales of DCFDA in ILC2 from naive, papain-only, and chronic *T. muris*-infected and papain mice. ILC2s were identified as $CD45^+$ Lin^- $Thy1.2^+$ $IL33R^+$ in (C-K). ILC2s were identified as $CD45^+$ Lin Lin^- $Thy1.2^+$ $GATA3^+$ in (A-B). Results display three independent experiments with three to five mice in each experimental group. All graphs display means ± SEM; ns (not significant) $p > 0.05$, * $p \leq 0.05$, ** $p \leq 0.01$, *** $p \leq 0.001$, **** $p \leq 0.0001$. One-way ANOVA with Tukey's multiple comparisons test.

Pathogenic ILC2 decrease ROS to enable their surival in allergic airway inflammation (Wientjens et al., 2025). In addition, ROS can accumulate under conditions of mitochondrial dysfunction, and general ROS were assessed using 2',7'-dichlorodihydrofluorescein diacetate (DCFDA) staining. Lung ILC2 from chronically infected mice exhibited increased intracellular ROS levels compared with papain-only controls (Figure 3.12I–J), consistent with altered redox homeostasis. As the ILC2 from *T. muris*–infected mice displayed impairments in lipid metabolism, we also investigated cellular fuel dependencies and capacities using the SCENITH™assay (Figure 3.13A). However, airway ILC2 from *T. muris*-infected mice and papain maintained displayed similar fuel dependencies despite altered lipid metabolism (Figure 3.13B-E).

Although reduced type 2 inflammation and metabolic alterations in ILC2 were evident in the day 14 papain model, the magnitude of protection varied between experiments for reasons that remain unclear. Given the improved reproducibility and more robust inflammatory readouts, subsequent mechanistic and metabolic analyses were therefore performed using the acute papain model (pap day 7), unless otherwise stated.

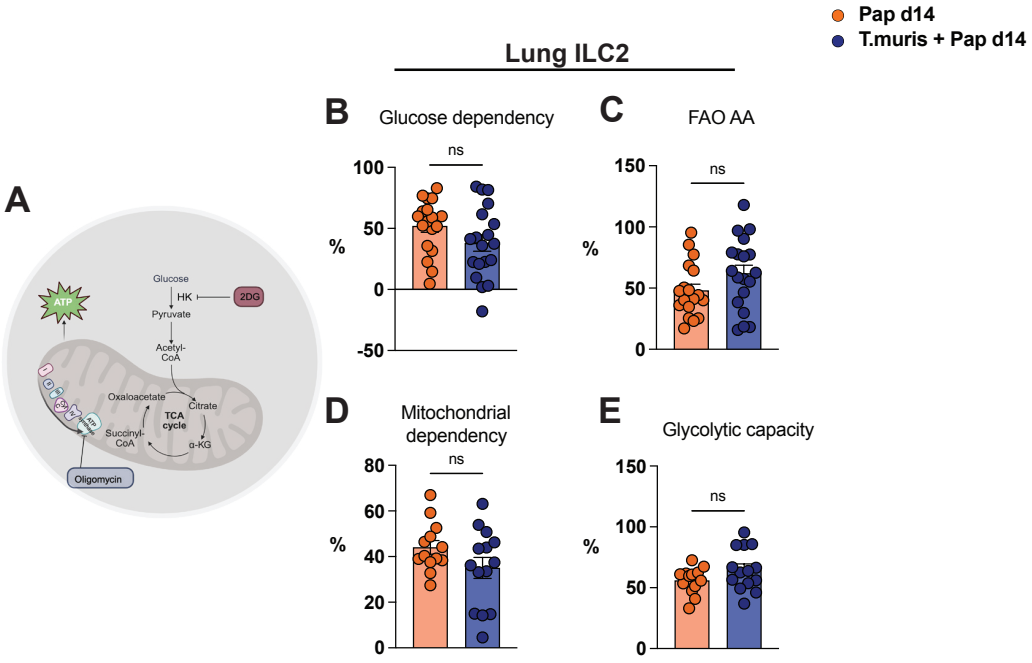

Figure 3.13: Chronic *T. muris* does not impact ILC2 fuel dependencies during day 14 papain. (A) Schematic of metabolic pathway targeted by 2-deoxyglucose (2-DG) (glucose dependency and FAO AA capacity) and oligomycin (mitochondrial dependency and glycolytic capacity). (B-E) Metabolic dependencies and capacities in ILC2 from papain only and chronic *T. muris* and papain mice. ILC2s were identified as $CD45^+$ Lin Lin^- $Thy1.2^+$ $GATA3^+$ in (B-E). Results display three independent experiments with three to five mice in each experimental group. All graphs display means ± SEM; ns (not significant) $p > 0.05$, * $p \leq 0.05$, ** $p \leq 0.01$, *** $p \leq 0.001$, **** $p \leq 0.0001$. Comparisons between two groups were analyzed by Welch's t-test.

To determine whether lung ILC2s in the acute day 7 model exhibit metabolic alterations similar to those observed at day 14, we next assessed lipid metabolism. ILC2s from *T. muris*–infected mice displayed reduced lipid uptake and decreased lipid droplet accumulation at day 7 compared with papain-only controls, consistent with findings from the chronic model (Figure 3.14A–D). At the transcriptional level, expression of genes associated with lipid uptake and storage, including *Pparg* and *Dgat1*, were unchanged in isolated ILC2s from infected mice (Figure 3.14E–F). In contrast, expression of *Pnpla2* (*Atgl*), a key mediator of triglyceride breakdown, was significantly upregulated (Figure 3.14G) (Colaço Gaspar et al., 2024). Together, these findings suggest that despite preserved transcriptional programs associated with lipid handling, ILC2s from *T. muris*–infected mice engage lipid catabolic pathways, consistent with a metabolically altered state.

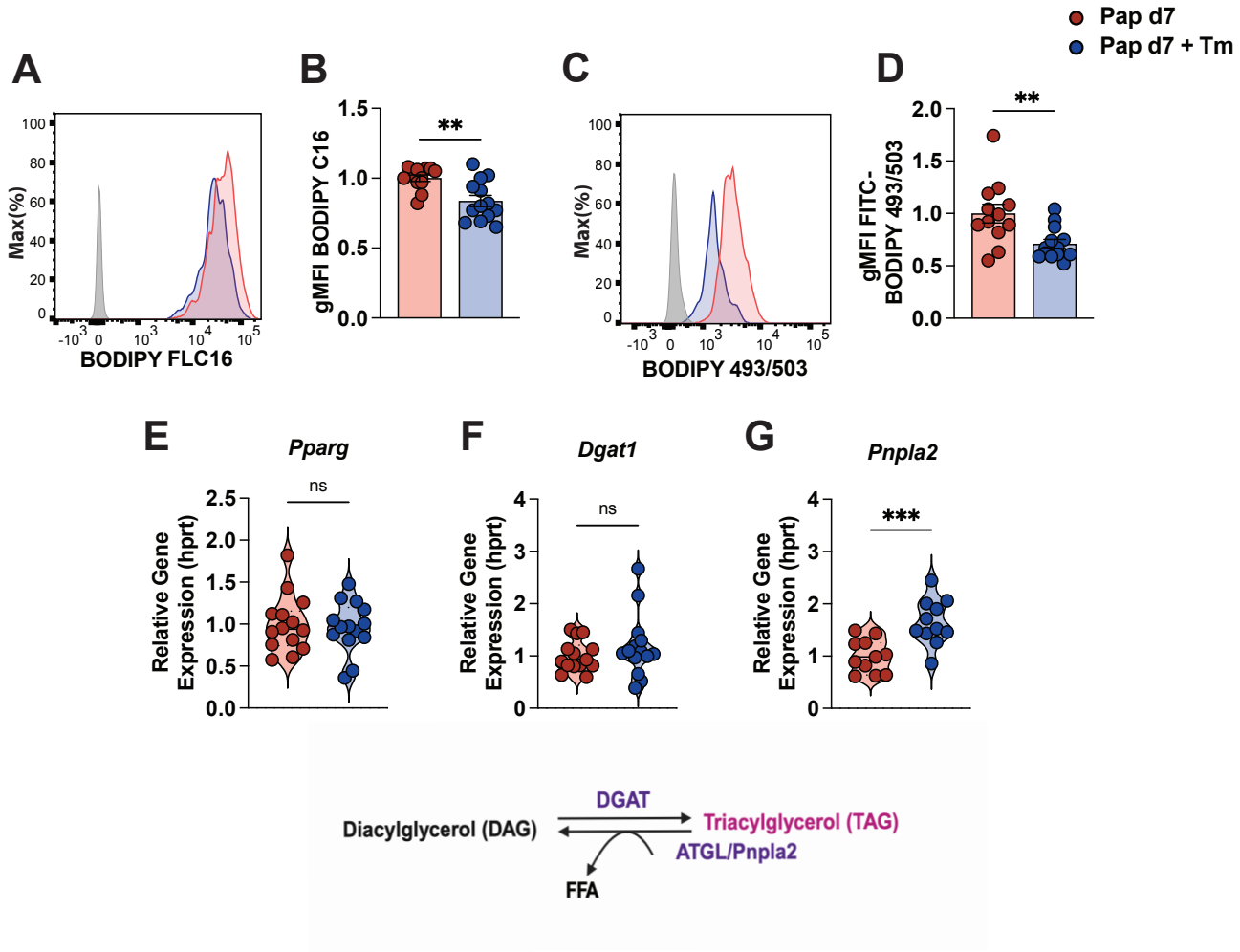

Figure 3.14: Chronic *T. muris* induces altered lipid metabolism in ILC2 during acute papain. (A-B) Histogram and gMFI values of BODIPY FLC16 uptake in ILC2 from papain-only and *T. muris*-infected and papain mice. (C-D) Histogram plot and gMFI values of BODIPY 493/503 uptake in ILC2 from papain-only and *T. muris* and papain. (E-F) Gene expression of *Pparg* and *DGAT1* in isolated ILC2 from papain-only and *T. muris*-infected and papain mice. (G) Gene expression of *Pnpla2* in isolated ILC2 from papain-only and chronic *T. muris*-infected and papain mice. ILC2s were identified as $CD45^+$ Lin^- $Thy1.2^+$ $IL33R^+$ in (E-G). ILC2s were identified as $CD45^+$ Lin Lin^- $Thy1.2^+$ $GATA3^+$ in (A-D). Results display three independent experiments with three to five mice in each experimental group. All graphs display means ± SEM; ns (not significant) $p > 0.05$, * $p \leq 0.05$, ** $p \leq 0.01$, *** $p \leq 0.001$, **** $p \leq 0.0001$. Comparisons between two groups were analyzed by Welch's t-test.

Helminth infection has been reported to influence host nutrient availability, including glucose, which is required for ILC2 proliferation and activation. Additionally, glucose uptake in ILC2 has been implicated in the regulation of lipid metabolism during allergic airway inflammation (Karagiannis et al., 2020). Although glucose-related metabolites were not altered in the metabolomic analysis, we directly assessed glucose levels in lung homogenates during papain challenge. Lung glucose concentrations were modestly reduced in *T. muris*–infected mice compared with papain-only controls (Figure 3.15A). Despite this reduction, expression

of the glucose transporter Glut1 or *Slc2a1* was comparable between *T. muris*–infected and papain-only groups at both the tissue level and in isolated ILC2 (Figure 3.15B–C). In addition, expression of *Arg1*, which has been linked to the regulation of glycolysis in activated ILC2, remained unchanged in ILC2 from infected mice (Figure 3.15D–E). Consistent with preserved glucose handling, Seahorse analysis revealed similar extracellular acidification rates (ECAR) between groups, indicating intact glycolytic capacity in lung ILC2 (Figure 3.15F). Together, these data indicate that although lipid metabolism is altered in ILC2 during chronic *T. muris* infection, glucose uptake and glycolytic capacity remain largely preserved.

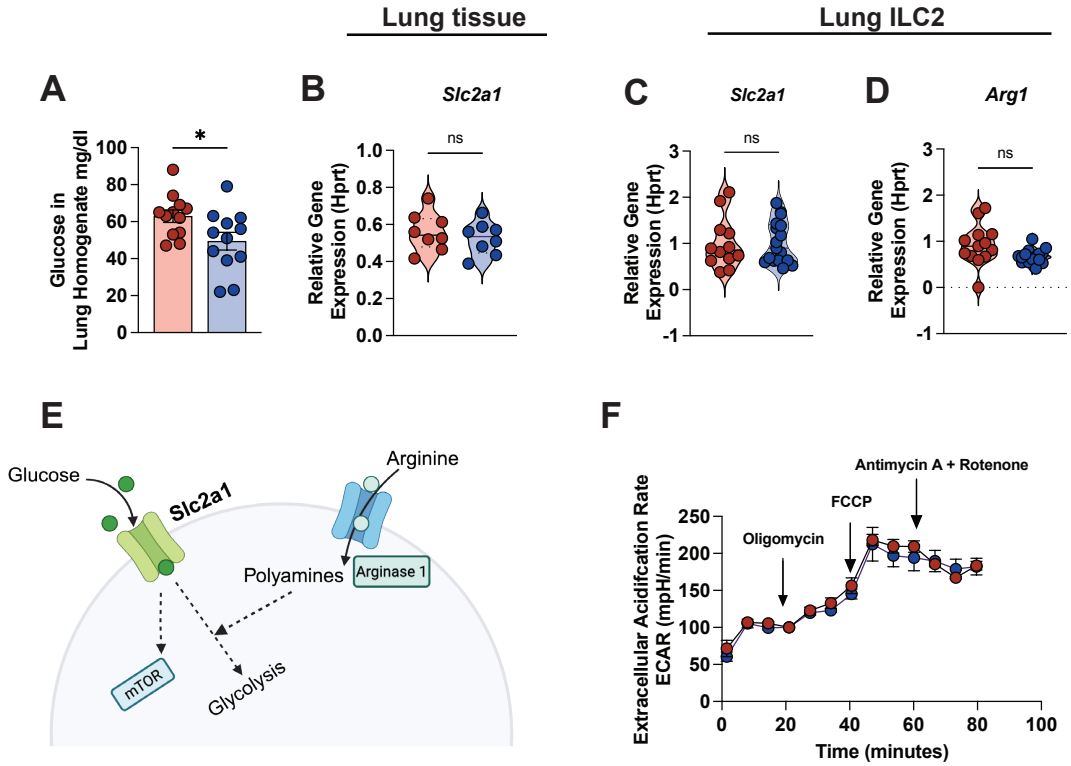

Figure 3.15: Glucose availability is reduced in the lung, but glycolysis is unaltered in chronic *T. muris* infection and acute papain. (A) Glucose measured in the lung homogenate of papain-only and *T. muris*-infected mice and papain. (B) Gene expression of *Glut1*/*Slc2a1* in lung tissue from papain and chronic *T. muris* and papain. (C) Gene expression of Glut1/*Slc2a1* mRNA in isolated ILC2 from papain-only and *T. muris*-infected mice and papain. (D) Gene expression of *Arg1* in isolated ILC2 from papain and *T. muris* and papain. (E) Schematic of glucose and arginine uptake to support glycolysis in ILC2. (F) ECAR was measured under basal conditions and in response to indicated drugs based on the Seahorse XF Mito Stress Test in isolated ILC2 from papain and *T. muris* and papain. ILC2s were identified as $CD45^+$ Lin^- $Thy1.2^+$ $IL33R^+$ in (B-D) and (F). Results display three independent experiments with three to five mice in each experimental group. All graphs display means ± SEM; ns (not significant) $p > 0.05$, * $p \leq 0.05$, ** $p \leq 0.01$, *** $p \leq 0.001$, **** $p \leq 0.0001$. Comparisons between two groups were analyzed by Welch's t-test.

As lung ILC2 from chronically infected mice exhibited reduced mitochondrial membrane potential in the day 14 papain model as well as altered redox balancing, we next assessed

these parameter during acute papain challenge. Lung ILC2 from *T. muris*–infected mice similarly displayed reduced mitochondrial membrane potential following acute papain exposure compared with papain-only controls (Figure 3.16A & C). In contrast to the day 14 model, mitochondrial mass was comparable between *T. muris*–infected and papain-only mice at day 7, as measured by MitoTracker Green fluorescence (Figure 3.16B & D). In addition, the ratio of TMRM to MitoTracker Green fluorescence was reduced, although not significantly (Figure 3.16E). This suggests subtle mitochondrial dysfunction rather than mitochondrial loss in the day 7 papain model. Seahorse analysis revealed a similar basal oxygen consumption rate (OCR) under steady-state conditions (Figure 3.16F). Following oligomycin addition (blocking ATP synthase), there was a bigger drop in OCR in ILC2 from *T. muris*–infected and papain mice compared to papain only, while maximal OCR after FCCP is similar. Thus, while ILC2 may rely more on ATP-synthase respiration, they did not compensate by increasing ECAR more than the ECAR of papain only, which may suggest the ILC2 are more metabolically inflexible under certain assay conditions. However, a full interpretation is limited, as OCR after rotenone/antimycin A remained high, suggesting incomplete mitochondrial inhibition.

Changes in membrane potential often coincide with increased mitochondrial ROS, therefore, we measured superoxide using MitoSOX Green (Park et al., 2023). Mitochondrial ROS levels were unchanged in ILC2s from infected mice compared to papain-only (Figure 3.16G & H). Although mitochondrial superoxide ROS was unaltered, total cellular ROS measured by DCFDA was elevated in ILC2s from infected mice compared to papain only, as was observed at day 14 (Figure 3.16 I-J). Additionally, an increased ROS environment could lead to enhanced peroxidation of lipids. To assess whether lipid peroxidation contributed to this signal, lipid ROS levels were measured and found to be unchanged (Figure 3.16K). Together, these findings indicate that ILC2 from *T. muris*–infected mice exhibit mild mitochondrial dysfunction accompanied by increased cytosolic redox stress during both acute (day 7) and chronic (day 14) papain challenge, which may contribute to impaired ILC2 function during allergic airway inflammation.

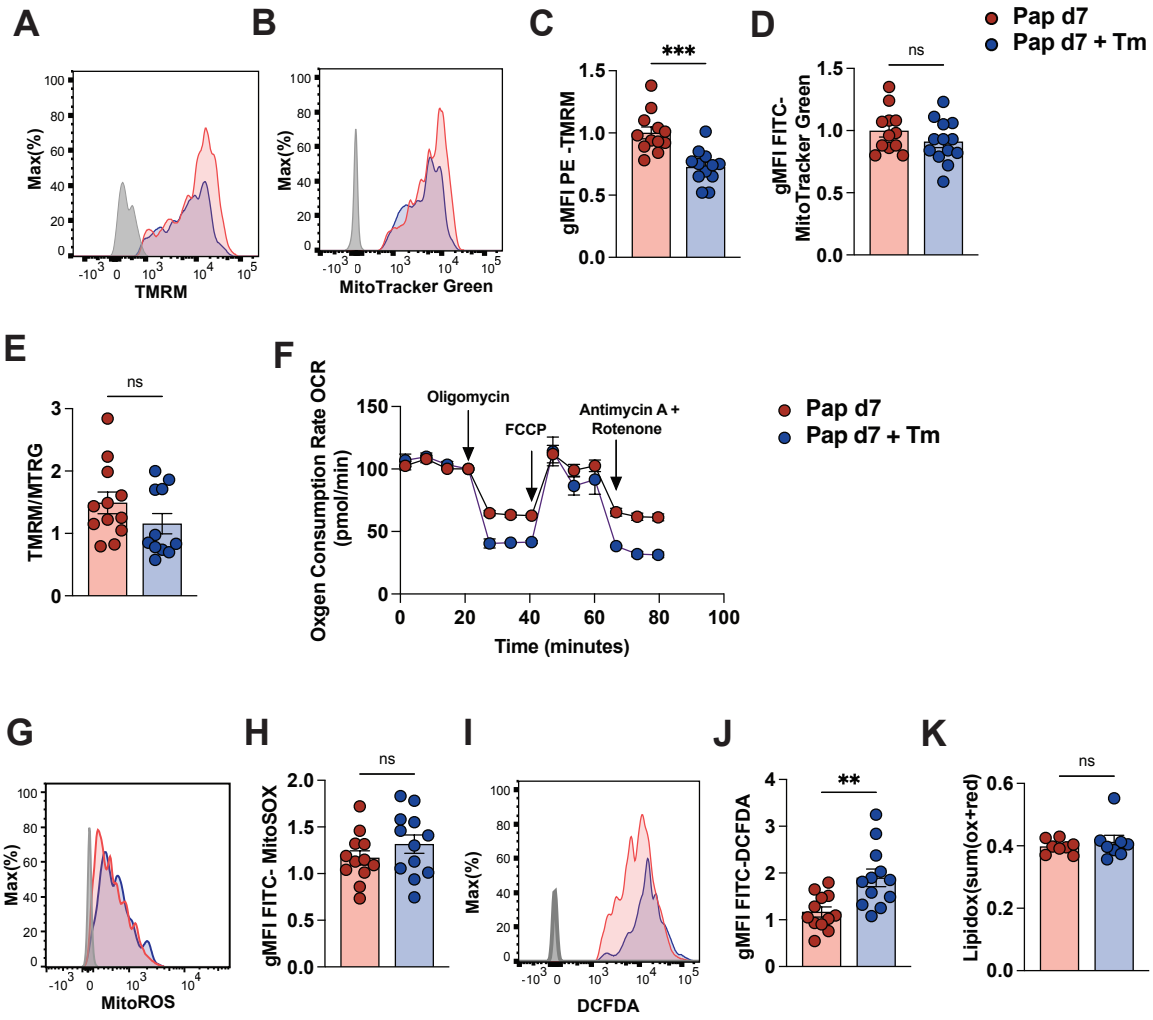

Figure 3.16: Chronic *T. muris* alters redox balancing and mitochondria in ILC2 during acute papain. (A-B) Representative Histograms of TMRM and MitoTracker Green from papain only and *T. muris* and papain. (C-D) gMFI values of TMRM and MitoTracker Green in ILC2 from papain only and *T. muris* and papain. (E) Ratio of TMRM to MitoTracker Green in ILC2. (F) OCR of isolated ILC2 as measured using Seahorse Mito stress test in response to indicated drugs. (G-H) Representative histogram and gMFI values of of MitoSOX Green in ILC2 from papain only and chronic *T. muris* and papain. (I-J) Representative flow cytometry histogram and gMFI values of DCFDA expression in ILC2 from papain only and *T. muris* and papain. (K) gMFI values of lipid peroxidation using BODIPY C11 dye in ILC2 from papain only and *T. muris* and papain. ILC2s were identified as $CD45^+$ Lin^- $Thy1.2^+$ $IL33R^+$ in (A-J). ILC2s were identified as $CD45^+$ Lin^- $Thy1.2^+$ $GATA3^+$ in (K). Results display three independent experiments with three to five mice in each experimental group. All graphs display means ± SEM; ns (not significant) $p > 0.05$, * $p \leq 0.05$, ** $p \leq 0.01$, *** $p \leq 0.001$, **** $p \leq 0.0001$. Comparisons between two groups were analyzed by Welch's t-test.

Elevated cellular ROS can arise from multiple sources, including altered redox buffering capacity. Amino acid signalling can support antioxidant defense as well as mTOR signalling which regulates energy metabolism in a cell (Bar-Peled and Sabatini, 2014; Egbujor et al., 2024). We therefore investigated amino acid transport in ILC2 during chronic *T. muris* in-

fection and papain. The amino acid transporters LAT1 and LAT2, encoded by *Slc7a5* and *Slc7a8*, respectively, play key roles in amino acid import in activated ILC2 (Hodge et al., 2023; Panda et al., 2022). ILC2 isolated from *T. muris*–infected and papain-challenged mice exhibited a modest increase in *Slc7a8* expression compared with papain-only controls, while expression of *Slc7a5* remained unchanged (Figure 3.17A–B). Expression of CD98, the heterodimeric partner of LAT1, was also unchanged (Figure 3.17D). To assess amino acid uptake directly, kynurenine, a fluorescent substrate of LAT1 and LAT2, was used as a functional proxy. ILC2 from *T. muris*–infected mice displayed a modest reduction in kynurenine uptake compared with papain-only controls (Figure 3.17C), indicating a mild impairment in amino acid transport despite preserved transporter expression. Recent work has highlighted a role for cystine uptake in supporting redox balance in pathogenic ILC2 (Wientjens et al., 2025). However, intracellular cystine levels were comparable between ILC2 from *T. muris*–infected and papain-only mice (Figure 3.17E). In contrast, expression of *Slc1a5*, a transporter implicated in pathogenic ILC2 function and known to preferentially transport glutamine (Wientjens et al., 2025), was significantly reduced in ILC2 from *T. muris*–infected mice compared with papain-only controls (Figure 3.17F). Consistent with this, uptake of the bioorthogonally reactive amino acid azidohomoalanine (AHA), which is transported via *Slc1a5*, was reduced in ILC2 from infected mice (Figure 3.17H) (Pelgrom et al., 2023). While glutamine is not the rate-limiting substrate for glutathione GSH synthesis, it contributes to GSH production by serving as a precursor for glutamate (Sappington et al., 2016). The amino acid transporter *Slc1a5* is also linked to cysteine availability, and cysteine is a rate-limiting substrate required for GSH synthesis (Scalise et al., 2018). Overall, these findings indicate a modest impairment in amino acid uptake in ILC2 during chronic *T. muris* infection and allergic airway inflammation. Additionally, impaired availability of amino acid substrates necessary for antioxidant production may contribute to the altered redox balance observed.

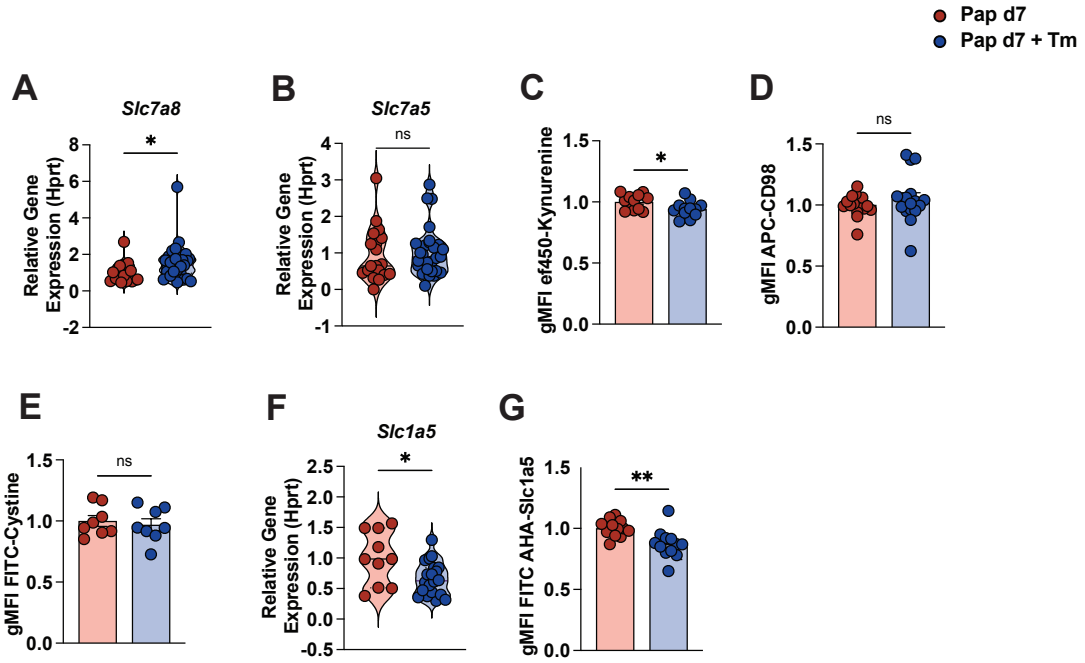

Figure 3.17: Chronic *T. muris* alters amino acid signalling in ILC2 during acute papain. (A-B) Gene expression of *Slc7a8* and *Slc7a5* in isolated ILC2 from papain only and *T. muris* and papain. (C) gMFI values of kynurenine uptake in ILC2 from papain only and *T. muris* and papain. (D) gMFI of values of CD98 expression on ILC2 from papain only and *T. muris* and papain. (E) gMFI values of cystine uptake on ILC2 from papain only and *T. muris* and papain. (F) Gene expression of *Slc1a5* in isolated ILC2 from papain and *T. muris* and papain. (H) gMFI values of bioorthogonal amino acid AHA uptake in ILC2 from papain only and *T. muris* and papain. ILC2s were identified as $CD45^+$ Lin^- $Thy1.2^+$ $IL33R^+$ in (A-F). Results display three independent experiments with three to five mice in each experimental group. All graphs display means ± SEM; ns (not significant) $p > 0.05$, * $p \leq 0.05$, ** $p \leq 0.01$, *** $p \leq 0.001$, **** $p \leq 0.0001$. Comparisons between two groups were analyzed by Welch's t-test.

As cellular energy metabolism and redox homeostasis rely on the cofactors NAD^+/NADH and $NADP^+$/NADPH, we next assessed these ratios in isolated lung ILC2 from *T. muris*–infected and papain-challenged mice compared with papain-only controls. ILC2 from *T. muris*–infected mice exhibited a significantly reduced NAD^+/NADH ratio, which reflects a relative depletion of the oxidised NAD^+ pool (Figure 3.18A). A similar, though non-significant, reduction in the $NADP^+$/NADPH ratio was also observed (Figure 3.18B). In parallel, expression of *Nampt*, a key enzyme in the NAD^+ salvage pathway, was consistently increased in ILC2 from *T. muris*–infected mice compared with papain-only controls (Figure 3.18C). While *Ido1* expression was elevated in whole lung tissue during chronic infection, it was also significantly increased in isolated ILC2 from *T. muris*–infected mice (Figure 3.18D). Increased *Nampt* expression may reflect an increased reliance on the NAD^+ salvage pathway to maintain cellular NAD^+ under metabolic and redox stress during *T. muris* infection and allergic asthma. Additionally, the induction of *Ido1* may reflect exposure to a type 1 inflammatory environment and

may further contribute to functional suppression through tryptophan catabolism and kynurenine production. Additionally, there is evidence that *Ido1* can limit lipid peroxidation and protect cells from ferroptotic stress, providing the possibility that its upregulation in ILC2 may be a consequence of increased cellular ROS (Tian et al., 2025). Together, these findings suggest that ILC2 from chronically infected mice experience altered NAD^+ homeostasis and engage compensatory metabolic programmes.

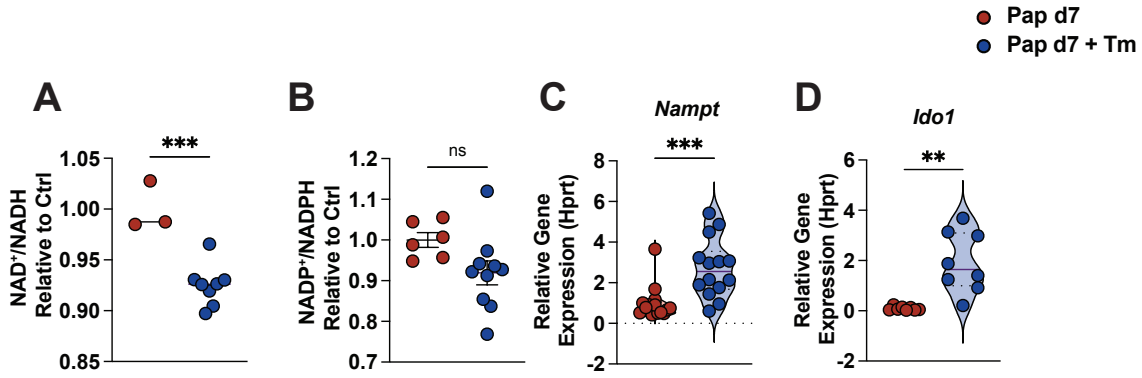

Figure 3.18: Chronic *T. muris* induces NAD salvage pathway in ILC2 during acute papain. (A-B) Normalised values of NAD^+/NADH and $NADP^+$/NADPH ratio in isolated ILC2 from papain only and chronic *T. muris* and papain. (C-D) Gene expression of *Nampt* and *Ido1* in isolated ILC2 from papain only and *T. muris* and papain. ILC2s were identified as $CD45^+$ Lin^- $Thy1.2^+$ $IL33R^+$ in (A-D). Results display two to three independent experiments with three to five mice in each experimental group. All graphs display means ± SEM; ns (not significant) $p > 0.05$, * $p \leq 0.05$, ** $p \leq 0.01$, *** $p \leq 0.001$, **** $p \leq 0.0001$. Comparisons between two groups were analyzed by Welch's t-test.

3.4 Chronic *T. muris* Infection Preferentially Alters Th2 Rather Than ILC2 Responses in a Chronic House Dust Mite Model

To determine whether the cellular metabolic alterations observed in ILC2 during chronic *T. muris* infection and acute papain were specific to ILC2 or extended to adaptive type 2 immunity, we employed a chronic HDM model, which is more strongly driven by Th2 cells. Mice were infected with *T. muris* and subsequently exposed to repeated HDM challenges as outlined in (Figure 3.19A). As observed in the papain model, total lymphocytes, including eosinophils, were decreased in the airways of infected mice (Figure 3.19B-C). Despite the reduction in eosinophils, total ILC2 numbers were unchanged. However, total Th2 cells were significantly reduced in infected mice compared to HDM-only controls (Figure 3.19E). While the percentage of IL-5 and IL-13 producing $CD4^+$ T cells was unchanged, the total number was reduced (Figure 3.19F-I). In contrast to the ILC2 in the acute papain models, lipid uptake and lipid droplet formation were unchanged in Th2 of infected mice suggesting alterations in lipid metabolism may be less prominent in Th2 cells in this model (Figure 3.19J-K). However,

cellular ROS was also increased and mitochondrial membrane potential was decreased in Th2 of infected mice (Figure 3.19L-M). In addition, amino acid uptake using kynurenine fluorescence was modestly decreased in infected mice (Figure 3.19N). Collectively, this data suggests similarities in Th2 and ILC2 susceptibility to increased ROS, mitochondrial dysfunction, and changes in amino acid uptake during *T. muris* infection. However, unlike ILC2, Th2 cells experienced fewer alterations in lipid metabolism.

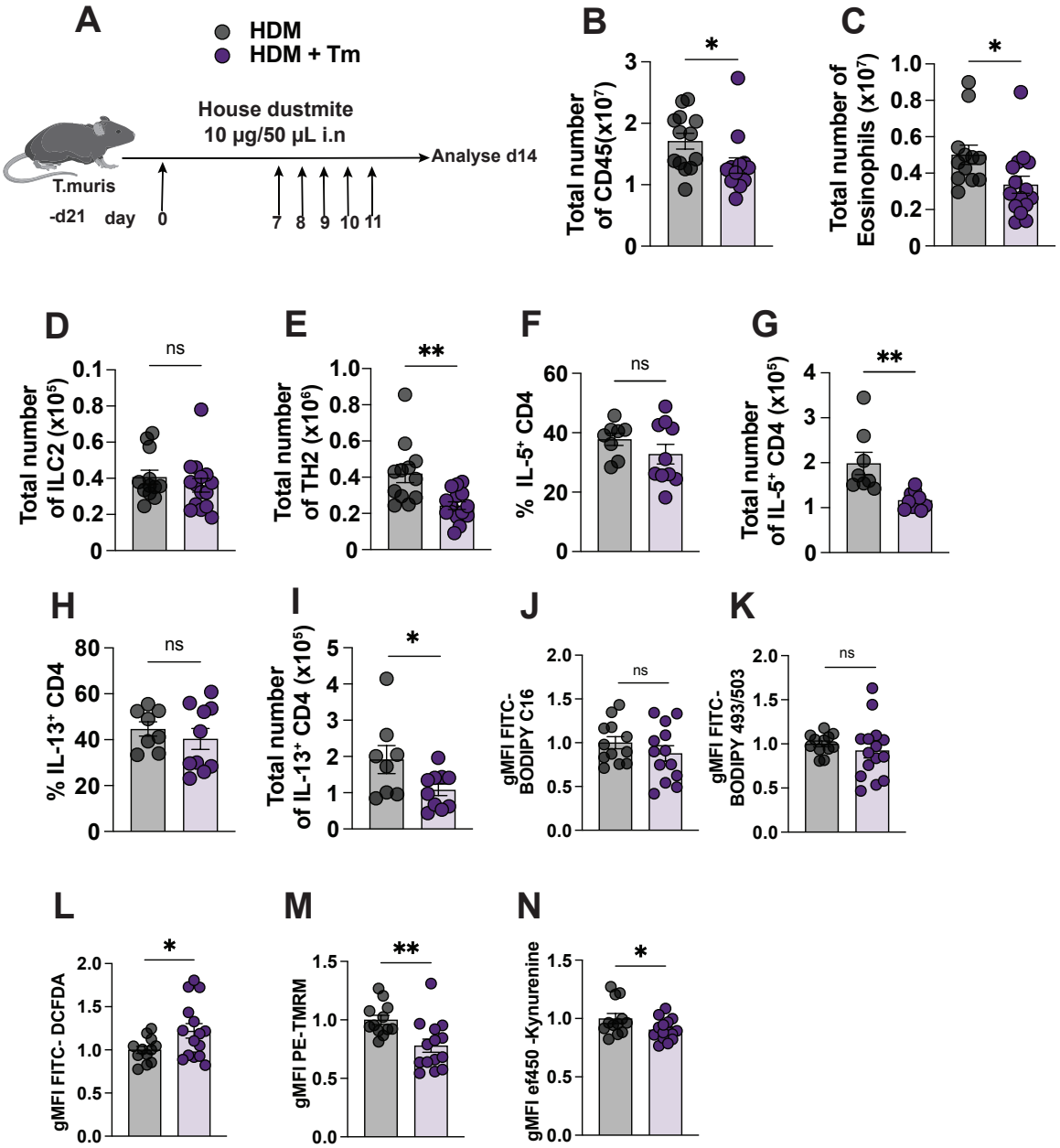

Figure 3.19: Chronic *T. muris* alters TH2 metabolism, not ILC2 during house dust mite exposure. (A) Schematic of infection and allergy model. (B-D) Total lymphocytes, eosinophils, and ILC2 from HDM only and *T. muris* and HDM. (E) Total Th2 from HDM only and *T. muris* and HDM. (F-I) Percentage and total number of IL-5 and IL-13 producing CD4 T cells from HDM only and *T. muris* and HDM. (J) gMFI values of BODIPY FLC16 in Th2 from HDM only and *T. muris* and HDM. (K) gMFI values of BODIPY 493/503 in Th2 from HDM only and *T. muris* and HDM. (L) gMFI values of DCFDA in Th2 from HDM only and *T. muris* and HDM. (M) gMFI values of TMRM uptake in Th2 from HDM only and *T. muris* and HDM. (N) gMFI values of kynurenine uptake in Th2 from HDM only and chronic *T. muris* and HDM. ILC2s were identified as $CD45^+$ Lin^- $Thy1.2^+$ $GATA3^+$ in (D). Th2 were identified as $CD4^+$ $TCRb^+$ $CD8b^-$ $FOXP3^-$ $GATA3^+$ in (E). Th2 were identified as $CD4^+$ $TCRb^+$ $CD8b^-$ $IL33R^+$ in (J-N). Results display three independent experiments with three to five mice in each experimental group. All graphs display means ± SEM; ns (not significant) $p > 0.05$, * $p \leq 0.05$, ** $p \leq 0.01$, *** $p \leq 0.001$, **** $p \leq 0.0001$. Comparisons between two groups were analyzed by Welch's t-test.

3.5 Chronic *T. muris* Induces Type 1 Skewing at day 21 Post Infection.

As discussed previously, chronic *T. muris* infection induces a heterogeneous immune response, with low-dose infection driving a systemic type 1 immune skewing that extends to distal organs (Else and Grencis, 1991). We hypothesised that the changes in the cytokine and immune cell landscape may contribute to the protection observed during papain exposure. To determine when immune skewing arises in the lung, mice were infected with a low dose of *T. muris* and analysed at days 14, 21, and 27 post infection, corresponding to the timeline of papain challenges (Figure 3.20A). On days 21 and 27, total $CD45^+$ numbers showed a modest, albeit nonsignificant, increase compared to naive controls (Figure3.20B). Total eosinophil, neutrophil, $CD4^+$ and $CD8^+$ counts remained unchanged at these time points (Figure 3.20C-F). However, components of the myeloid compartment were selectively altered. Alveolar macrophages were modestly increased at day 21, and airway-infiltrating monocytes were significantly elevated (Figure 3.20G–H). In parallel, analysis of lung homogenates revealed elevated CCL2 and CCL5 protein levels, peaking at day 21 post infection (Figure 3.20I-J). Both chemokines are potent monocyte chemoattractants (Haberstroh et al., 2002), indicating enhanced recruitment of myeloid cells to the lung during this stage of chronic infection. Cxcl10 and IFNγ (Figure 3.20K-L) were also increased at 21 days post infection in the lung homogenate, which is consistent with the literature that type 1 immune skewing occurs in chronic *T. muris* at approximately 21 days post infection (Taylor et al., 2000).

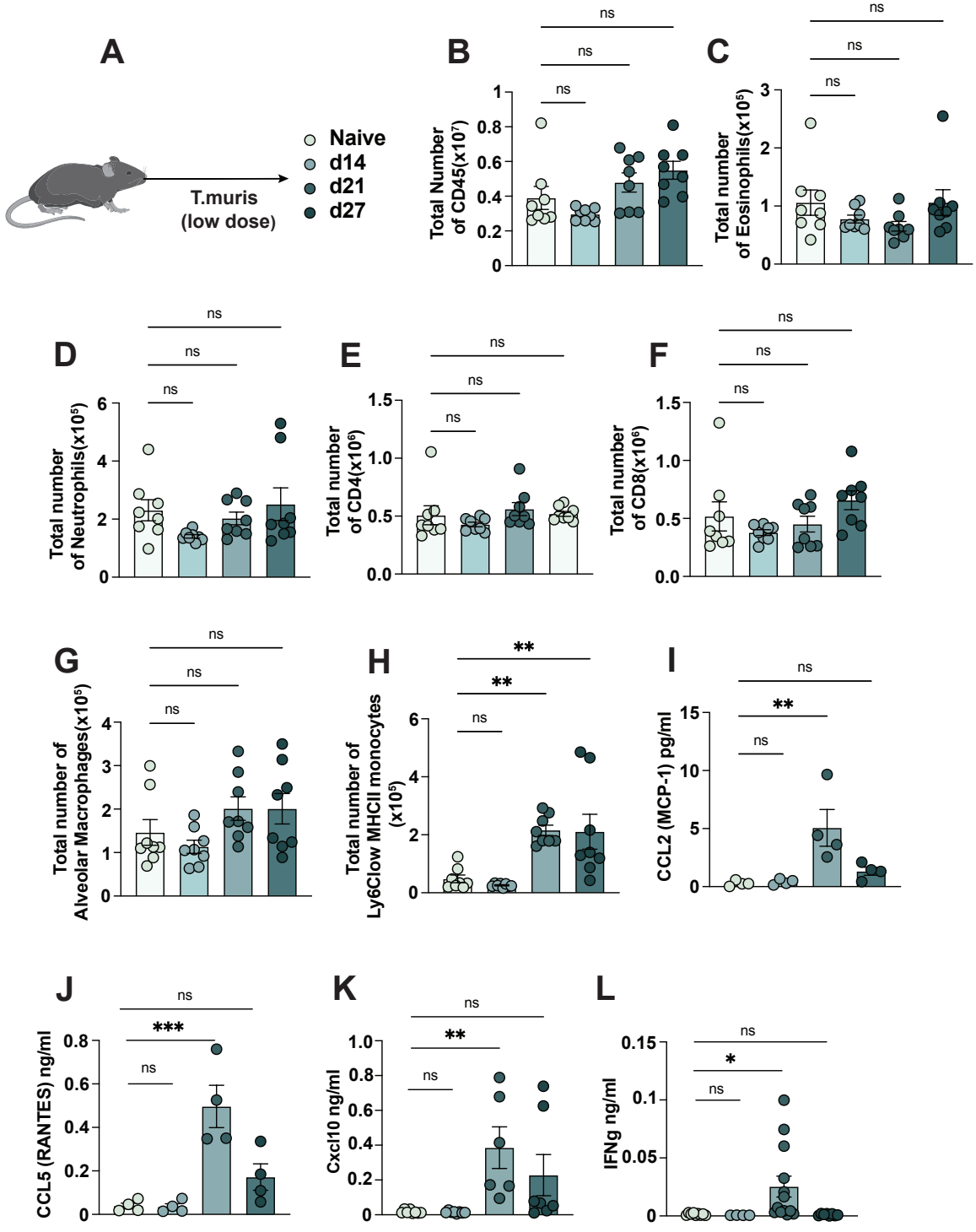

Figure 3.20: Chronic *T. muris* induces type 1 skewing at day 21 post infection. (A) Schematic of infection model: Mice were infected at various time points and compared to naive. (B) Total number of $CD45^+$ cells at d14, d21, and d27 compared to naive. (C-H) Total numbers of eosinophils, neutrophils, $CD4^+$ and $CD8^+$ T cells, alveolar macrophages, and infiltrating monocytes 14, 21, and 27 compared to naive. (I-L) Concentrations of CCL2, CCL5, Cxcl10 and IFNγ in lung homogenates were determined by LEGENDplex 14, d21, and d27 compared to naive. Results display two to three independent experiments with three to five mice in each experimental group. All graphs display means ± SEM; ns (not significant) $p > 0.05$, * $p \leq 0.05$, ** $p \leq 0.01$, *** $p \leq 0.001$, **** $p \leq 0.0001$. One-way ANOVA with Tukey's multiple comparisons test.

Although total $CD4^+$ T cell numbers did not change over time, a clear increase in Th1 cells was observed at 21 days post infection, accompanied by a significant increase in IFNγ-producing $CD4^+$ T cells (Figure 3.21A-D). Consistent with previous reports identifying $CD4^+$ T cells as a key source of IFNγ during chronic infection (Chenery et al., 2016), a significant contribution to IFNγ-producing populations was detected among non-$CD4^+$/$CD8^+$ cells, partly attributable to NK cells (Figure 3.21E-F). Collectively, these findings suggest that while overall immune cell composition remains largely stable, *T. muris* infection drives a type 1 skewing in the lung by reshaping the cytokine milieu as well as altering the myeloid compartment and IFNγ-producing populations of the lung at steady-state.

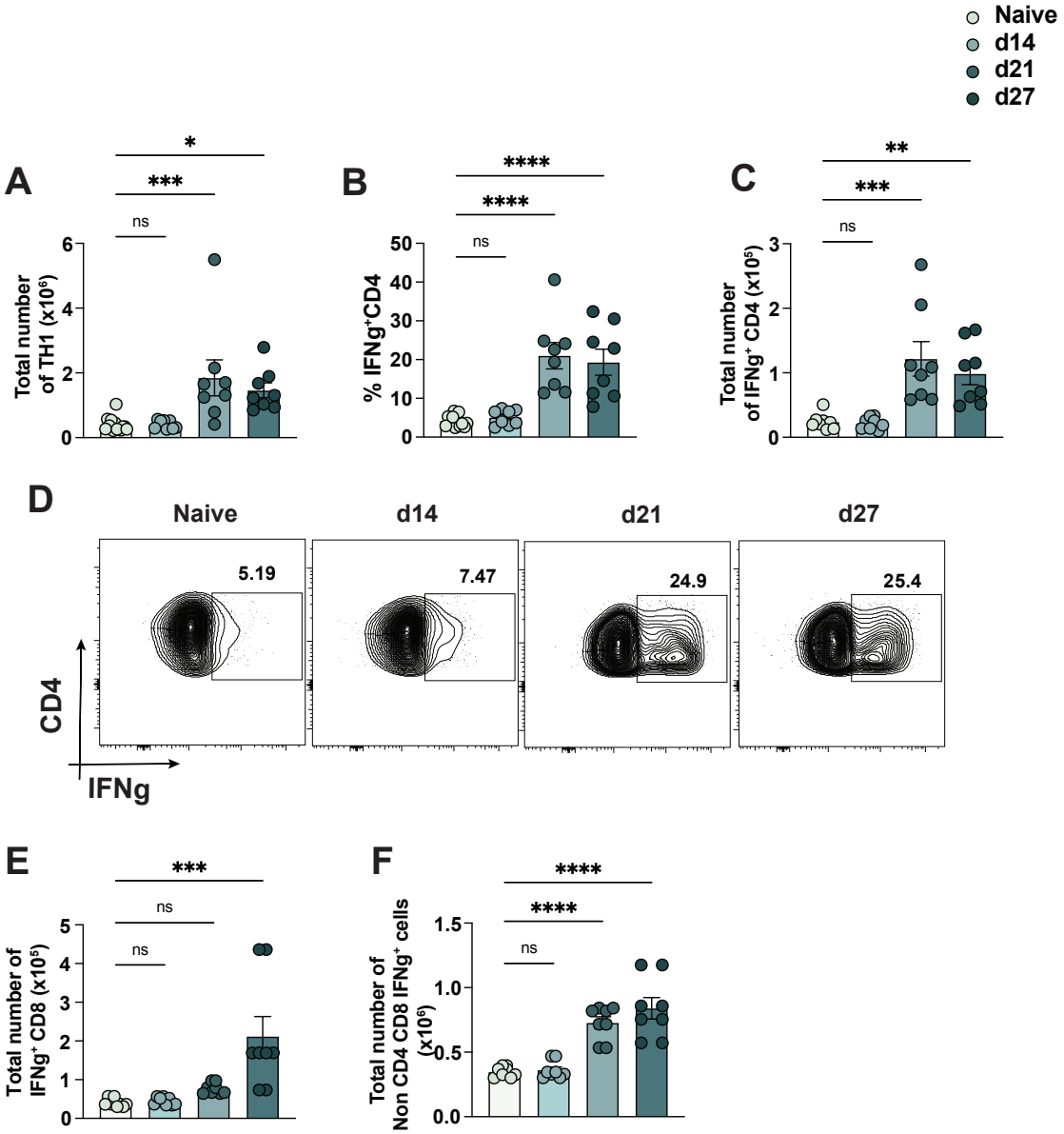

Figure 3.21: Chronic *T. muris* increased IFNγ-producing cells at day 21 post infection. (A) Total number of Tbet$^+$ CD4 T cells (Th1). (B-D) Chronic *T. muris* increased IFNγ-producing CD4 T cells. (E-F) IFNγ-producing cells in infected versus papain-only controls. Results display two to three independent experiments with three to five mice in each experimental group. All graphs display means ± SEM; ns (not significant) $p > 0.05$, * $p \leq 0.05$, ** $p \leq 0.01$, *** $p \leq 0.001$, **** $p \leq 0.0001$. One-way ANOVA with Tukey's multiple comparisons test.

As chronic *T. muris* infection induces a type 1–skewed immune environment in the lung at 21 days post infection, coinciding with the first papain exposure, we examined ILC2 characteristics at this time point (Figure 3.22A). Indeed, the lung tissue at 21 days post infection displays enhanced type 1 skewing, including increased *Ifng*,*Tbx21*, *Stat1*, and *Ido1* mRNA expression (Figure 3.22B). While Chenery et al. (2016) reported increased regulatory T cells and a myeloid-derived IL-10 increase during chronic infection, which may contribute to the suppres-

sion of ILC2 in our model, Treg frequencies remained stable in the lung at day 21, however, IL-10 gene expression was upregulated in the lung tissue (Figure 3.22D-E). Equally, Th2 and ILC2 numbers were comparable to naive controls (Figure 3.22F-G), and ILC2s maintained normal IL-5 and IL-13 production (Figure 3.22 H-J).

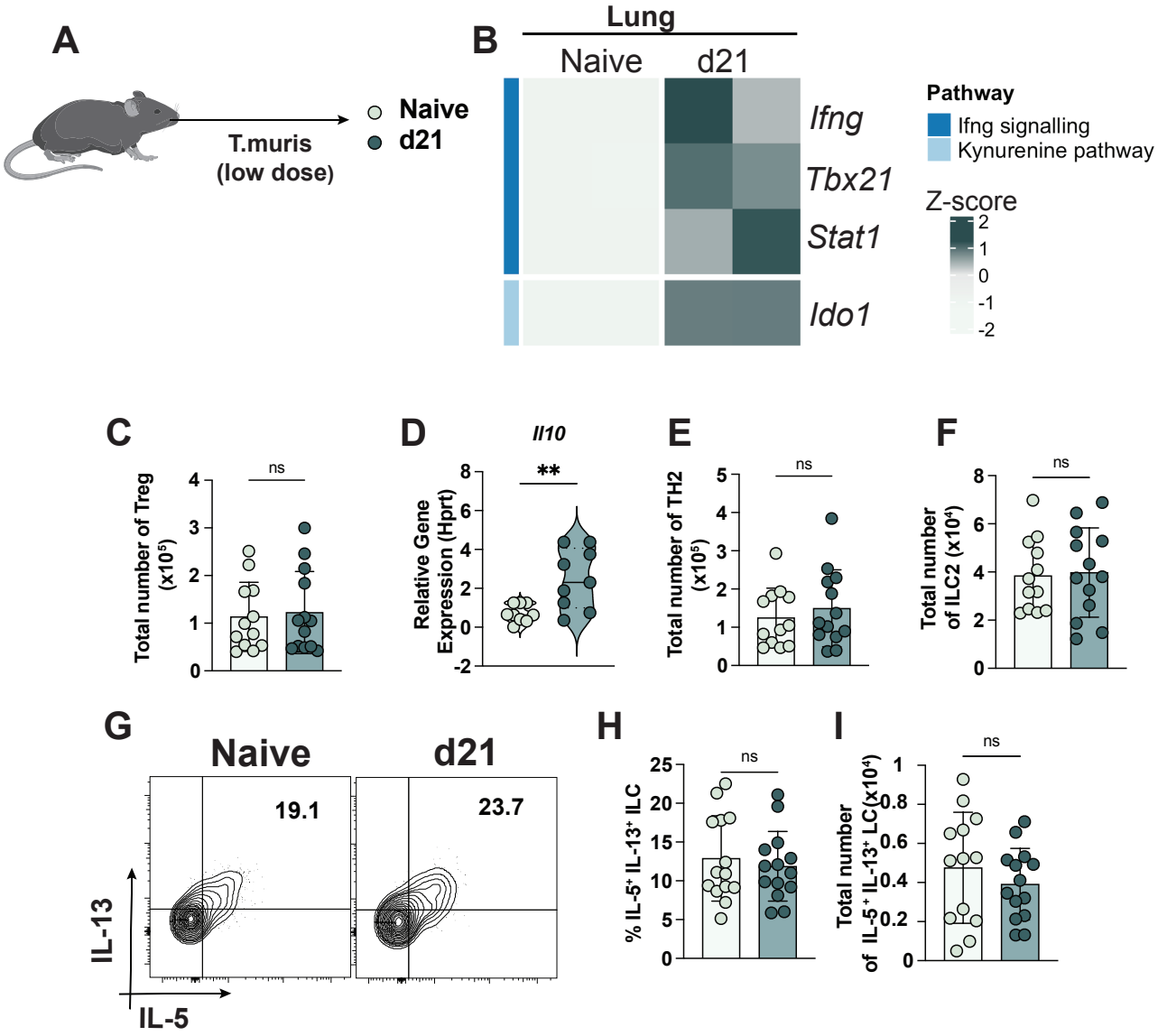

Figure 3.22: Chronic *T. muris* does not alter ILC2 functionality at steady-state. (A) Schematic of infection model: Mice were infected and sacrificed 21 days later. (B) Heatmap of *Ifng*,*Tbx21*, *Stat1*, and *Ido1* gene expression in naive and *T. muris* lung tissue. (C) Total number of regulatory T cells in naive and *T. muris*-infected mice. (D) Gene expression of *Il10* in lung tissue of naive and *T. muris*-infected mice. (E-F) Total number of airway Th2 and ILC2 numbers in naive and *T. muris*-infected mice. (G-I) IL-5^{+} IL-13 $^{+}$ double-producing ILCs in naive and *T. muris*-infected mice. Treg were identified as CD4^{+} TCRb^{+} CD8b^{-} FOXP3^{+}. ILC2s were identified as CD45^{+} Lin^{-} Thy1.2 $^{+}$ GATA3^{+} in (G). Th2 were identified as CD4^{+} TCRb^{+} CD8b^{-} FOXP3^{-} GATA3^{+} in (F). Results display three to four independent experiments with three to five mice in each experimental group. All graphs display means ± SEM; ns (not significant) $p > 0.05$, * $p \leq 0.05$, ** $p \leq 0.01$, *** $p \leq 0.001$, **** $p \leq 0.0001$. Comparisons between two groups were analyzed by Welch's t-test.

Despite unchanged cytokine output and cell numbers, ILC2s from day 21–infected mice displayed modestly reduced lipid uptake, while lipid droplet formation remained unaltered (Figure 3.23 A-B). These cells also exhibited decreased mitochondrial membrane potential without changes in cellular ROS (Figure 3.23 C-D). Thus, while the type 1 environment at day 21 does not alter ILC2 numbers or effector function, the observed reductions in lipid uptake and mitochondrial potential suggest a potential metabolic tissue restraint that may limit their responsiveness upon exposure to papain.

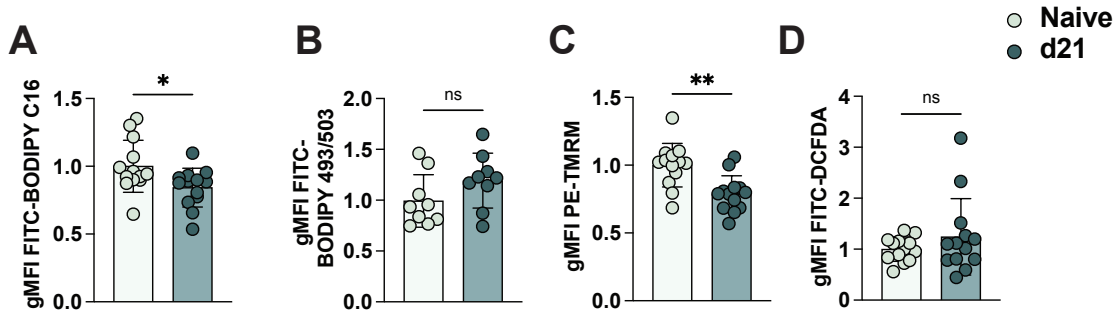

Figure 3.23: Chronic *T. muris* may alter ILC2 metabolism at steady-state. (A-B) gMFI values of BODIPY FLC16 and BODIPY 493/503 in ILC2 in naive and *T. muris*-infected mice. (C-D) gMFI values of mitochondrial membrane potential and cellular ROS in ILC2 in naive and *T. muris*-infected mice. ILC2s were identified as $CD45^+$ Lin^- $Thy1.2^+$ $GATA3^+$ in (A-B). ILC2s were identified as $CD45^+$ Lin^- $Thy1.2^+$ $IL33R^+$ in (C-D). Results display three to four independent experiments with three to five mice in each experimental group. All graphs display means ± SEM; ns (not significant) $p > 0.05$, * $p \leq 0.05$, ** $p \leq 0.01$, *** $p \leq 0.001$, **** $p \leq 0.0001$. Comparisons between two groups were analyzed by Welch's t-test.

To assess whether lung ILC2s from chronically infected mice are intrinsically impaired prior to activation, ILC2s were sorted from naive and day 21 *T. muris*–infected lungs and stimulated in vitro with IL-33 and IL-7. However, ILC2s from day 21 infected mice expanded and proliferated comparably to naive controls (Figure 3.24 A-B). In addition, lipid droplet formation was also comparable between day 21 *T. muris*–infected ILC2 and naive controls upon activation (Figure 3.24 C). Thus, a key feature of lipid metabolism in activated ILC2 is intact. Collectively, these data indicate that ILC2s from infected mice are not intrinsically defective when removed from their in vivo environment during *T. muris* infection but may instead be acutely influenced by the lung microenvironment.

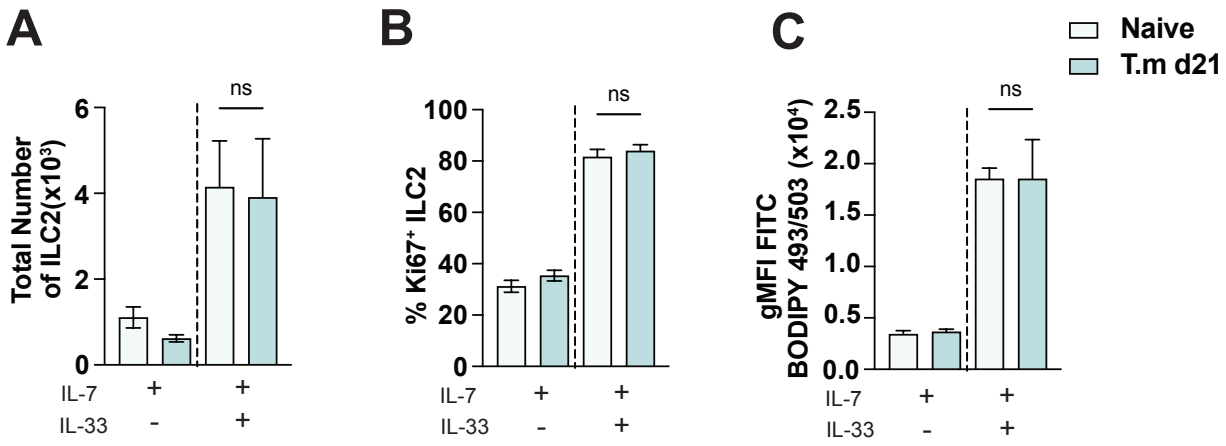

Figure 3.24: ILC2 from d21 chronic *T. muris* infection can proliferate in culture. (A) Total ILC2 numbers from naive and day 21 *T. muris*–infected mice cultured with a combination of IL-7 and IL-33. (B) Percentage of Ki67$^+$ ILC2 from naive and day 21 *T. muris*–infected mice. (C) gMFI values of BODIPY 493/503 in ILC2 in the presence of IL-33. ILC2s were identified as CD45$^+$ Thy1.2 $^+$ GATA3$^+$ in (A-C). Results display two independent experiments with five mice in each experimental group. All graphs display means ± SEM; ns (not significant) $p > 0.05$, * $p \leq 0.05$, ** $p \leq 0.01$, *** $p \leq 0.001$, **** $p \leq 0.0001$. One-way ANOVA with Tukey's multiple comparisons test.

As IFNγ peaks both in protein and mRNA levels at 21 days post infection, we investigated whether IFNγ in the lung environment contributes to the suppression of ILC2 upon activation. To do so, we cultured whole-lung cells from naive and day 21–infected mice with IL-33 or IL-33 + anti-IFNγ antibody. ILC2s from infected lungs were less responsive to IL-33, and the production of IL-5 and IL-13 cytokine levels were lower in supernatants (Figure 3.25 A-D). Blocking IFNγ restored ILC2 responsiveness and IL-5 and IL-13 cytokine production (Figure 3.25 E-H). Together, these findings indicate that while the airway ILC2 from *T. muris*–infected mice are not intrinsically impaired and can proliferate ex vivo, the lung environment of chronically infected mice contributes to the suppression of ILC2 activation.

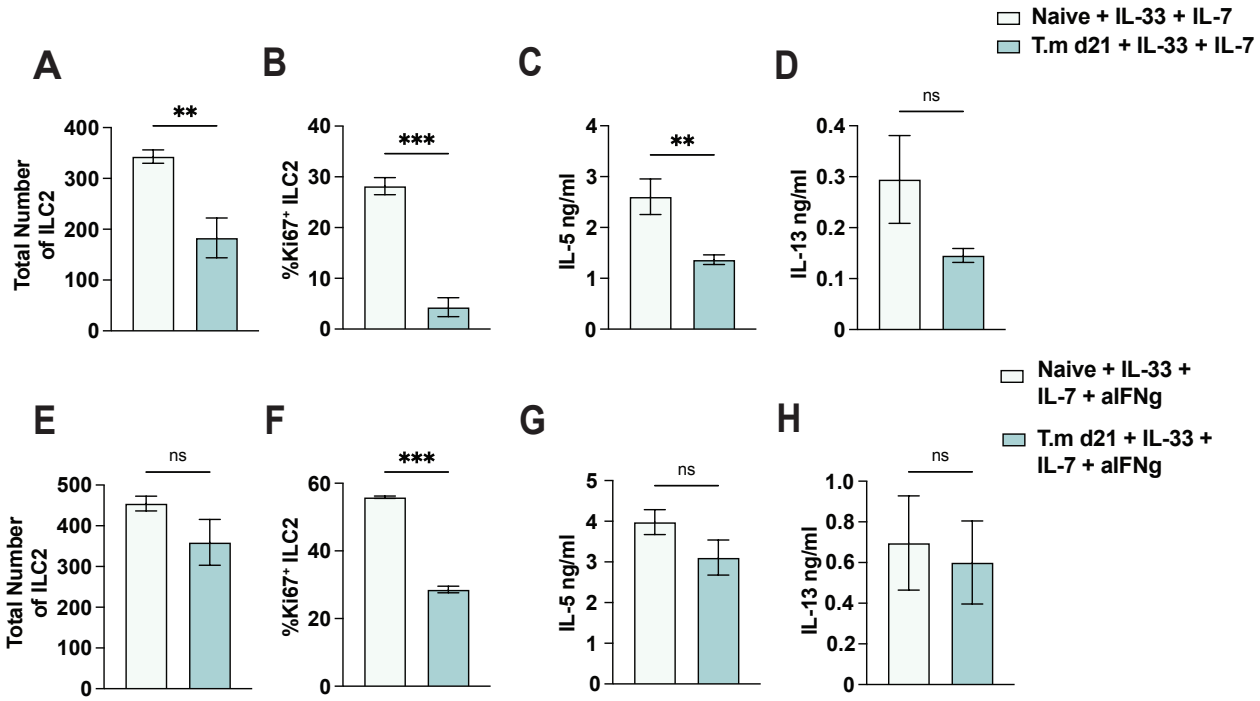

Figure 3.25: Chronic *T. muris* promotes an environment that suppresses ILC2 proliferation and function in vitro. (A-B) Total numbers of ILC2 from whole lung culture of naive and day 21 *T. muris*–infected mice in the presence of IL-33 and IL-7. (C-D) Quantification of IL-5 and IL-13 from supernatant using LEGENDplex in the presence of IL-33 and IL-7. (E-F) Total numbers of ILC2 from whole lung culture of naive and day 21 *T. muris*–infected mice in the presence of IL-33 and IL-7 and anti-IFNγ antibody. (G-H) Quantification of IL-5 and IL-13 from supernatant using LEGENDplex in the presence of IL-33 and IL-7 and anti-IFNγ antibody. ILC2s were identified as $CD45^+$ $Thy1.2^+$ Lin^- $GATA3^+$ in (A-B) and (E-F). Results display two independent experiments with three to five mice in each experimental group. All graphs display means ± SEM; ns (not significant) $p > 0.05$, * $p \leq 0.05$, ** $p \leq 0.01$, *** $p \leq 0.001$, **** $p \leq 0.0001$. Comparisons between two groups were analyzed by Welch's t-test.

3.6 Chronic *T. muris* Infection Induces IFNγ Signalling in ILC2 during Airway Inflammation

Increased IFNγ and type 1 immune skewing were also evident in *T. muris*–infected mice during papain exposure. Serum levels of CXCL10 and IFNγ were elevated in infected mice (Figure 3.26 A-B), and IFNγ was similarly increased in lung homogenates, accompanied by enhanced T-bet expression in lung tissue (Figure 3.26 C-D). Consistent with these findings, $CD4^+$T cells from infected mice displayed a greater capacity to produce IFNγ (Figure3.26 E-G). IFNγ signalling was also apparent in ILC2 from *T. muris*–infected. Expression of Sca-1, a marker of IFNγ responsiveness in ILC2s (Cautivo et al., 2022), was elevated on lung ILC2s from *T. muris* and papain mice (Figure3.26 H). Moreover, isolated ILC2s from these mice showed increased expression of *Irf1* and *Cxcl10*, downstream targets of IFNγ signalling.

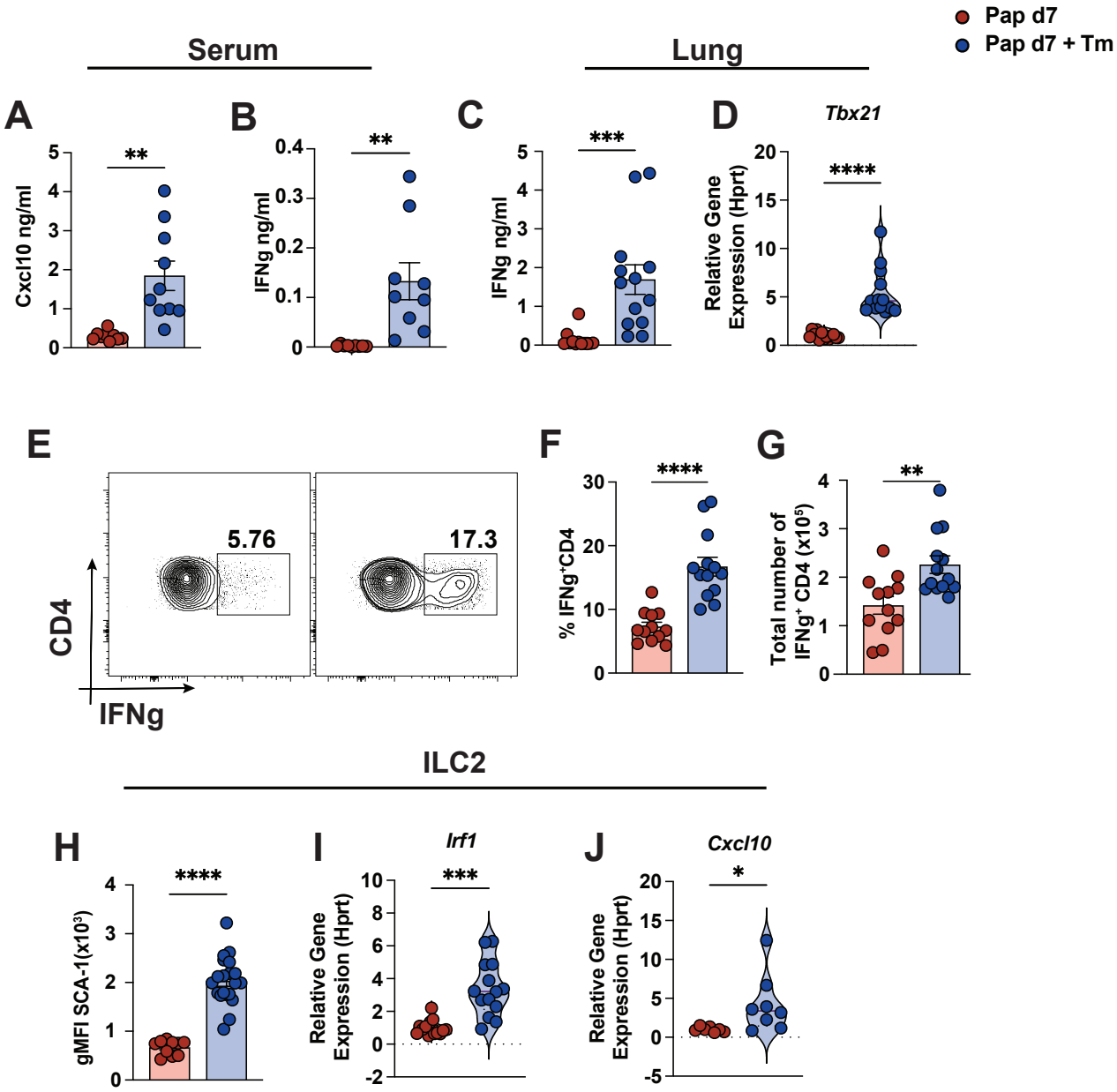

Figure 3.26: Chronic *T. muris* induces IFNγ signalling in ILC2. (A-B) Cxcl10 and IFNγ in the serum of *T. muris*-infected mice quantified by LEGENDplex. (C) IFNγ in the lung homogenate of *T. muris*-infected mice and papain only quantified by LEGENDplex. (D) Gene expression of *Tbx21* in lung tissue from papain and *T. muris*-infected mice. (E) Representative flow plot of IFNγ$^+$ CD4$^+$ T cells in the lung from papain and *T. muris*-infected mice. (F-G) Bar plot quantification of percentage and total number of IFNγ-producing CD4 T cells from papain and *T. muris*-infected mice. (H) gMFI values of Sca-1 expression on ILC2 from papain and *T. muris*-infected mice. (I-J) Gene expression of *Irf1* and *Cxcl10* in isolated ILC2 from papain and *T. muris*-infected mice. ILC2s were identified as CD45$^+$ Thy1.2 $^+$ Lin$^-$ IL33R$^+$ in (H) and (I-J). IFNγ-producing CD4 T cells were identified as CD45$^+$ CD4$^+$ TCRb$^+$ IFNγ$^+$ in (E-G). Results display three to four independent experiments with three to five mice in each experimental group. All graphs display means ± SEM; ns (not significant) $p > 0.05$, * $p \leq 0.05$, ** $p \leq 0.01$, *** $p \leq 0.001$, **** $p \leq 0.0001$. Comparisons between two groups were analyzed by Welch's t-test.

While ILCs are sometimes described as plastic, and there are reports that ILC2 can convert

to ILC1 under type 1 driven factors (Shao et al., 2021), we did not observe increased Tbet expression in ILC2 from *T. muris*–infected mice during papain exposure (Figure 3.27 A-B). Together, these data demonstrate robust IFNγ signalling in lung ILC2s during *T. muris* infection and allergic airway inflammation, which may contribute to the observed suppression and metabolic alterations in ILC2.

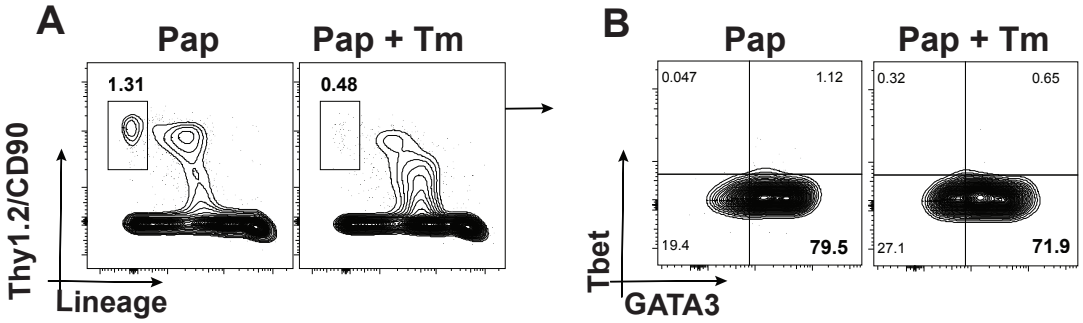

Figure 3.27: ILC2 are not upregulating Tbet during chronic *T. muris* infection. (A) Representative flow cytometry plot gating on ILC2 Thy1.2/CD90$^+$ vs lineage from papain and *T. muris*-infected mice. (B) Representative flow cytometry plot, subgating on Thy1.2$^+$ lineage$^-$ followed by Tbet vs GATA3 from papain and *T. muris*-infected mice. ILCs were identified as CD45$^+$ Thy1.2 $^+$ Lin$^-$. Results display three to four independent experiments with three to five mice in each experimental group. All graphs display means ± SEM; ns (not significant) $p > 0.05$, * $p \leq 0.05$, ** $p \leq 0.01$, *** $p \leq 0.001$, **** $p \leq 0.0001$. Comparisons between two groups were analyzed by Welch's t-test.

As IFNγ signalling in ILC2 was apparent during chronic *T. muris* infection, we hypothesised that local blocking of IFNγ through intranasal application may reverse the suppression of ILC2 proliferation and function (Figure 3.28A). Indeed, blocking IFNγ using an anti-IFNγ antibody during papain exposure reversed total ILC2 and eosinophils in the airways of aIFNγ-treated mice compared to the isotype control (Figure 3.28B-C). Importantly, blocking local IFNγ did not cause expulsion of worms (Figure 3.28D). Notably, ILC2 function was also restored both in percentage and total numbers of IL-5$^+$ and IL-13 IL-5$^+$ double-positive ILC (Figure 3.28E-G). Furthermore, type 2 cytokines IL-5, IL-13, and IL-9 were increased in the lung homogenate of aIFNγ-treated mice compared to the isotype control (Figure 3.28H-K). At the same time, IFNγ was decreased in the lung homogenate of aIFNγ-treated mice (Figure 3.28L).

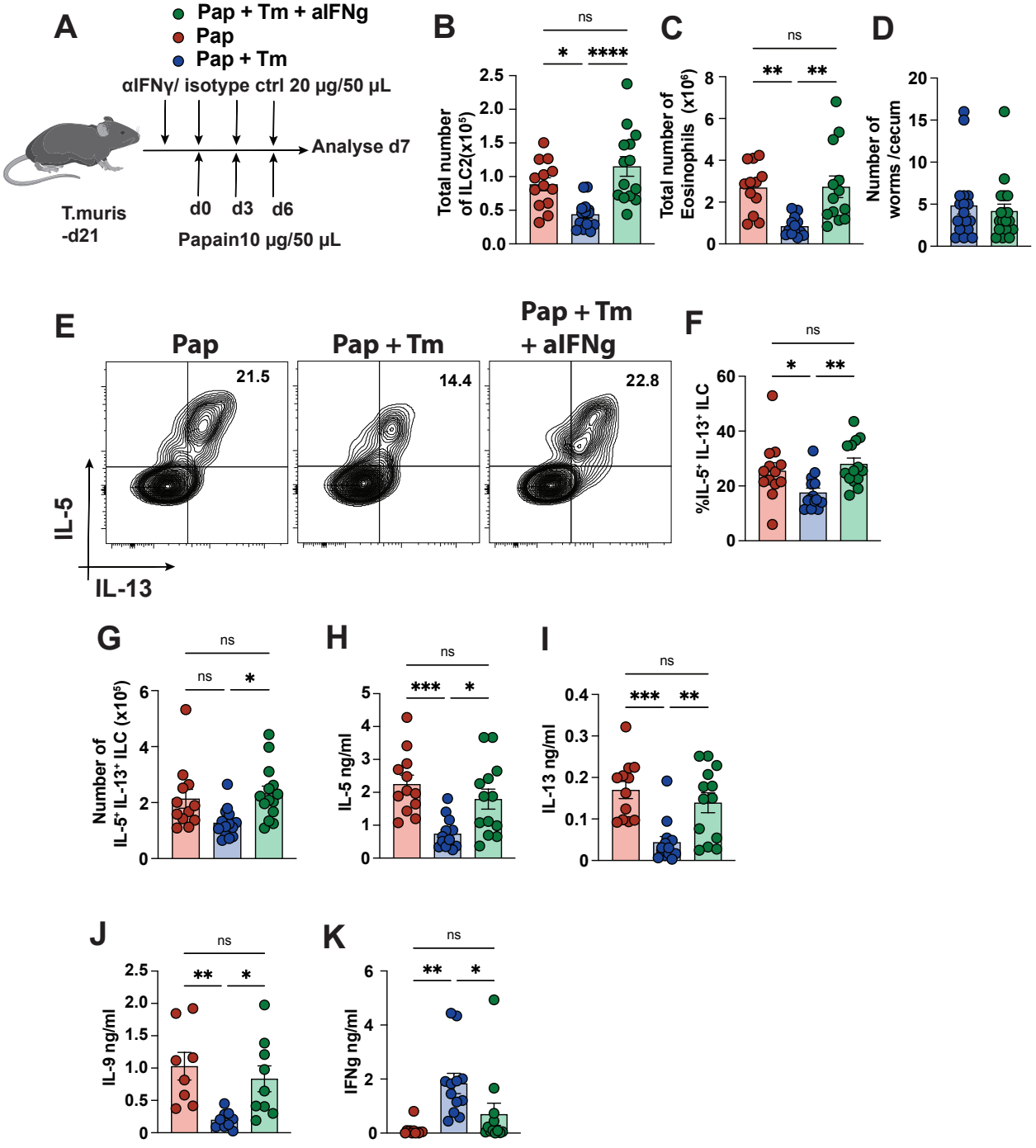

Figure 3.28: Blocking local IFNγ during chronic *T. muris* reverses altered functional suppression of ILC2. (A) Schematic of animal model. (B) Total ILC2 numbers from papain, papain and *T. muris* + isotype, and papain and *T. muris* + a-IFNγ antibody. (C) Total eosinophils from papain, papain and chronic *T. muris* + isotype, and papain and *T. muris* + a-IFNγ antibody. (D) Total worm count in cecum from papain and *T. muris* + isotype and papain and *T. muris* + a-IFNγ antibody. (E) Representative flow cytometry plot of IL-5$^+$ and IL-13$^+$ producing ILC from papain, papain and *T. muris* + isotype, and papain and *T. muris* + a-IFNγ antibody. (F-G) Quantification of IL-5$^+$ and IL-13$^+$ producing ILC in percentage and total numbers from papain, papain and *T. muris* + isotype, and papain and chronic *T. muris* + a-IFNγ antibody. (H-K) IL-5, IL-13, IL-9, and IFNγ protein in the lung homogenate as quantified by LEGENDplex. ILCs were identified as CD45$^+$ Thy1.2 $^+$ Lin$^-$ GATA3$^+$ in (B). Results display three to four independent experiments with three to five mice in each experimental group. All graphs display means ± SEM; ns (not significant) $p > 0.05$, * $p \leq 0.05$, ** $p \leq 0.01$, *** $p \leq 0.001$, **** $p \leq 0.0001$. One-way ANOVA with Tukey's multiple comparisons test.

Blocking local IFNγ also restored key features of ILC2 metabolism that are suppressed by the presence of chronic *T. muris* infection. Lipid droplets and fatty acid uptake were restored in ILC2 during IFNγ blockade (Figure 3.29A-B). In addition, cellular ROS was reduced, and mitochondrial membrane potential was increased (Figure 3.29C-D). Furthermore, AHA uptake was increased and Sca-1 expression was decreased on ILC2 with IFNγ blockade (Figure 3.29E-F). Collectively, these data imply that the IFNγ cytokine environment induced by chronic *T. muris* infection is contributing to the suppression of ILC2 proliferation and function in the airways of papain-challenged mice. Furthermore, IFNγ is contributing to the metabolic changes we observe in ILC2 during chronic *T. muris* infection.

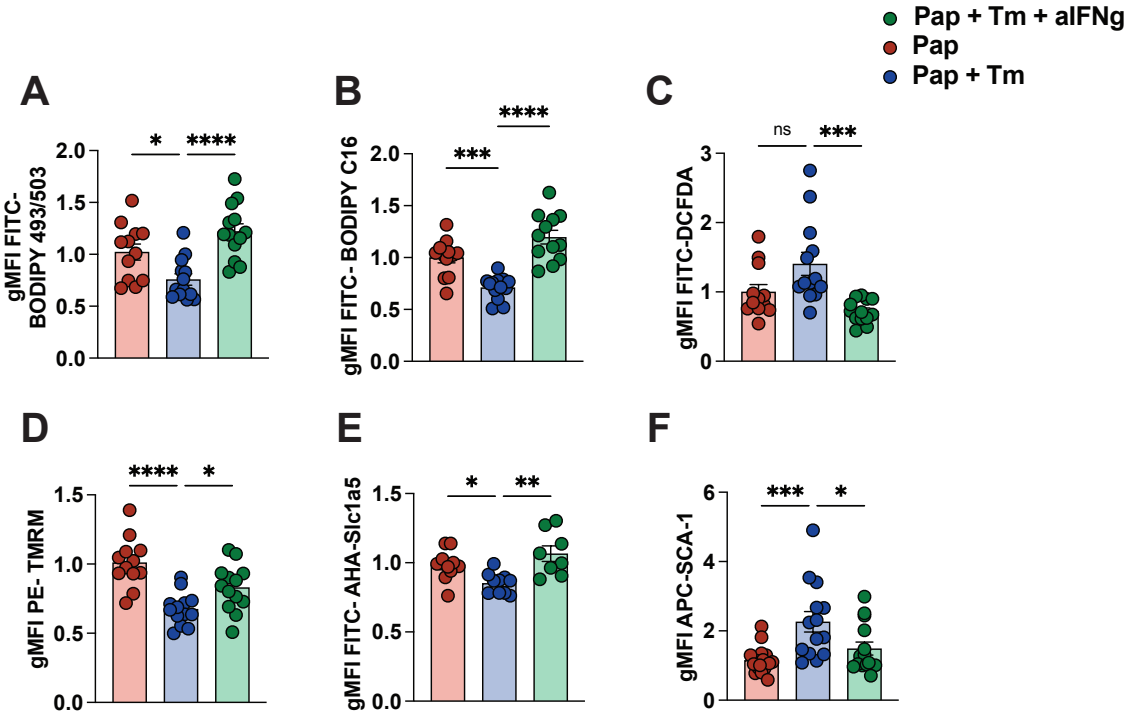

Figure 3.29: Blocking local IFNγ reverses metabolism in ILC2. (A-B) gMFI values of BODIPY 493/503 and BODIPY FLC16 in ILC2 from papain, papain and *T. muris* + isotype, and papain and *T. muris* + a-IFNγ antibody. (C) gMFI values of DCFDA in ILC2 papain, papain and *T. muris* + isotype, and papain and *T. muris* + a-IFNγ antibody. (D) gMFI of TMRM values in ILC2 from papain, papain and *T. muris* + isotype, and papain and *T. muris* + a-IFNγ antibody. (E) gMFI values of AHA uptake in ILC2 from papain only, papain and *T. muris* + isotype, and papain and *T. muris* + a-IFNγ antibody. (F) gMFI values of Sca-1 expression on ILC2. ILCs were identified as $CD45^+$ $Thy1.2^+$ Lin^- $GATA3^+$ (A-B) and (F). $CD45^+$ $Thy1.2^+$ Lin^- $IL33R^+$ (C-E). Results display three to four independent experiments with three to five mice in each experimental group. All graphs display means ± SEM; ns (not significant) $p > 0.05$, * $p \leq 0.05$, ** $p \leq 0.01$, *** $p \leq 0.001$, **** $p \leq 0.0001$. One-way ANOVA with Tukey's multiple comparisons test.

As chronic *T. muris* infection alters the metabolism of visceral adipose tissue (see Figure 3.7), we examined the effect of blocking local IFNγ with changes in host metabolism induced

by *T. muris* in a distal organ such as the adipose tissue. qPCR performed on VAT revealed that blocking IFNγ locally in the lung did not impact the effect the helminth has on the host visceral adipose tissue metabolism, such that *Fasn*, *Retn* were decreased in both infected mice that received anti-IFNγ and isotype control compared to papain only (Figure 3.30A-B). While *Insr* remained unchanged as previously observed (see Figure 3.7). In addition, *Tbx21* and *Ifng* mRNA remained upregulated in the adipose tissue compared to the papain-only control, demonstrating sustained type 1 skewing despite local depletion of IFNγ in the lung (Figure 3.30D-E). Overall, this suggests that the helminth can exert effects on host metabolism independent of the amelioration of airway inflammation.

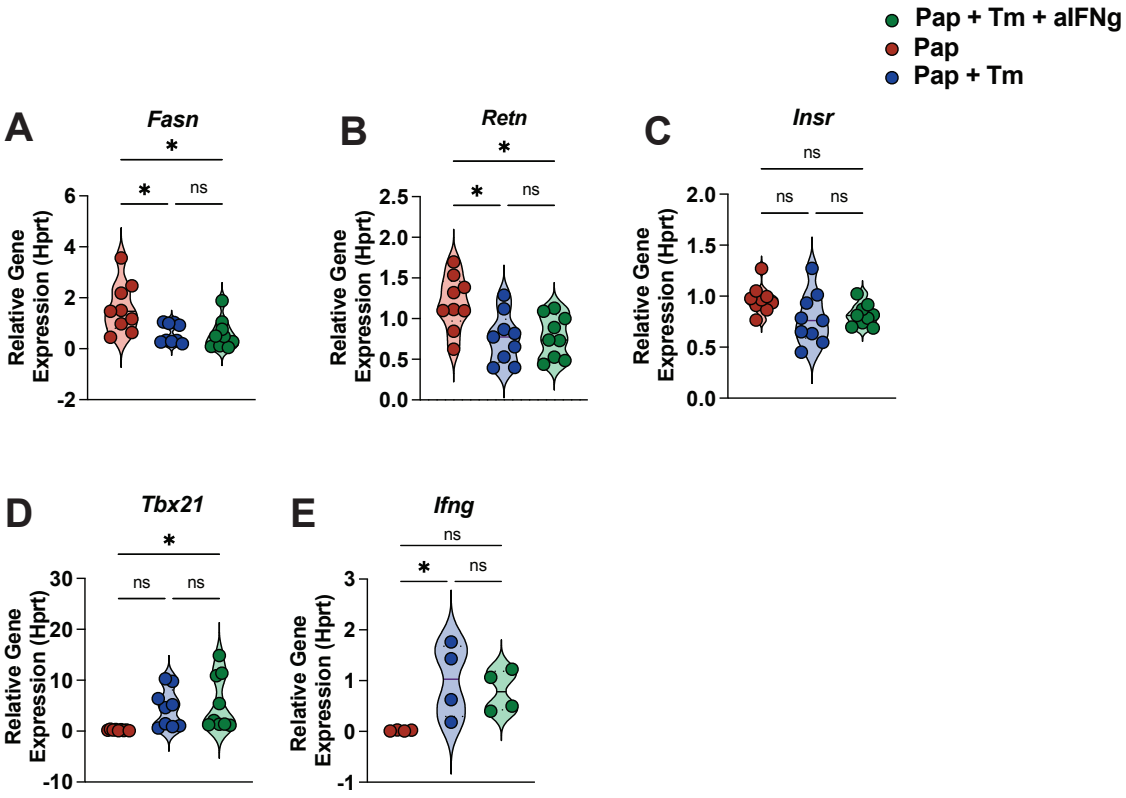

Figure 3.30: Blocking local IFNγ does not alter the helminth effect on adipose tissue metabolism. (A-C) Gene expression of *Fasn*, *Insr*, and *Retn* in VAT from papain, papain and *T. muris* + isotype, and papain and *T. muris* + a-IFNγ antibody. (D-E) Gene expression of *Tbx21* and *Ifng* in VAT from papain, papain and *T. muris* + isotype, and papain and *T. muris* + a-IFNγ antibody. Results display two independent experiments with three to five mice in each experimental group. All graphs display means ± SEM; ns (not significant) $p > 0.05$, * $p \leq 0.05$, ** $p \leq 0.01$, *** $p \leq 0.001$, **** $p \leq 0.0001$. One-way ANOVA with Tukey's multiple comparisons test.

3.7 IFNγ in vivo Recapitulates Changes in ILC2 Metabolism

Given that IFNγ signalling occurs in lung ILC2s from *T. muris* + papain–treated mice and contributes to their altered metabolism, we next examined whether IFNγ administration alone can reproduce these effects during mixed type 1/ type 2 inflammation in vivo. Mice were acutely challenged intranasally with IL-33 alone or in combination with IFNγ to assess metabolic and functional changes in ILC2s (Figure 3.31A). Consistent with previous reports demonstrating IFNγ-mediated suppression of ILC2s during mixed inflammatory responses (Cautivo et al., 2022; Moro et al., 2016), co-administration of IFNγ and IL-33 significantly reduced ILC2 numbers and proliferation (Figure 3.31B-C). This suppression was accompanied by a decrease in eosinophil recruitment (Figure 3.31D) and impaired ILC2 effector function, with reductions observed in both IL-5^{+}IL-13^{+} double-producing and single cytokine–producing ILC2s (Figure 3.31E-G).

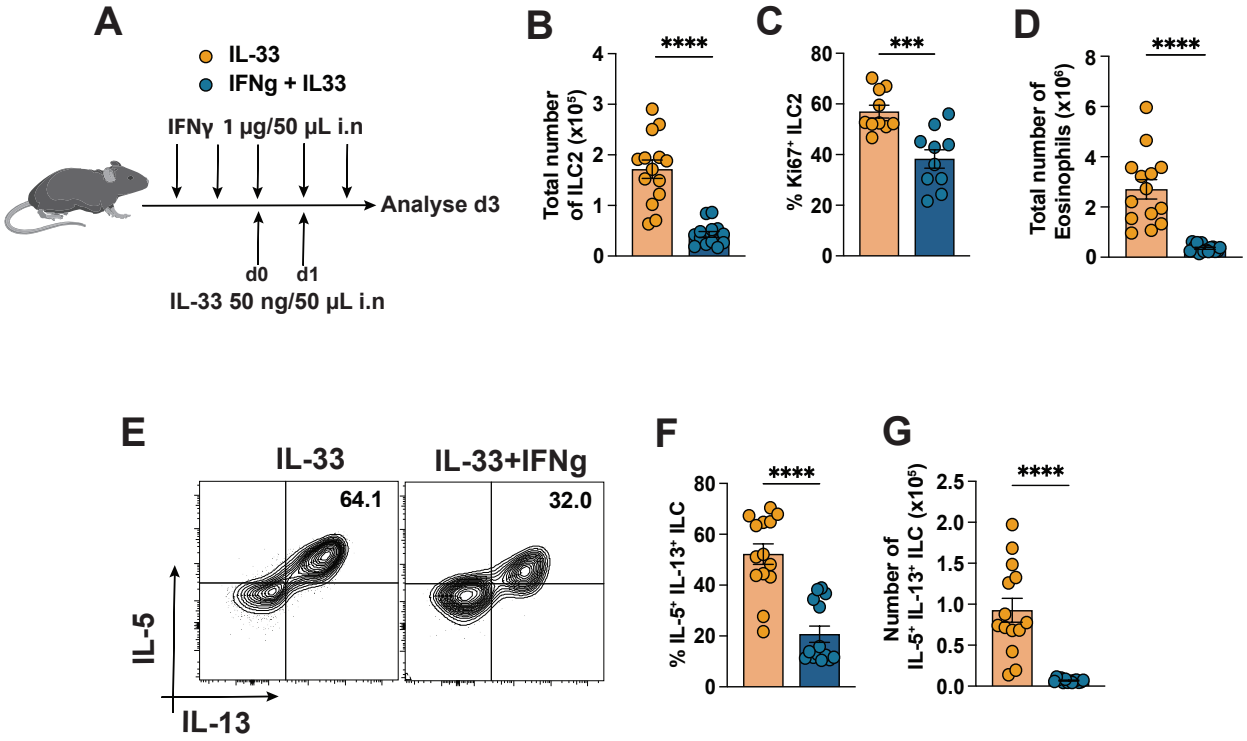

Figure 3.31: IFNγ suppresses ILC2 and eosinophils in mixed type 1/type 2 immune responses. (A) Schematic of in vivo administration of mixed type 1 / type 2 immune response. (B-C) Total ILC2 numbers and percentage of Ki67$^+$ ILC2 in IFNγ + IL-33-treated compared to IL-33 only. (D) Total airway eosinophils in IFNγ + IL-33-treated compared to IL-33 only. (E) Representative flow cytometry plot of IL-5$^+$ vs IL-13$^+$ ILC in IFNγ + IL-33-treated compared to IL-33 only. (F-G) Percentage and total number of IL-5$^+$ and IL-13$^+$ ILC in IFNγ + IL-33-treated compared to IL-33 only. ILCs were identified as CD45$^+$ Thy1.2 $^+$ Lin$^-$ IL33R/GATA3$^+$. Results display three independent experiments with three to five mice in each experimental group. All graphs display means ± SEM; ns (not significant) $p > 0.05$, * $p \leq 0.05$, ** $p \leq 0.01$, *** $p \leq 0.001$, **** $p \leq 0.0001$. Comparisons between two groups were analyzed by Welch's t-test.

In contrast to the metabolic phenotype observed during chronic *T. muris* infection and papain exposure, acute IFNγ signalling in the context of IL-33 stimulation induced a stronger metabolic reprogramming in ILC2. IFNγ treatment resulted in reduced expression of the amino acid transporters LAT1 and LAT2, encoded by *Slc7a5* and *Slc7a8*, respectively (Figure 3.32A), as well as reduced expression of *Arg1*, the absence of which has been shown to impair ILC2 function (Monticelli et al., 2016). However, *Slc1a5* expression was increased in ILC2 from IFNγ + IL-33–treated mice, whereas *Slc1a5* was reduced in ILC2 during chronic *T. muris* infection and papain challenge (Figure 3.32A). This upregulation may reflect a compensatory response to reduced expression of the glutamine transporter *Slc38a1* observed under IFNγ stimulation as well as differing expansion kinetics in the different models (Figure 3.32A). In addition, IFNγ signalling reduced expression of *Pparg* in ILC2 (Figure 3.32A),

consistent with the observed decrease in lipid uptake (Figure 3.32B).

While lipid and amino acid transport were impaired, expression of the glucose transporter *Slc2a1* was increased in ILC2 following IFNγ + IL-33 treatment (Figure 3.32A). In contrast, expression of key metabolic enzymes involved in glycolysis (*Hk1*), fatty acid oxidation (*Cpt1a*), and amino acid metabolism (*Got1*) remained unchanged compared with IL-33–only controls (Figure 3.32A). IFNγ + IL-33–treated ILC2 displayed reduced lipid droplet accumulation, alongside decreased expression of CD98 and CD71, which are required for amino acid and iron uptake, respectively (Figure 3.32C–E). In addition, puromycin incorporation was reduced in ILC2 from IFNγ + IL-33–treated mice, indicating impaired protein translation under acute IFNγ exposure (Figure 3.32F).

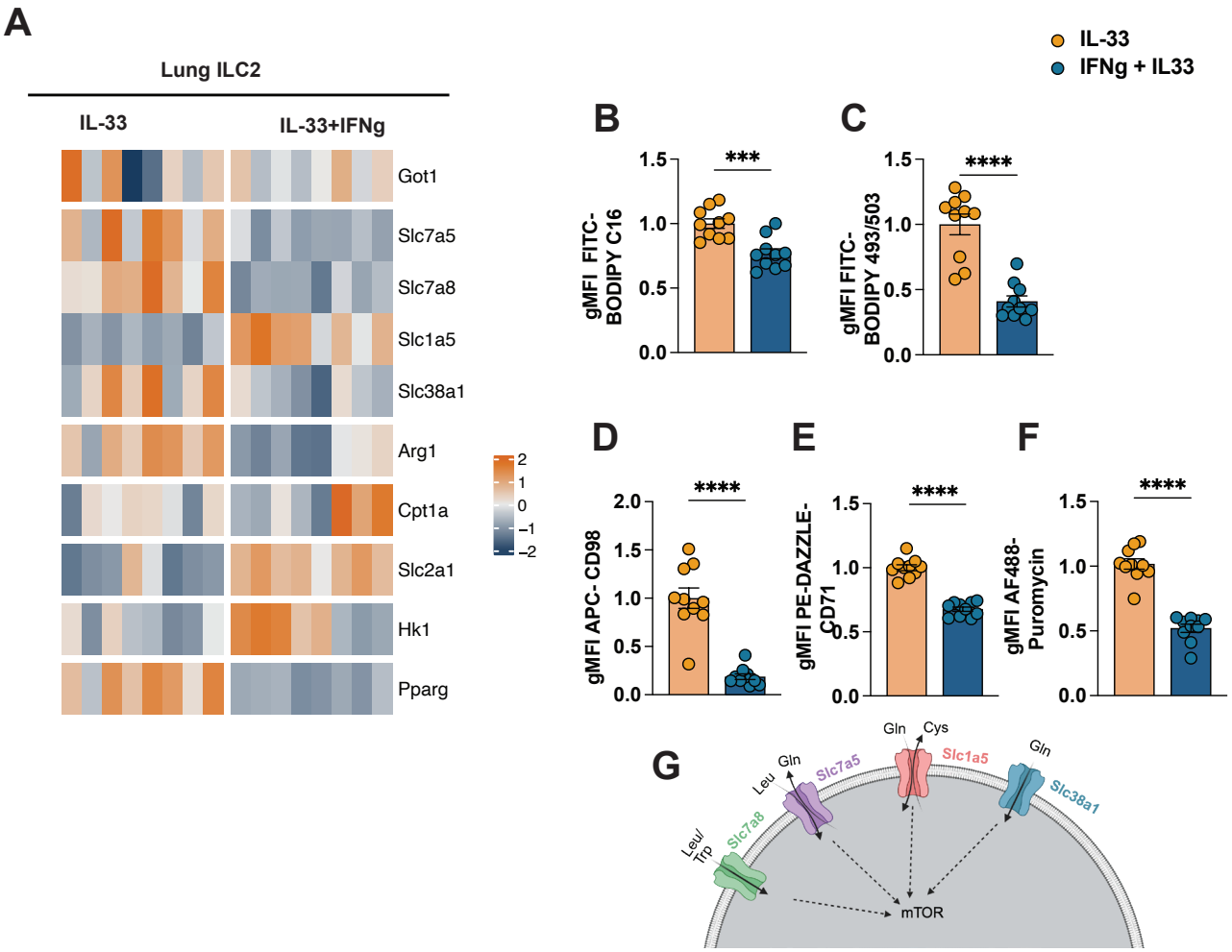

Figure 3.32: IFNγ alters amino acid and lipid metabolism in a model of mixed type 1 / type 2 inflammation. (A) Heatmap of qPCR of select genes in ILC2 from IFNγ + IL-33 mice compared to IL-33-only controls. (B-C) gMFI values of BODIPY FLC16 and BODIPY 493/503 in ILC2 from IFNγ + IL-33 mice compared to IL-33-only. (D-E) gMFI values of CD98 and CD71 in ILC2 from IFNγ + IL-33 mice compared to IL-33-only. (F) gMFI values of Puromycin in ILC2 from IFNγ + IL-33 mice compared to IL-33-only controls. (G) Schematic of important amino acid transporters in ILC2. ILC2 were identified as $CD45^+$ $Thy1.2^+$ Lin^- $GATA3^+$ (B-C) and (F). ILC2 were identified as $CD45^+$ $Thy1.2^+$ Lin^- $IL33R^+$ (D-E). Results display three independent experiments with three to five mice in each experimental group. All graphs display means ± SEM; ns (not significant) $p > 0.05$, * $p \leq 0.05$, ** $p \leq 0.01$, *** $p \leq 0.001$, **** $p \leq 0.0001$. Comparisons between two groups were analyzed by Welch's t-test.

ILC2s from IFNγ + IL-33 have reduced mitochondrial mass and membrane potential was decreased, resulting in a reduced TMRM/MitoTracker Green ratio (Figure 3.33A-C), suggesting decreased mitochondrial activity. In addition, ILC2s from IFNγ + IL-33–treated mice exhibited increased cellular ROS compared to IL-33 only, indicating elevated oxidative stress (Figure 3.33D).

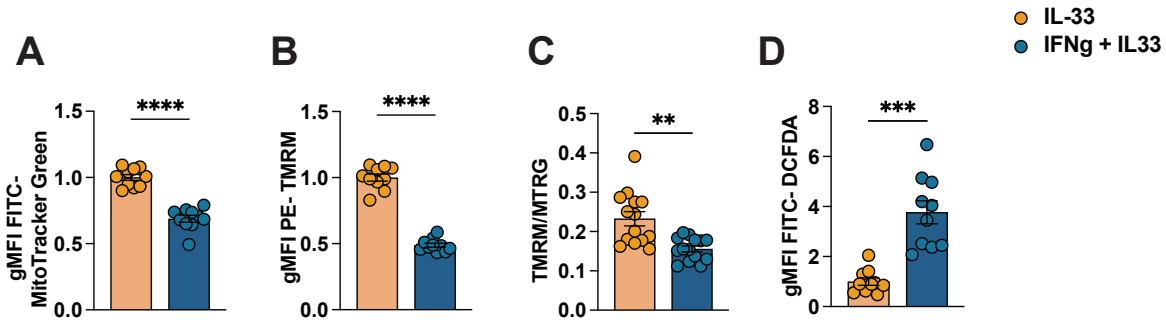

Figure 3.33: Acute IFNγ alters mitochondria and redox balance in ILC2 during mixed type 1/ type 2 inflammation. (A) gMFI values of MitoTracker Green in ILC2 from IFNγ + IL-33 mice compared to IL-33-only controls. (B) gMFI values of TMRM in ILC2 from IFNγ + IL-33 mice compared to IL-33-only controls. (C) The ratio of TMRM to MitoTracker Gree in ILC2 from IFNγ + IL-33 mice compared to IL-33-only controls. (D) gMFI values of DCFDA in ILC2 from IFNγ + IL-33 mice compared to IL-33-only controls. ILC2 were identified as $CD45^+$ $Thy1.2^+$ Lin^- $IL33R^+$. Results display three independent experiments with three to five mice in each experimental group. All graphs display means ± SEM; ns (not significant) $p > 0.05$, * $p \leq 0.05$, ** $p \leq 0.01$, *** $p \leq 0.001$, **** $p \leq 0.0001$. Comparisons between two groups were analyzed by Welch's t-test.

In isolated ILC2 from IFNγ + IL-33–treated and IL-33 alone, ROS can be reduced in an overnight culture with ROS scavengers NAC and GSH (Figure 3.33A). However, the reduction in ROS was not able to rescue mitochondrial potential or mitochondrial mass (Figure 3.33B-C). In addition, neutralising ROS overnight was not sufficient to boost IL-5 and IL-13 production of ILC2s (Figure 3.33D-E). Overall, these findings demonstrate that acute IFNγ exerts a stronger impact on ILC2 metabolism than the chronic IFNγ environment induced by *T. muris* infection, yet both models share features of impaired lipid metabolism, mitochondrial dysfunction, and redox imbalance, which contributes to the suppression of ILC2 abundance and function.

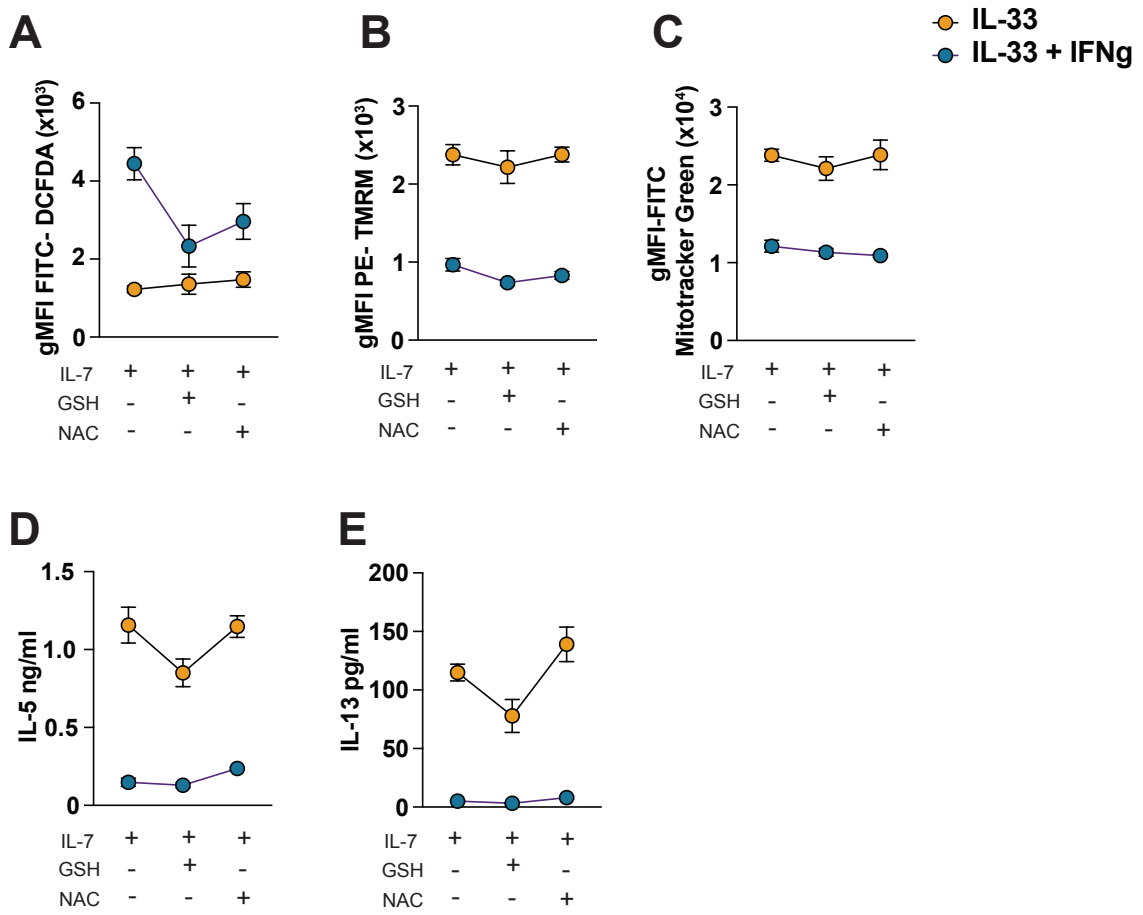

Figure 3.34: Neutralising ROS does not rescue mitochondrial potential or ILC2 function in an overnight culture. (A) gMFI values of DCFDA in ILC2 from IFNγ + IL-33 mice compared to IL-33-only controls. (B-C) gMFI values of TMRM and MitoTracker Green in ILC2 from IFNγ + IL-33 mice compared to IL-33-only controls. (D-E) IL-5 and IL-13 protein in supernatant quantified by LEGENDplex from IFNγ + IL-33 mice compared to IL-33-only controls. Results display one independent experiment with five mice in each experimental group. All graphs display means ± SEM. ILC2 were identified as $CD45^+$ $Thy1.2^+$ Lin^- $IL33R^+$.

3.8 Redox Imbalance Links Chronic *T. muris* Infection and IFNγ Signalling in ILC2

Using publicly available RNA-seq data from (Cautivo et al., 2022; Moro et al., 2016), we reanalyzed transcriptomic profiles of ILC2s isolated from IL-33 and IFNγ/IL-27-treated fat-associated lymphoid cluster (FALC) ILC2 and IL-33- and IFNγ-lung ILC2, focusing on genes linked to ILC2 metabolism. Interestingly, *Txnip* expression was elevated in FALC ILC2s exposed to both IFNγ/IL-27 and IL-33 compared with IL-33 alone (Figure 3.35A). *Txnip* expression was also upregulated in lung ILC2 from IL-33+IFNγ compared to IL-33 alone or IFNγ receptor–deficient ILC2s (Figure 3.35B). Suggesting that IFNγ signal in ILC2 can directly regulate TXNIP. TXNIP, a key regulator of cellular redox balance, promotes ROS accumulation by inhibiting thioredoxin (Trx) and can itself be induced by ROS, forming a feed-forward amplification loop (Mohamed et al., 2021). In both FALC and lung ILC2, IFNγ+IL-33 induced

increased *Nampt* expression. IL-27 + IL33 also induced an increase in *Nampt* expression. FALC ILC2 had an increase in *Slc1a5* with a decrease in *Slc38a1* similar to what we observe in ILC2 after intranasal administration of acute IFNγ+IL-33 (Figure 3.35A)(Moro et al., 2016). In contrast, lung ILC2s from (Cautivo et al., 2022) have decreased expression of *Slc1a5* and increased expression of *Slc38a1*(Figure 3.35B). The subtle differences in amino acid transporters could reflect the differences in the models used, as both our model and (Moro et al., 2016) is acute exposures, whereas they (Cautivo et al., 2022) examined the ILC2 two weeks after the last exposure to IL-33.

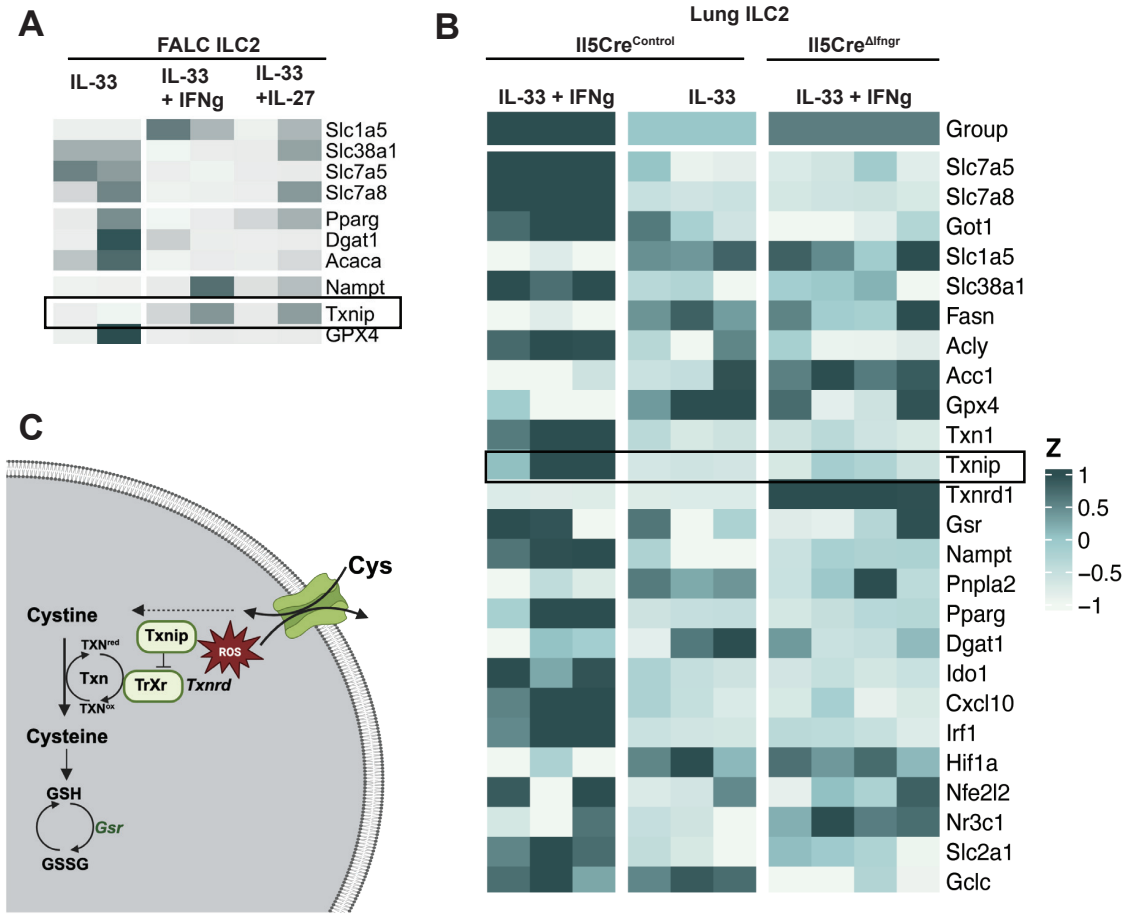

Figure 3.35: IFNγ alters redox proteins during mixed type 1/ type 2 inflammation. (A) Heatmaps of differentially expressed genes associated with amino acid signalling, lipid metabolism, and redox systems from FALC ILC2 in the presence of IL-33, IL-33+IFNγ/IL-27. (B) Heatmaps of differentially expressed genes associated with amino acid signalling, lipid metabolism, and redox systems from airway ILC2 in th presence of IL-33 and IL-33+IFNγ. Data reanalysed from (Moro et al., 2016) in (A) and (Cautivo et al., 2022) in (B). (C) Schematic of the thioredoxin system, including TXNIP.

In *T. muris*–infected + papain-challenged mice, isolated ILC2 have increased *Txnip* and *Gsr* expression in isolated lung ILC2s (Figure 3.36 A-B). Glutathione reductase (*gsr*), which regenerates reduced glutathione (Carlberg and Mannervik, 1985), was also increased, sug-

gesting an attempt at a compensatory response to oxidative stress. In parallel to this, a similar upregulation of *Txnip* and *Gsr* was observed in ILC2s from our in vivo model of IL-33 and IFNγ (Figure 3.36 C-D). This indicates that type 1–driven redox reprogramming is a shared feature across both models. *Gsr* was also upregulated in the ILC2 from (Cautivo et al., 2022) (Figure 3.35B). However, glutamate-cysteine ligase, catalytic subunit (*Gclc*) involved in the first step of glutathione synthesis (Ngo and Duennwald, 2022), is unchanged in ILC2 from chronic *T. muris*–infected + papain-challenged mice (Figure 3.36E) as well as ILC2 from IL-33 + IFNγ from (Cautivo et al., 2022) (Figure 3.35B). Nuclear factor erythroid 2-related factor 2 (*Nfe2l2*) a transcription factor that regulates a cell's response to oxidative stress, (Ngo and Duennwald, 2022) was unchanged in ILC2 from chronic *T. muris*–infected + papain-challenged mice compared to papain only (Figure 3.36F). In contrast, *Nfe2l2* is significantly upregulated in ILC2 from IL-33 and IFNγ compared to IL-33 alone. This comparison could reflect a threshold level of redox imbalance during acute IFNγ exposure compared to a more sustained exposure and metabolic adaptation of ILC2 during chronic *T. muris* infection and papain.

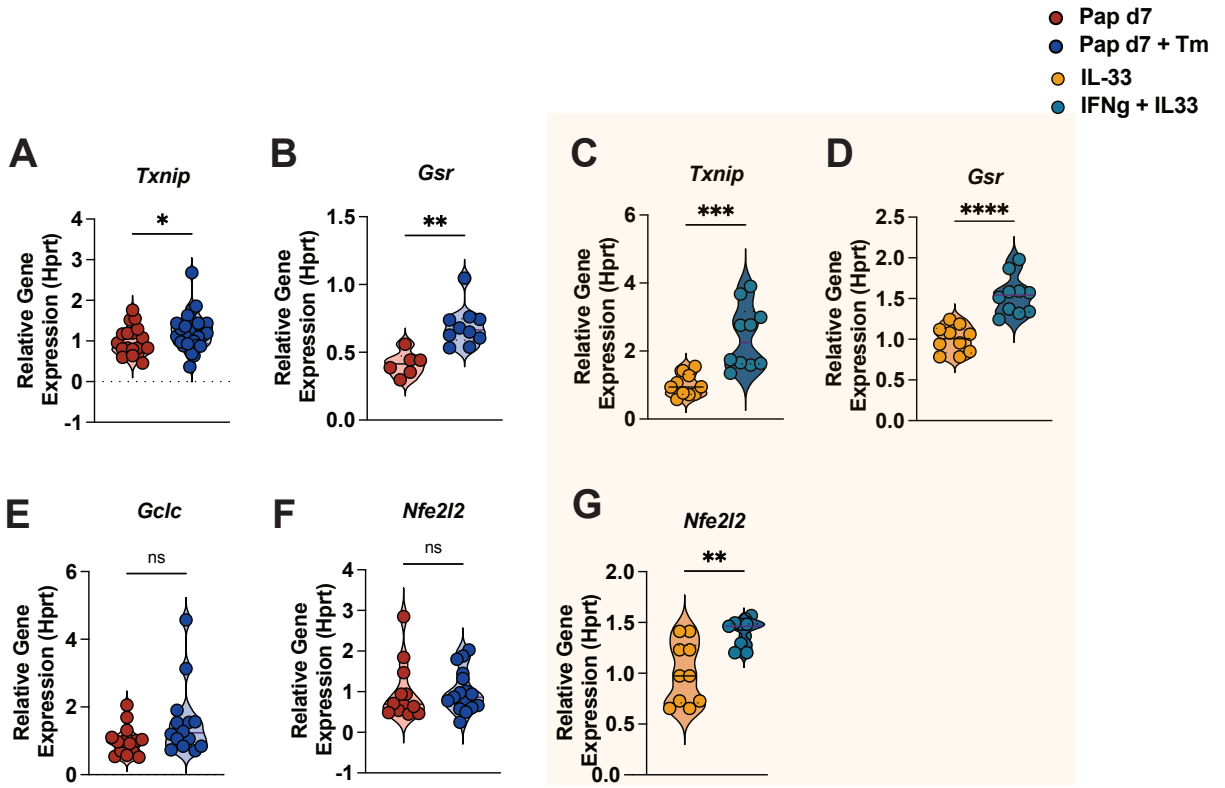

Figure 3.36: Chronic *T. muris* infection and IFNγ drive TXNIP upregulation during type 2 airway inflammation. (A-D) Gene expression of *Txnip* and *Gsr* in isolated ILC2 from *T. muris* and papain and IFNγ + IL-33 compared to papain only and IL-33 only. (E-F) Gene expression of *Gclc* and *Nfe2l2* in isolated ILC2 from *T. muris* and papain compared to papain only. (G) Gene expression of *Nfe2l2* in isolated ILC2 from IFNγ + IL-33 compared to IL-33 only. Results display three to four independent experiments with three to five mice in each experimental group. All graphs display means ± SEM; ns (not significant) $p > 0.05$, * $p \leq 0.05$, ** $p \leq 0.01$, *** $p \leq 0.001$, **** $p \leq 0.0001$. Comparisons between two groups were analyzed by Welch's t-test.

To investigate the role of increased TXNIP expression in ILC2 from chronic *T. muris*-infected mice and allergic asthma, we made use of the Red5 x Txnip$^{fl/lfl}$ mice. By crossing Red5 mice carrying a reporter for IL-5 expression and Cre recombinase under the endogenous Il5 locus to mice carrying a loxP-flanked TXNIP gene (Txnip$^{fl/lfl}$ mice), TXNIP is selectively ablated in IL-5-expressing cells. Results generated in our lab have shown that in naive mice and allergen-challenged mice, the majority of IL-5-producing cells (Red5+) are ILC2 (Wientjens et al., 2025). Red5 control mice will be referred to as ILC2^{WT} and ILC2 without TXNIP will be defined as ILC2$^{\Delta TXNIP}$. At steady-state, ILC2 and eosinophil numbers in ILC2$^{\Delta TXNIP}$ are comparable to ILC2^{WT} controls (Figure 3.37A-B). However, upon acute in vivo activation with IL-33, ILC2 and eosinophils are non significantly reduced in ILC2$^{\Delta TXNIP}$ compared to ILC2^{WT} controls (Figure 3.37C-D).

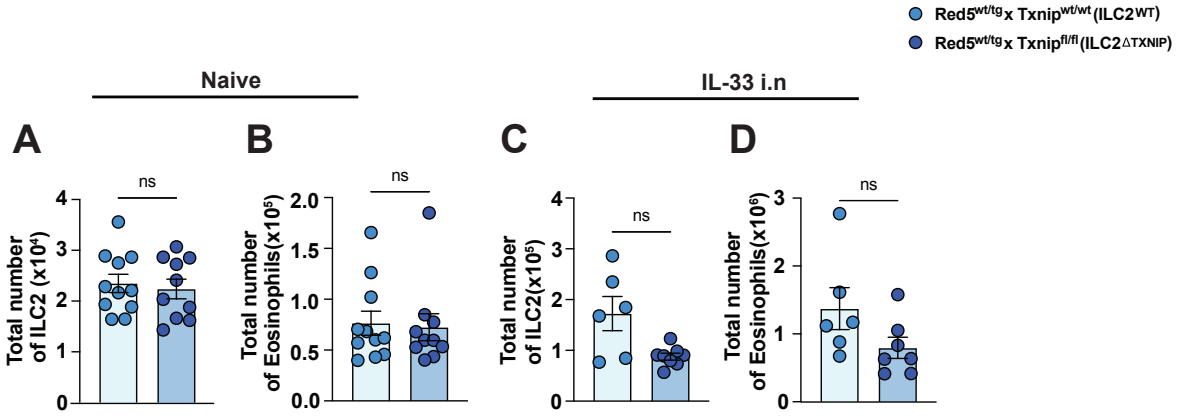

Figure 3.37: TXNIP KO in ILC2 does not impact steady-state or activated ILC2 numbers. (A-B) Total number of ILC2s and eosinophils from ILC2^{WT} and ILC2$^{\Delta TXNIP}$. (C-D) Total number of in vivo IL-33 activated ILC2 and eosinophils from ILC2^{WT} and ILC2$^{\Delta TXNIP}$. ILC2s were identified as CD45^{+} Thy1.2 $^{+}$ Lin^{-} GATA3^{+} in (A) and (C). Results display two independent experiments with three to five mice in each experimental group. All graphs display means ± SEM; ns (not significant) $p > 0.05$, * $p \leq 0.05$, ** $p \leq 0.01$, *** $p \leq 0.001$, **** $p \leq 0.0001$. Comparisons between two groups were analyzed by Welch's t-test.

As TXNIP expression was upregulated in ILC2 during acute papain and chronic *T. muris* infection and the acute model gave a more robust phenotype, we investigated the role of TXNIP at day 7 papain and chronic *T. muris* infection. ILC2$^{\Delta TXNIP}$ mice were infected with chronic *T. muris* and 21 days later were challenged with papain according to the schematic in (Figure 3.38A) and compared to controls. The absence of TXNIP in ILC2 did not prevent suppression of total ILC2 numbers during chronic *T. muris* infection and papain (Figure 3.38B). Equally, total eosinophil numbers were reduced in ILC2^{WT}Pap+Tm and ILC2$^{\Delta TXNIP}$Pap+Tm as compared with ILC2^{WT}Pap only (Figure 3.38C). Moreover, IL-5-producing ILCs were reduced in both ILC2^{WT}Pap+Tm and ILC2$^{\Delta TXNIP}$Pap+Tm as compared to ILC2^{WT}Pap only (Figure 3.38D-F). IL-5^{+}IL-13^{+} ILC were also significantly reduced in both ILC2^{WT}Pap+Tm and ILC2$^{\Delta TXNIP}$Pap+Tm compared to control in both percentage and total numbers (Figure 3.38G-H). In addition, IL-13 was reduced in the lung homogenate (Figure 3.38I). Cellular ROS was also increased in ILC2 from both groups exposed to *T. muris* (Figure 3.38J). These results indicate that although TXNIP is consistently upregulated in ILC2s during chronic *T. muris* infection and acute papain, TXNIP alone may not be sufficient to explain the redox imbalance and functional suppression observed in ILC2.

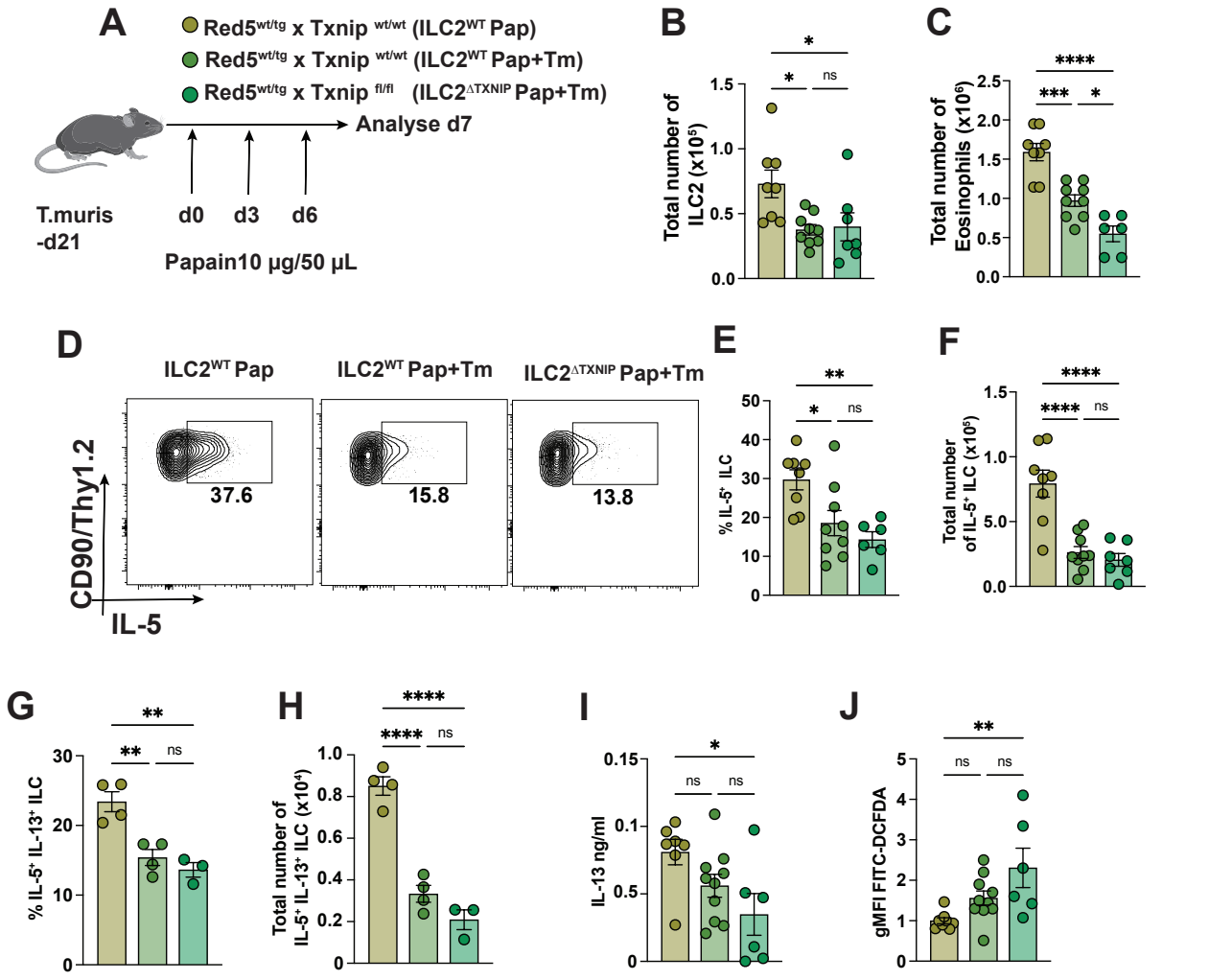

Figure 3.38: TXNIP KO in ILC2 does not prevent supression of ILC2 during chronic *T. muris* infection and papain. (A) Schematic of mouse infection model. (B-C) Total number of ILC2 and eosinophils from ILC2^{WT}Pap, ILC2^{WT}Pap+Tm, and ILC2$^{\Delta TXNIP}$Pap+Tm. (D-F) Percentage and total number of IL-5^{+} ILCs from ILC2^{WT}Pap, ILC2^{WT}Pap+Tm, and ILC2$^{\Delta TXNIP}$Pap+Tm. (G-H) Percentage and total number of IL-5^{+}IL-13^{+} ILC from ILC2^{WT}Pap, ILC2^{WT}Pap+Tm, and ILC2$^{\Delta TXNIP}$Pap+Tm. (I) IL-13 protein detected using LEGENDplex in the lung homogenate from ILC2^{WT}Pap, ILC2^{WT}Pap+Tm, and ILC2$^{\Delta TXNIP}$Pap+Tm. (J) Cellular ROS measured in ILC2 by flow cytometry from ILC2^{WT}Pap, ILC2^{WT}Pap+Tm, and ILC2$^{\Delta TXNIP}$Pap+Tm. ILC2s were identified as CD45^{+} Thy1.2 $^{+}$ Lin^{-} GATA3^{+} in (B). ILC2s were identified as CD45^{+} Thy1.2 $^{+}$ Lin^{-} IL33R^{+} in (J). Results display two independent experiments with three to five mice in each experimental group. All graphs display means ± SEM; ns (not significant) $p > 0.05$, * $p \leq 0.05$, ** $p \leq 0.01$, *** $p \leq 0.001$, **** $p \leq 0.0001$. One-way ANOVA with Tukey's multiple comparisons test

In vitro, isolated naive ILC2s have increased expression in *Txnip* when cultured with IFNγ and IL-33 compared to the IL-33 control (Figure 3.39A). Additionally, ILC2 express less *Slc1a5* when cultured with IFNγ and IL-33 as well as increased cellular ROS (Figure 3.39B-C). Thus a reduction of *Slc1a5* may reduce the availability of glutamine and cysteine in the ILC2s that is needed to handle the increase in ROS.

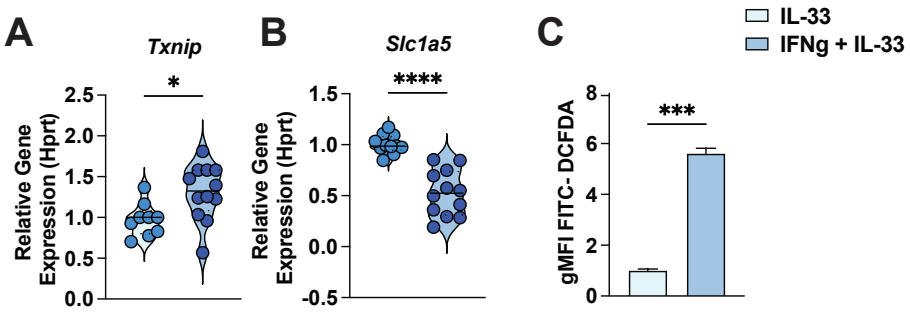

Figure 3.39: TXNIP is increased in ILC2 after in vitro culture with IL-33 and IFNγ. (A) Gene expression of *Txnip* in ILC2 cultured with a combination of IL-7 and IL-33 with/without IFNγ. (B) Gene expression of *Slc1a5* in ILC2 cultured with a combination of IL-7 and IL-33 with/without IFNγ. (C) gMFI values of DCFDA in ILC2 with a combination of IL-7 and IL-33 with/without IFNγ. ILC2s were identified as $CD45^+$ $Thy1.2^+$ Lin^- $IL33R^+$ in (C). Results display three independent experiments (A-B) and two independent experiments (C) with five mice in each experimental group. All graphs display means ± SEM; ns (not significant) $p > 0.05$, * $p \leq 0.05$, ** $p \leq 0.01$, *** $p \leq 0.001$, **** $p \leq 0.0001$. Comparisons between two groups were analyzed by Welch's t-test.

As chronic *T. muris* infection is a more complex environment, we wanted to investigate if direct IFNγ signalling in the absence of TXNIP can restore ILC2 numbers in vitro and in vivo. Naive ILC2 from $ILC2^{\Delta TXNIP}$ and $ILC2^{WT}$ were sorted and cultured for four days in the presence of IL-33 and IL-7 with or without IFNγ. $ILC2^{\Delta TXNIP}$ and $ILC2^{WT}$ had comparable expansion in numbers after activation with IL-33 (Figure 3.40A). Additionally, proliferation was also comparable in both groups (Figure 3.40B). The combination of IFNγ and IL-33 suppressed both total numbers and proliferation of $ILC2^{\Delta TXNIP}$ and $ILC2^{WT}$(Figure 3.40A-B). Production of cytokines also remained intact between $ILC2^{\Delta TXNIP}$ and $ILC2^{WT}$ after activation of IL-33 (Figure 3.40C-D). Upon the addition of IFNγ, both groups reduced secretion of IL-5 and IL-13.

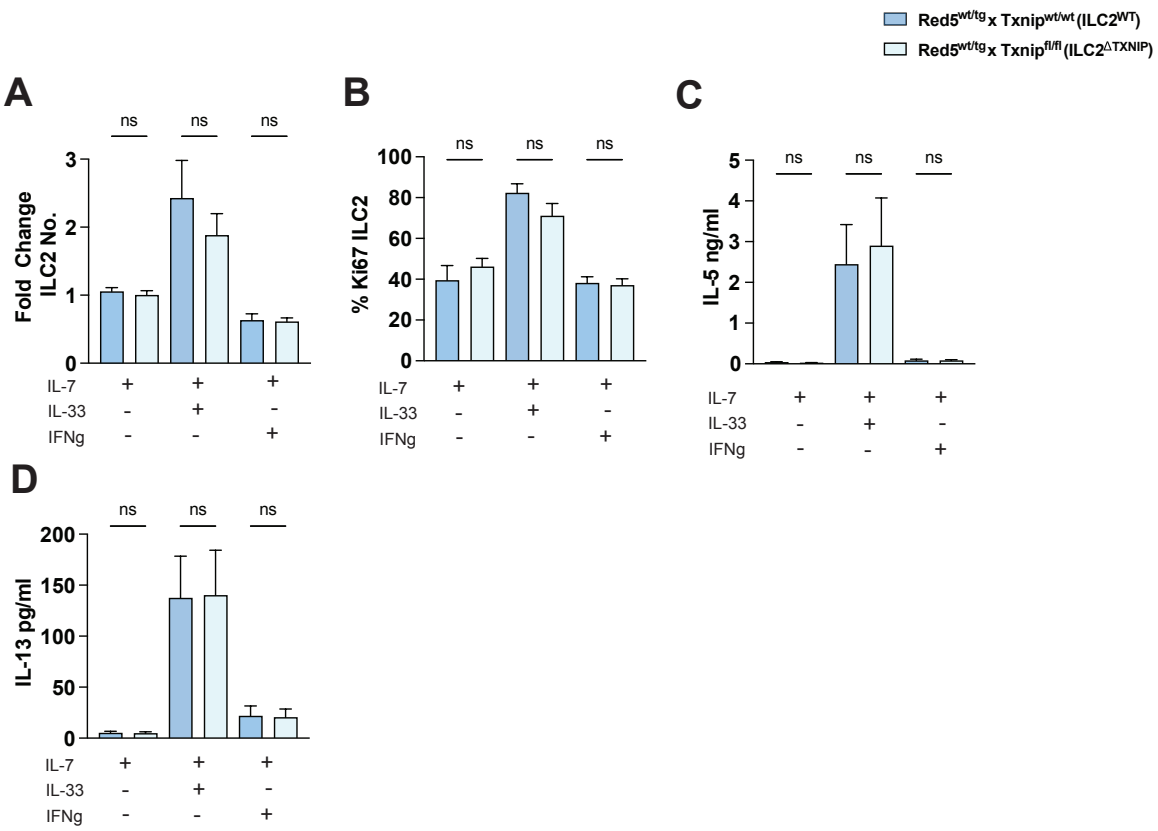

Figure 3.40: TXNIP KO in ILC2 does not prevent IFNγ-induced suppression in vitro. (A) Normalised cell counts of ILC2 from in vitro culture of ILC2$^{\Delta TXNIP}$ and ILC2^{WT} in combination of IL-33 + IL-7 with/without IFNγ. (B) Ki67^{+} percentage of ILC2 from in vitro culture of ILC2$^{\Delta TXNIP}$ and ILC2^{WT} in combination of IL-33 + IL-7 with/without IFNγ. (C-D) IL-5 and IL-13 measured in the supernatant by LEGENDplex. ILC2s were identified as CD45^{+} Thy1.2 $^{+}$ Lin^{-} GATA3^{+}. Results display three independent experiments with five mice in each experimental group. All graphs display means ± SEM; ns (not significant) $p > 0.05$, * $p \leq 0.05$, ** $p \leq 0.01$, *** $p \leq 0.001$, **** $p \leq 0.0001$. Comparisons between two groups were analyzed by Welch's t-test.

Similarly, in vivo, using our model of acute IFNγ and IL-33 to induce a mixed type 1/ type 2 response in the airways, ILC2$^{\Delta TXNIP}$IL-33 + IFNγ and ILC2^{WT}IL-33 + IFNγ did not prevent IFNγ-induced suppression of ILC2 and eosinophils in the lungs compared to ILC2^{WT}IL-33 only (Figure 3.41B-C).

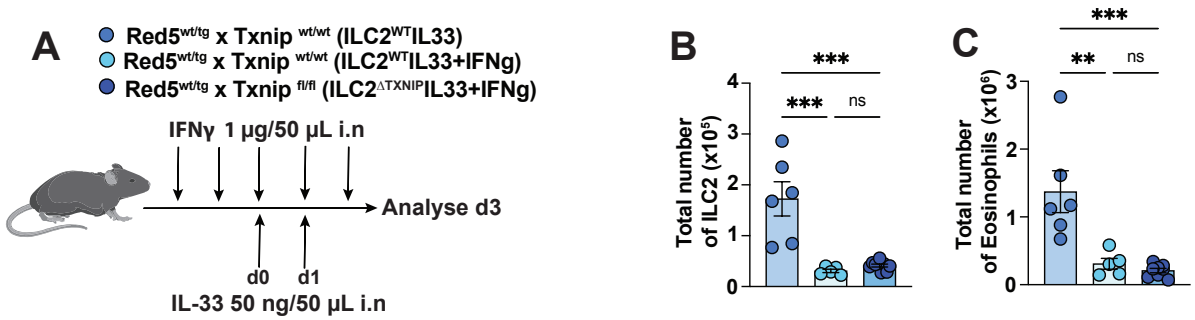

Figure 3.41: TXNIP KO in vivo does not prevent IFNγ-induced suppression during mixed type 1/type 2 airway inflammation. (A) Schematic model showing induction of type 1/type 2 inflammation. (B-C) Total lung ILC2 and eosinophil numbers from $ILC2^{WT}$ IL-33, $ILC2^{WT}$ IL-33+IFNγ, and $ILC2^{\Delta TXNIP}$ IL-33+IFNγ. ILC2s were identified as $CD45^+$ $Thy1.2^+$ Lin^- $GATA3^+$. Results display two independent experiments with three to five mice in each experimental group. All graphs display means ± SEM; ns (not significant) $p > 0.05$, * $p \leq 0.05$, ** $p \leq 0.01$, *** $p \leq 0.001$, **** $p \leq 0.0001$. Comparisons between two groups were analyzed by Welch's t-test.

Effective induction of Cre recombinase in the Il5cre mice used for the TXNIP model requires Il5 to be transcribed after activation of ILC2 (Nussbaum et al., 2013). As this may be a limitation to the model, we examined the effects of TXNIP regulator, SRI-37330, on cell proliferation and function in the context of IFNγ and IL-33. SRI-37330 blocks the E-Box promoter region of TXNIP and prevents transcription of TXNIP in a dose-dependent manner in islet pancreas cells under high glucose conditions (Thielen et al., 2020). However, we observed in a preliminary experiment that *Txnip* in ILC2 is reduced at the literature-reported IC50 value and did not decrease further at increasing concentrations (Figure 3.42A). *Txnip* upregulation in certain cell types is a negative regulator of glucose transporter *Slc2a1*. Indeed, Thielen et al. (2020) observed that by blocking TXNIP translation, SRI-37330 enabled the upregulation of *Slc2a1*. However, in vitro ILC2 in the presence of IFNγ downregulate *Slc2a1* and this was not rescued by SRI-37330 (Figure 3.42B).

As the IC50 value of SRI-37330 was able to lower TXNIP expression to similar levels as IL-33 only in ILC2, we examined its effects on cell number and function. ILC2 cultured with SRI-37330 were modestly increased in number, albeit nonsignificantly, and remained significantly lower than IL-33 only (Figure 3.42D). Although proliferation was slightly increased upon SRI-37330 treatment compared to IFNγ and IL-33, a full rescue was not achieved (Figure 3.42E). Finally, IL-5 and IL-13 production measured in the supernatant was modestly increased with SRI-37330 but remained significantly reduced when compared to IL-33 only (Figure 3.42F-

G). Overall these data indicate that impairment of TXNIP expression in ILC2, either by genetic modification or in the form of small molecules such as SRI-37330, does not protect ILC2 from IFNγ-induced redox imbalance and suppression.

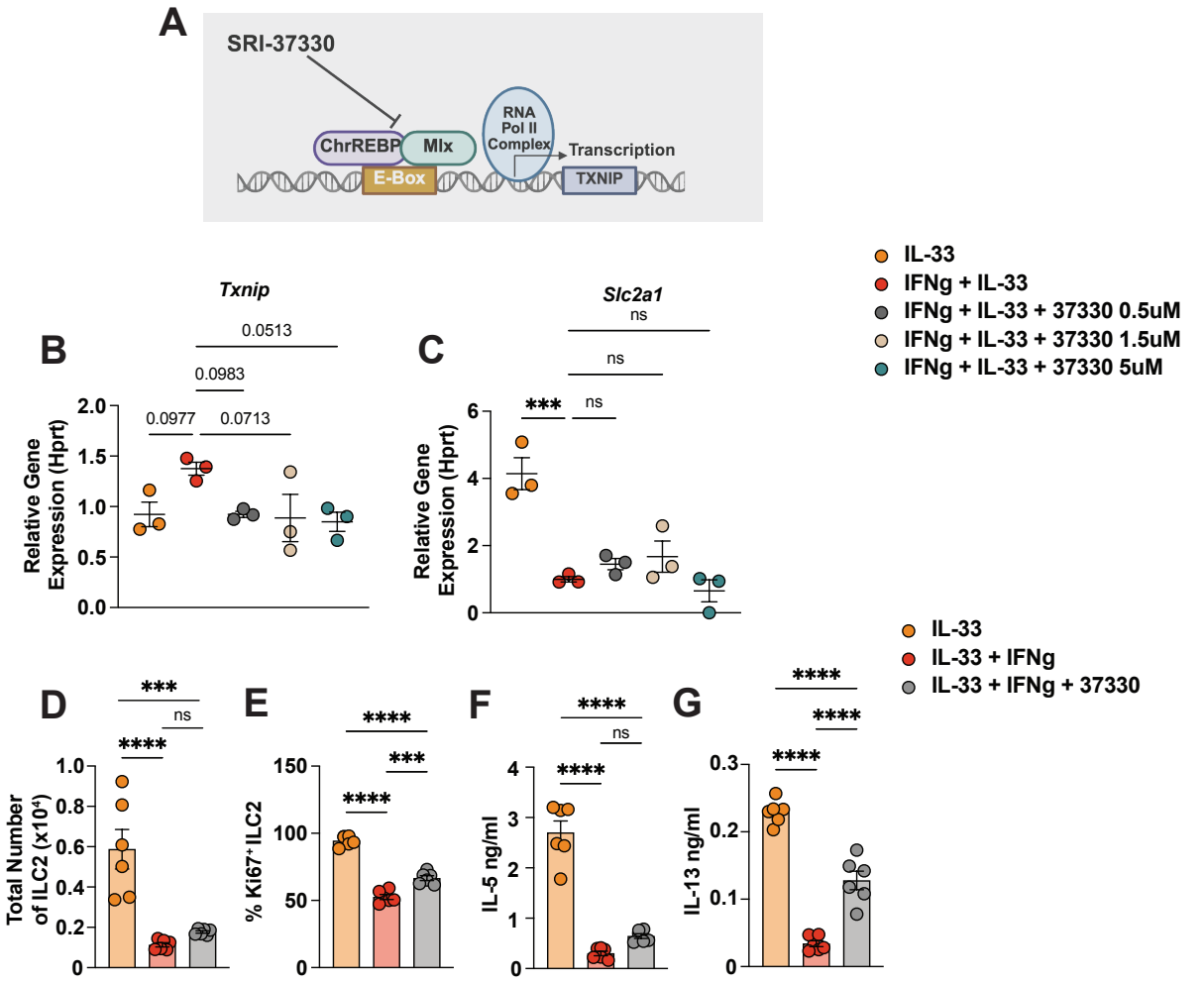

Figure 3.42: Small molecule regulator of TXNIP, SRI-37330, does not rescue ILC2 from IFNγ-induced suppression. (A) Schematic of the proposed mechanism of action of SRI-37330 on regulating TXNIP mRNA. (B-C) Gene expression of *Txnip* and *Slc2a1* in in vitro activated ILC2 cultured in a combination of IL-33 + IL-7 with/without IFNγ and varying concentrations of SRI-37330. (D-E) Total number and proliferative capacity of ILC2 after culturing in a combination of IL-33 + IL-7 with/without IFNγ and SRI-37330. (F-G) Supernatant IL-5 and IL-13 were measured by LEGENDplex. ILC2s were identified as $CD45^+$ $Thy1.2^+$ Lin^- $GATA3^+$. Results display two to three independent experiments with five mice in each experimental group. All graphs display means ± SEM; ns (not significant) $p > 0.05$, * $p \leq 0.05$, ** $p \leq 0.01$, *** $p \leq 0.001$, **** $p \leq 0.0001$. One-way ANOVA with Tukey's multiple comparisons test.

3.9 Redox Balancing Can Protect ILC2 from IFNγ-induced suppression but Does Not Restore All Aspects of Metabolism

While TXNIP increase alone is not accounting for the total suppression of ILC2, it is clear that ILC2 in the presence of an IFNγ-rich environment experiences significant oxidative stress and impaired redox balancing. Moreover, the reduced expression of amino acids, including glutamine transporters *Slc38a1* in vivo and *Slc1a5* in vitro, could be contributing to a reduced synthesis of glutathione GSH, and the ILC2 may have impaired reducing equivalents. We sought to examine if the antioxidants NAC (precursor for GSH) and GSH itself could prevent reduction in ILC2 numbers by balancing ROS. As one limitation of naive in vitro culture is the low cell number of ILC2 in naive mice, ILC2 were activated in vivo with intranasal IL-33 to maximise the number of ILC2. IFNγ can suppress ILC2 in vivo that have already been activated by IL-33, thus we hypothesised the same could be true in vitro (Moro et al., 2016).

$ST2^+$ ILCs were sorted and cultured for 72 hours with IL-7 (ctrl) or a combination of IL-7 and IFNγ with/without GSH or NAC. In vivo activated ILC2 numbers were repressed by IFNγ, which was rescued by either GSH and NAC (Figure 3.43A). Additionally, increased ROS was observed in ILC2 in the presence of IFNγ which was reduced by the presence of GSH and NAC (Figure 3.43B). The rescue of ILC2 production of IL-5 produced a split phenotype where GSH and NAC either completely restored IL-5 function or did not (Figure 3.43C). In contrast to this, IL-13 production was sufficiently rescued by the presence of GSH and NAC with IFNγ (Figure 3.43D). IFNγ suppressed the expression of CD71 on in vivo activated ILC2 compared to control, which could be partially rescued by the presence of GSH and NAC (Figure 3.43E). CD98 expression was also suppressed by IFNγ but this could not be rescued by GSH and NAC (Figure 3.43F). As increased expression of CD98 and CD71 are linked with mTOR signalling (De Federicis et al., 2024; Yang et al., 2013; Zheng et al., 2020), we hypothesised that a decrease in both induced by IFNγ signalling in ILC2 may disrupt mTOR signalling. Indeed, IFNγ modestly suppressed phospho mTOR and the downstream target phosphorylated S6 ribosomal protein (pS6) signalling in ILC2 (Figure 3.43G-H). The expression of both phospho mTOR and pS6 was not restored by GSH and NAC treatment (Figure 3.43G-H). In addition, IFNγ reduced *c-Myc*, which is closely linked to mTOR regulation and amino acid import in activated ILC2 (Panda et al., 2022).

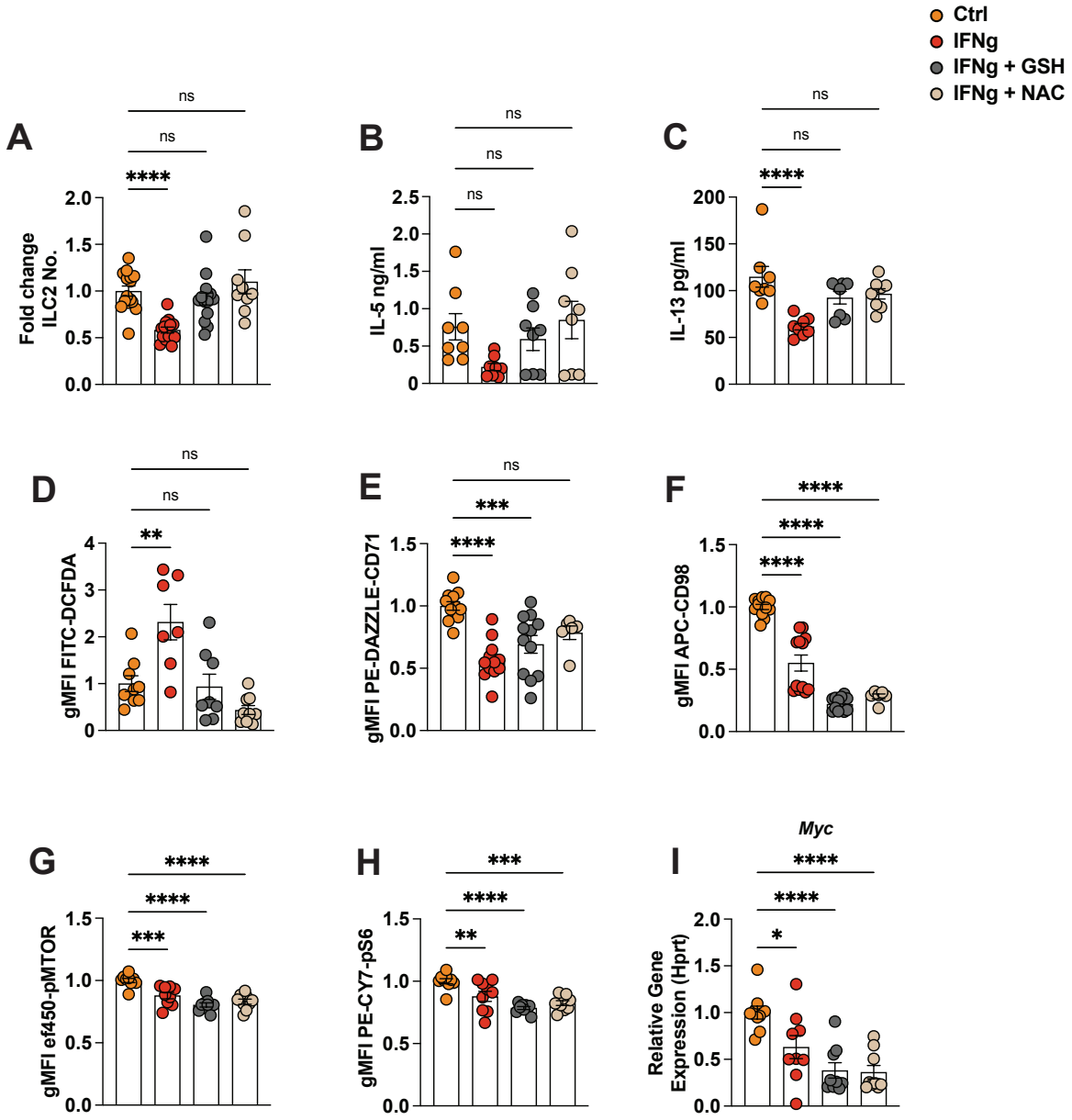

Figure 3.43: Buffering ROS can rescue IFNγ-induced suppression of in vivo activated ILC2. (A) Normalised counts of ILC2 in culture with IL-7 with/without IFNγ and GSH/NAC. (B-C) IL-5 and IL-13 were measured in the supernatant by LEGENDplex. (C) gMFI values of DCFDA in ILC2. (E-F) gMFI values of CD71 and CD98 expression on ILC2 from Ctrl, IFNγ, IFNγ + GSH/NAC. (G-H) gMFI values of phospho mTOR and phoso S6 on ILC2 from Ctrl, IFNγ, IFNγ + GSH/NAC. (I) Gene expression of *c-Myc* mRNA expression in ILC2 from Ctrl, IFNγ, IFNγ + GSH/NAC. ILC2s were identified as $CD45^+$ $Thy1.2^+$ Lin^- $GATA3^+$ (A). ILC2s were identified as $CD45^+$ $Thy1.2^+$ Lin^- $IL33R^+$ (D-H). Results display three independent experiments with five mice in each experimental group. All graphs display means ± SEM; ns (not significant) $p > 0.05$, * $p \leq 0.05$, ** $p \leq 0.01$, *** $p \leq 0.001$, **** $p \leq 0.0001$. One-way ANOVA with Tukey's multiple comparisons test.

Increased *Nampt* expression appears to be an effect of IFNγ signalling in ILC2 and in vivo activated ILC2 cultured with IFNγ also have increased *Nampt* and expression was not de-

creased by GSH or NAC (Figure 3.44A). In addition, mitochondrial membrane potential was reduced by IFNγ, but balancing ROS with GSH and NAC could not restore the mitochondrial potential (Figure 3.44B). Thus, increased ROS can contribute to cell loss, but mitochondrial dysfunction and possible NAD^+ stress cannot be buffered by reduced ROS in this model. Interestingly, *Txnip* expression is not upregulated in in vivo activated ILC2 cultured with IFNγ suggesting a more complex regulation of *Txnip* that may depend on activation kinetics (Figure 3.44C). However, this may indicate the increase in ROS induced by IFNγ in this context is not driven by *Txnip* upregulation but instead through another pathway, which requires further investigation. Unsurprisingly, culturing ILC2 induced phospho STAT1 expression as well as increased *Irf1* mRNA expression in the ILC2 cultured with IFNγ, including the conditions with GSH and NAC (Figure 3.44D-E). This could highlight that while buffering ROS is important for cell numbers and function in ILC2, STAT1 signalling is governing another pathway of repression that may repress mTOR as well as disrupt mitochondrial function in ILC2.

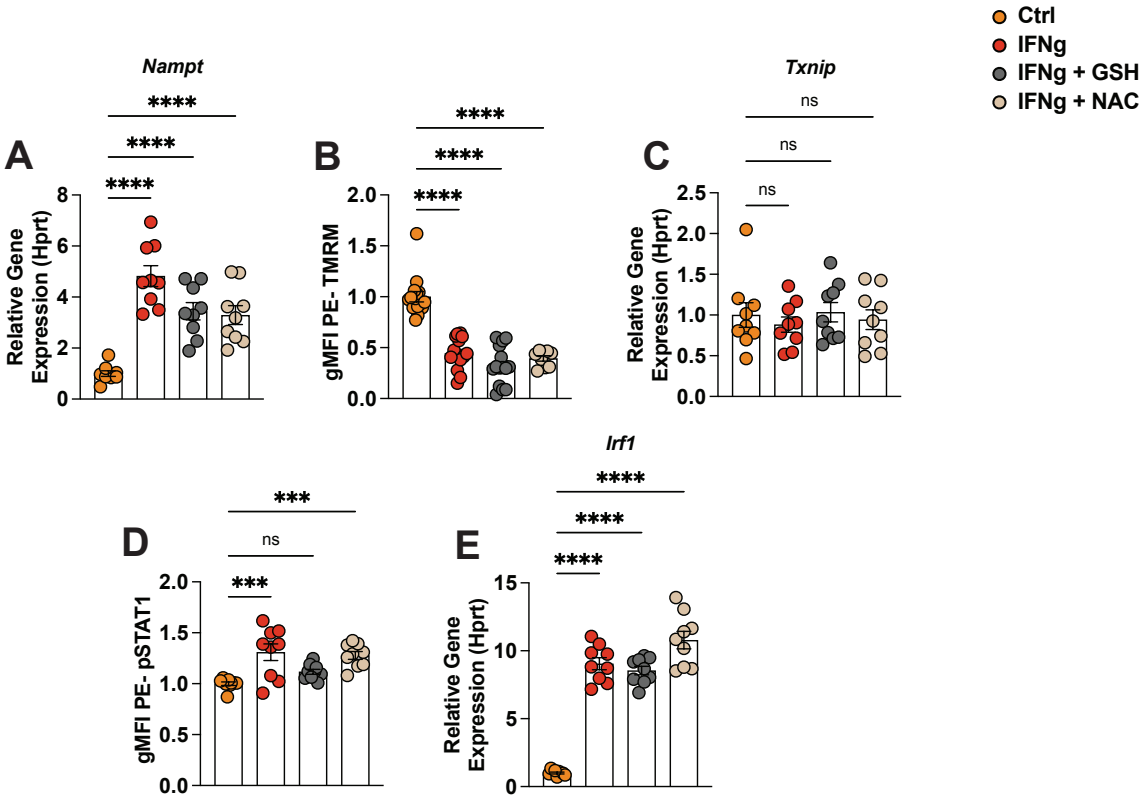

Figure 3.44: Buffering ROS cannot prevent mitochondrial dysfunction and NAD$^+$ stress. (A) Gene expression of *Nampt* in ILC2 from Ctrl, IFNγ, IFNγ + GSH/NAC. (B) gMFI values of TMRM in ILC2 from Ctrl, IFNγ, IFNγ + GSH/NAC. (C) Gene expression of *Txnip* in ILC2 from Ctrl, IFNγ, IFNγ + GSH/NAC. (D) gMFI values of phospho STAT1 in ILC2 from Ctrl, IFNγ, IFNγ + GSH/NAC. (E) Gene expression of *Irf1* in ILC2 from Ctrl, IFNγ, IFNγ + GSH/NAC. ILC2s were identified as CD45$^+$ Thy1.2 $^+$ Lin$^-$ IL33R$^+$ (B) and (D). Results display three independent experiments with five mice in each experimental group. All graphs display means ± SEM; ns (not significant) $p > 0.05$, * $p \leq 0.05$, ** $p \leq 0.01$, *** $p \leq 0.001$, **** $p \leq 0.0001$. One-way ANOVA with Tukey's multiple comparisons test.

Understanding the role of activating cytokines such as IL-2 and IL-33 in driving metabolic programmes in ILC2 is important to consider. Culturing naive ILC2 with a combination of IL-33 and IL-7 with/without IFNγ and GSH or NAC, boosted ILC2 numbers and proliferation (Figure 3.45A-B). However, IL-5 production was only mildly rescued, whereas IL-13 was fully rescued with GSH and partially rescued by NAC (Figure 3.45C-D). Lipid droplet formation was also boosted in the conditions supplemented with GSH and NAC, suggesting restored lipid metabolism (Figure 3.45E). Furthermore, mitochondrial membrane potential was mildly increased in the presence of GSH and NAC compared to IL-33+IFNγ (Figure 3.45F). However, like the in vivo activated ILC2, supplementation with NAC and GSH did not restore CD98 expression (Figure 3.45G). Furthermore, CD71 expression was only rescued by NAC and not GSH, although further experiments are required to confirm this phenotype (Figure 3.45G). Collectively this data highlights that balancing ROS can rescue ILC2 numbers in the

presence of survival factor IL-7 alone, but STAT1 signalling dominates and prevents active metabolism. However, when ILC2 have activating cytokines such as IL-33, GSH and NAC can restore certain aspects of ILC2 metabolism, including lipid metabolism and mitochondrial potential, as well as partial functional rescue. These results support a model in which IFNγ signalling exerts dual control over ILC2, coupling transcriptional repression with sustained metabolic and redox imbalance that limits lipid metabolism and effector function.

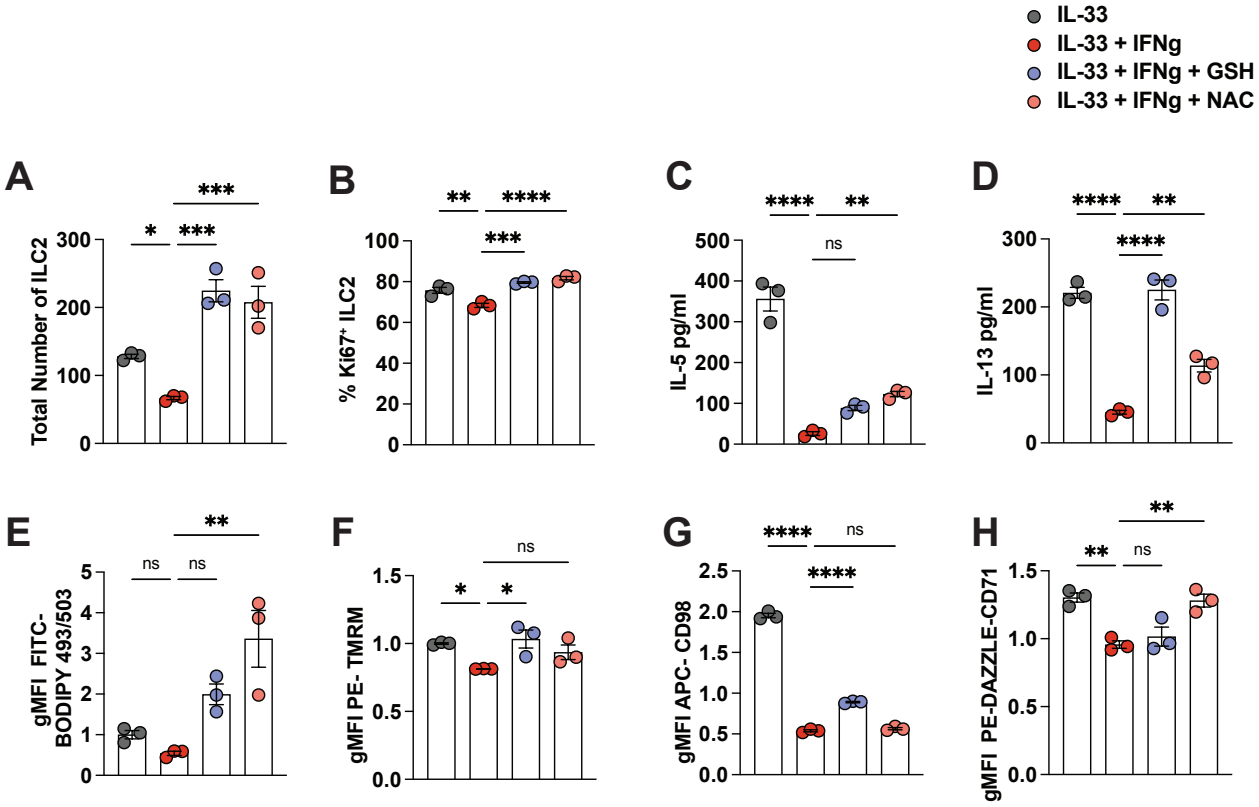

Figure 3.45: Activating cytokine IL-33 can boost rescue with GSH and NAC. (A) Total ILC2 numbers of naive ILC2 cultured with IL-33+IL-7 and a combination of IFNγ and GSH or NAC. (B) Percentage of Ki67$^+$ of ILC2 from IL-33, IL-33 + IFNγ, IL-33 + IFNγ + GSH/NAC. (C-D) IL-5 and IL-13 in the supernatant measured using LEGENDplex from IL-33, IL-33 + IFNγ, IL-33 + IFNγ + GSH/NAC. (E) gMFI values of BODIPY 493/503 in ILC2 from IL-33, IL-33 + IFNγ, IL-33 + IFNγ + GSH/NAC (F) gMFI values of TMRM in ILC2 from IL-33, IL-33 + IFNγ, IL-33 + IFNγ + GSH/NAC. (G-H) gMFI values of CD98 and CD71 expression on ILC2 from IL-33, IL-33 + IFNγ, IL-33 + IFNγ + GSH/NAC. ILC2s were identified as CD45$^+$ Thy1.2 $^+$ Lin$^-$ GATA3$^+$ (A-B) and (E). ILC2s were identified as CD45$^+$ Thy1.2 $^+$ Lin$^-$ IL33R$^+$ (F-H). Results display a representative of three independent experiments with five mice in each experimental group. All graphs display means ± SEM; ns (not significant) $p > 0.05$, * $p \leq 0.05$, ** $p \leq 0.01$, *** $p \leq 0.001$, **** $p \leq 0.0001$. One-way ANOVA with Tukey's multiple comparisons test.

4. Discussion

The incidence of chronic inflammatory diseases such as asthma has increased markedly over the past century, coinciding with industrialisation, changes in diet, and altered exposure to microbes and parasites (Adolph and Tilg, 2024; Stiemsma et al., 2015). This observation is the basis of the hygiene hypothesis and more recently the “old friends” hypothesis, which proposes that reduced exposure to helminths and other pathogens contributes to dysregulated immune responses and increased susceptibility to allergic disease. Parasitic helminths, despite eliciting strong type 2 immune responses that promote their clearance, have evolved sophisticated strategies to dampen host immunity and enable chronic infection. While adaptive Th2 cells are central to the development and maintenance of allergic memory, ILC2 play a crucial role in the initiation and amplification of allergic airway inflammation. ILC2 rapidly respond to epithelial-derived cytokines such as IL-33, IL-25, and TSLP, and their activation shapes downstream adaptive responses. Consequently, understanding how helminths modulate ILC2 function is essential for elucidating mechanisms of helminth-mediated protection against allergic disease. Chenery et al. (2016) previously demonstrated that chronic *T. muris* protects mice from allergic airway inflammation in both papain and HDM models. Although that study did not report a reduction in ILC2 numbers in bronchoalveolar lavage fluid, it clearly established chronic *T. muris* as a modulator of allergic pathology. Building on this work, we aimed to define the cellular and metabolic mechanisms by which chronic *T. muris* suppresses allergic airway inflammation, with a particular focus on ILC2 and their metabolic regulation.

Using both acute and chronic papain models of allergic airway inflammation, we demonstrated that chronic *Trichuris muris* results in a reduction in airway inflammation, characterised by decreased eosinophil infiltration, reduced type 2 cytokine production, and diminished expansion of ILC2 in the lung. In contrast to Chenery et al. (2016) that assessed ILC2 in bronchoalveolar lavage fluid, analysis of lung tissue in this model revealed a significant reduction in lung-resident ILC2 numbers and effector function. This discrepancy may reflect differences in tissue compartmentalisation, as lung tissue more accurately captures the resident ILC2 population that drives local inflammatory responses. In addition to reduced immune cell infiltration, chronic *T. muris* infection altered the lung structural cell compartment. Expression of genes associated with extracellular matrix remodelling and fibrosis was reduced, and IL-33 protein levels in lung homogenates were significantly reduced. As structural cells such as epithelial cells and fibroblasts provide cytokine signals and a structural

framework that support ILC2 activation and expansion (Atakkatan et al., 2025; Dahlgren et al., 2019), these changes suggest that chronic *T. muris* infection can remodel the lung microenvironment in a manner that is less favourable for type 2 inflammation. While these changes are also occurring at the structural level, this impacts tissue-resident cells such as ILC2 that are in close contact with the structural cell compartment, and their activation relies on cytokines and nutrients provided by the tissue niche.

Indeed, like all immune cells, ILC2 activation and proliferation are tightly coupled to cellular metabolism, and the current literature suggests that metabolic rewiring is required to sustain pathogenic ILC2 responses during allergic inflammation (Hodge et al., 2023; Hurrell et al., 2024; Karagiannis et al., 2020; Monticelli et al., 2016; Wientjens et al., 2025). In the context of chronic *T. muris* infection, ILC2 displayed a distinct metabolic phenotype that impaired their proliferation and effector function. Importantly, however, this phenotype does not support a model of global metabolic shutdown. Translational capacity, assessed by puromycin incorporation, remained intact in ILC2 from chronic *T. muris*–infected mice, indicating that these cells retain the capacity for protein synthesis. Equally, glycolytic capacity, measured by extracellular acidification rate, was preserved despite reduced ILC2 expansion. Oxygen consumption rate analyses revealed only modest impairments in mitochondrial respiration, further suggesting that ILC2 are not in complete metabolic failure. Thus, the environment induced by chronic *T. muris* infection is imposing a metabolic constraint on the ILC2 which is preventing full effector capacity and proliferation. The SCENITH™ assay indicated that although ILC2 from chronically *T. muris*-infected mice are functionally impaired, they retain metabolic flexibility. However, this assay is performed under nutrient-replete conditions, providing all major substrates required to support cellular metabolism. An important step to further define the nature of this metabolic constraint could be to assess ILC2 responses under selective nutrient limitation. Single nutrient depletion or add-back assays could help determine whether lung ILC2 during chronic *T. muris* infection exhibit stable metabolic alterations or heightened dependence on specific nutrient pathways during activation.

Amino acid availability is a critical regulator of ILC2 activation, proliferation, and redox homeostasis (Hodge et al., 2023; Panda et al., 2022; Wientjens et al., 2025). To determine whether altered amino acid signalling contributes to ILC2 suppression during chronic *T. muris* infection, expression and functional activity of key amino acid transporters were examined. In ILC2 isolated from *T. muris*–infected mice, expression of *Slc7a8* (LAT2) was modestly increased, while expression of *Slc7a5* (LAT1) remained unchanged. LAT transporters mediate

uptake of large neutral amino acids as well as function as antiporters, requiring intracellular exchange substrates to facilitate transport. *Slc7a8* imports arginine and large neutral amino acids and is important for homeostasis and activation of ILC2 (Panda et al., 2022). While the amino acid arginine was not significantly altered in the metabolomics of the lung tissue, immune cells such as NK cells, myeloid cells and T cells also use arginine for proliferation and function. The competition for arginine may deprive the ILC2 of adequate arginine levels, causing an upregulation in transporter expression to optimise availability (Martí et al., 2021). While *Slc7a5* transcript levels were preserved, they displayed altered transporter function, as uptake of kynurenine, a commonly used proxy for LAT-mediated amino acid transport, was modestly reduced in ILC2 from chronic *T. muris*-infected mice. This reduction occurred despite unchanged expression of CD98, the heavy chain that heterodimerises with *Slc7a5*, which may suggest that impaired uptake reflects functional constraints rather than loss of transporter expression. Because LAT1-mediated import of kynurenine requires glutamine efflux, reduced availability of intracellular glutamine could limit kynurenine uptake even when transporter expression is maintained (Meier et al., 2002). In support of this interpretation, expression of *Slc1a5*, which preferentially transports glutamine but also transports cysteine and is implicated in pathogenic ILC2 responses, was reduced in ILC2 during chronic *T. muris* infection (Wientjens et al., 2025). In addition, functional uptake of the *Slc1a5*-transported amino acid analogue AHA was also decreased. Together, these findings suggest that glutamine or cysteine import capacity may be constrained in ILC2 during chronic *T. muris* infection and allergic asthma. Cystine uptake is important to support redox balance and lipid metabolism in activated ILC2 and cystine uptake appeared comparable between ILC2 from *T. muris*-infected mice and papain-only mice. This indicates that cystine import is not impaired and suggests that redox imbalance in ILC2 is unlikely to arise solely from defective cystine. However, it is possible that this reveals a sensitivity to glutamine depletion within the cell. 13-C glutamine tracing or untargeted metabolomics would more accurately reveal such nutrient depletion within the ILC2.

While amino acid metabolism plays a significant role in ILC2 activation, the availability of glucose and the switch to glycolysis are common features of activated immune cells during inflammation. While glucose availability in the lung is tightly regulated under homeostatic conditions to prevent bacterial overgrowth, it increases during inflammation due to enhanced vascular permeability and epithelial barrier disruption (Baker and Baines, 2018; Roth-Walter et al., 2024). In the papain model of allergic airway inflammation, glucose concentrations in lung homogenates were elevated, consistent with tissue damage and inflammation. This

increase was modestly reduced in mice chronically infected with chronic *T. muris* infection. However, this reduction in lung glucose is unlikely to reflect direct glucose sequestering by the helminth infection. Although *T. muris* has a specialised glucose uptake structure known as a bacillary band, it does not fully develop until the adult stage of infection (around day 32). Mice in this study were sacrificed at day 28 post-infection, when worms remain in a late larval stage. Additionally, early larval stage 1 of *T. muris* have been reported to rely minimally on glucose metabolism compared to other nutrients, making helminth-mediated glucose depletion an unlikely explanation for reduced lung glucose levels (Hansen et al., 2016). While we are dealing with larval stage 4, this reflects different nutrient requirements of the helminth at various developmental stages. Instead, the reduced glucose concentration more likely reflects attenuated airway inflammation and reduced tissue damage in *T. muris*–infected mice. Consistent with preserved glucose utilisation by ILC2, expression of the glucose transporter *Slc2a1* (Glut1) remained unchanged in both lung tissue and isolated ILC2, and expression of *Arg1*, which is linked to glycolytic regulation in ILC2, was also stable (Monticelli et al., 2016). Functional assessment of glycolysis by extracellular acidification rate demonstrated preserved glycolytic capacity in ILC2 from *T. muris*–infected mice. Together, these data indicate that glucose uptake and glycolytic metabolism remain intact and unlikely represent the dominant metabolic restraint underlying ILC2 suppression in this model.

While activated ILC2 rely on glucose during activation, lipid metabolism remains a key feature of pathogenic ILC2 (Karagiannis et al., 2020; Wientjens et al., 2025). In contrast to preserved glycolysis, altered lipid metabolism emerged as a prominent altered pathway in ILC2 during *T. muris* infection. In this study, fatty acid uptake, assessed by BODIPY FLC16, was reduced in ILC2 isolated from *T. muris*-infected mice. In the acute papain model, this was accompanied by reduced neutral lipid droplet accumulation. At the transcriptional level, expression of *Pparg* and *Dgat1*, genes associated with lipid uptake and storage, remained unchanged, whereas expression of *Pnpla2* (Atgl), a key mediator of triglyceride lipolysis, was increased. This suggests that altered lipid handling in ILC2 is not necessarily driven by impaired lipid metabolism programmes but may reflect increased lipid catabolism under conditions of constrained metabolic support. When immune cells such as T cells undergo activation, they often switch from catabolic to anabolic metabolism in order to support the generation of new biomass (Frauwirth et al., 2002). Equally, naive, quiescent cells, and memory cells switch to catabolism for maintenance (Pearce et al., 2008). In chronic *T. muris* and papain, ILC2 may be entering a state of quiescence, and switching to catabolic metabolism is less energy taxing for their survival and maintenance within the tissue. Lipid tracing would provide

valuable insight into the mobilisation of the lipids in ILC2 during *T. muris* infection and papain challenge. In particular, if fewer lipids are entering phopholipid membranes, this could reflect the reduced proliferation of ILC2s during infection with *T. muris* and papain. Wilhelm et al. (2016) demonstrated that activated ILC2s in the context of helminth infections rely on the uptake of fatty acids to fuel fatty acid oxidation (FAO). Roy-Dorval et al. (2024) confirmed this finding by flow cytometry using FAO blue on cell-sorted, in vitro-activated lung ILC2. We made use of this dye in this thesis to investigate if ILC2 during chronic *T. muris* infection and papain rely more or less on FAO. However, we could not achieve a detectable signal. It is possible that the dye is more suitable to isolate cell cultures than whole lung staining and requires further optimisation in this experimental setting. Overall, these findings indicate that lipid uptake and storage pathways are selectively impaired in ILC2 during chronic *T. muris* infection and papain. Given the reliance of activated ILC2 on lipid metabolism, disruption of this pathway may contribute to reduced proliferative capacity and effector function, even in the presence of stable glucose metabolism.

Fatty acid oxidation occurs in the mitochondria, and mitochondrial fitness is essential for immune cell proliferation and effector responses. In the context of *T. muris* infection, ILC2 displayed multiple features that indicated the impairment of mitochondrial function during allergic airway inflammation. In particular, mitochondrial membrane potential was consistently reduced in ILC2 from *T. muris*-infected mice, while mitochondrial content remained largely unchanged or nonsignificantly reduced. This data suggests reduced mitochondrial efficiency rather than impaired mitochondrial biogenesis or loss of mitochondrial mass. However, mitochondrial biogenesis was not investigated but could be confirmed in the future using an antibody against peroxisome proliferator-activated receptor gamma coactivator 1 alpha (PGC-1α), which is the key regulator of mitochondrial biogenesis (Krisna et al., 2024). Seahorse analyses revealed only modest reductions in oxidative phosphorylation in ILC2 isolated from *T. muris*-infected mice compared with papain-only controls. Together with preserved glycolytic capacity and translational activity, these findings support the interpretation that ILC2 are not undergoing complete metabolic shutdown. Instead, reduced mitochondrial membrane potential may reflect impaired coupling or altered electron transport chain activity that constrains metabolic output during activation. Indeed, as the NAD^+/NADH ratio was lower in the ILC2 from *T. muris*-infected mice compared with papain-only controls, this imbalance may impact the functions of the electron transport chain (ETC). While there were alterations in NAD^+/NADH ratio along with reduced mitochondrial membrane potential, mitochondrial superoxide levels as measured by MitoSOX were not significantly altered in ILC2 from *T.*

muris-infected mice and papain. However, general ROS species including cytosolic ROS were increased as measured using DCFDA. DCFDA measures H_2O_2 and enters the cytosol, thus, the redox imbalance may be predominantly cytosolic in nature. While cellular ROS can be important for activation, excessive ROS can have damaging effects on immune cell function (Bassoy et al., 2021). Elevated ROS levels can also increase the likelihood of lipid peroxidation and ferroptosis Endale et al. (2023), however, lipid peroxidation measured by BODIPY C11 remained comparable between ILC2 from *T. muris*-infected mice and papain-only mice. The absence of increased lipid peroxidation argues against significant oxidative damage to membrane lipids and suggests that antioxidant systems may partially regulate oxidative stress, even in the presence of elevated cellular ROS. One potential contributor to the observed redox imbalance is altered amino acid availability, particularly glutamine, which supports synthesis of the antioxidant glutathione (Amores-Sánchez and Medina, 1999). Reduced expression of *Slc1a5* may impact glutamine or cysteine availability in ILC2 from *T. muris*-infected mice, which may limit glutathione production, thereby exacerbating cytosolic oxidative stress. While cystine uptake was preserved, de novo glutathione synthesis requires the availability of multiple glycine, cysteine and glutamate, and limitations in one of these could compromise redox homeostasis. Several methods of detecting GSH are available which would give insight into disruputed GSH availability within the ILC2 from *T. muris*-infected mice during papain. Wientjens et al. (2025) highlights the importance of both cystine and cysteine availability for redox balancing in ILC2 to support lipid metabolism. Thus, redox balancing is a central component of activated ILC2 which can restrain proliferation and effector function when dysregulated. Importantly,Wientjens et al. (2025) also demonstrated the importance of redox balancing in Th2s, suggesting that redox balancing is a feature of type 2 immunity. Equally, using a model of HDM in this thesis, we observed that chronic *T. muris* infection imposes redox stress on Th2 that may also impact their effector function.

Chronic *T. muris* infection is known to induce alterations in amino acid availability during infection (Holm et al., 2015). Such changes could extend to other nutrients and impact immune cell function. To determine whether systemic changes in nutrient availability could contribute to the metabolic phenotype observed in lung ILC2, we examined nutrient transporter expression in the small intestine, metabolic alterations in visceral adipose tissue, and tissue-level metabolomic changes in the colon and lung during chronic *T. muris* infection and papain. The small intestine is responsible for the absorption of the majority of dietary nutrients, however, the expression of key nutrient transporters in the small intestine remained largely unchanged during chronic *T. muris* infection. This included transporters involved in amino acid

and lipid uptake. In addition to nutrient transporters, expression of *Tbx21*, encoding the transcription factor T-bet, was significantly increased in the small intestine, consistent with a skewing toward a type 1 immune environment. In addition, expression of the glutamine transporter *Slc38a1* was reduced. Given that glutamine levels were elevated in the colon during chronic infection, it is difficult to determine whether reduced *Slc38a1* expression reflects decreased host absorption, altered availability, or feedback regulation in response to increased local glutamine concentrations. However, glutamine levels in the colonic tissue do not reflect availability in the small intestine. In addition, transcript levels alone do not provide information on transporter activity or nutrient availability, highlighting a limitation of these analyses. At the same time, chronic *T. muris* infection was associated with a reduction in visceral adipose tissue mass, despite infected mice maintaining overall body weight. This finding suggests an effect on host lipid storage and energy distribution. Gene expression analyses in visceral adipose tissue revealed reduced expression of *Lpl*, which hydrolyses circulating triglycerides to facilitate fatty acid uptake and storage, and *Dgat1*, a key enzyme in triglyceride synthesis (Kersten, 2023). Changes in these genes suggests impaired lipid storage and potential redistribution of fatty acids to provide energy to other organs during a state of altered nutrient availability. Expression of *Retn*, which encodes the adipokine resistin, was also reduced. *Retn* regulates glucose metabolism and insulin resistance and is typically downregulated in fasted states which may also highlight limited nutrient availability to the host during chronic *T. muris* infection (Banerjee et al., 2004). Together, these changes indicate that chronic *T. muris* infection induces a systemic metabolic state characterised by reduced lipid storage capacity and altered energy homeostasis. Consistent with immune skewing observed in the lung, visceral adipose tissue from chronically infected mice also exhibited increased expression of *Ifn*γ. This suggests that type 1 immune polarisation extends to distal tissues during chronic infection, reinforcing that the helminth-induced immune modulation is systemic. Such systemic metabolic changes may indirectly influence immune cell function in peripheral tissues, including the lung, by shaping nutrient distribution and inflammatory mediators. While Funjika et al. (2023) investigated whether chronic *T. muris* infection could prevent the development of obesity, they instead observed that mice developed an alternative Th2 response and effectively expelled the helminth and did not protect from diet-induced obesity. Commercially available high-fat diets are low in insoluble fiber which promotes obesity Chassaing et al. (2015), and Myhill et al. (2025) demonstrated that insoluble fiber is necessary for maintaining the chronicity of *T. muris* and generating a type 1 immune response. This finding could explain the observed phenotype of expulsion during high-fat diets and highlights a significant gap in the literature on the effects of diet and nutri-

ents during chronic *T. muris*infection that requires further investigation.

We performed untargeted metabolomic analyses which highlighted tissue metabolic changes during chronic *T. muris* infection and papain. While a significant number of metabolites were altered in colonic tissue, reflecting direct effects at the site of infection, relatively few metabolites were changed in the lung tissue. This may indicate that the metabolic environment of the lung is partially protected from systemic metabolic alterations during chronic *T. muris*. However, among the metabolites altered in both colon and lung, kynurenine was consistently increased, suggesting induction of systemic inflammatory or immunoregulatory pathways. In addition, the xenobiotic metabolite 3-(3-hydroxyphenyl)propionic acid sulfate was elevated in the lung, while its unsulfated precursor and structural isomers were increased in the colon.

Consistent with the increase in kynurenine, expression of *Ido1*, which catalyses the conversion of tryptophan to kynurenine, was increased in the lung during chronic infection, following acute papain exposure, and at steady-state compared with naive mice. Induction of *Ido1* is well described during infection and inflammation and can be induced by interferon signalling, particularly IFNγ (Huang et al., 2013; Taylor and Feng, 1991). Functionally, IDO1-mediated tryptophan depletion has been proposed as an evolutionary host defense mechanism that restricts pathogen growth (Grohmann and Puccetti, 2015). Kynurenine can also have pleiotropic effects on the immune system by inducing regulatory T cells and balancing the Th1/Th2 ratio (Grohmann and Puccetti, 2015). Additionally, a depleted local tryptophan environment may hamper immune cell function. We observed that increasing concentrations of kynurenine were able to suppress ILC2 numbers and proliferation in vitro. ILC2 expresses aryl hydrocarbon receptor (AhR, and kynurenine is an endogenous AhR ligand (Li et al., 2018a,b). Furthermore, enhancing IDO1 expression was shown to relieve a HDM model of asthma (Miao et al., 2024). However, the literature on direct suppression of ILC2 with kynurenine is lacking. Moreover, the concentration used in our assay to suppress ILC2 proliferation was significantly above physiological conditions during inflammation (Bizjak et al., 2024). Thus, while increased kynurenine and depleted tryptophan may be contributing to an altered environment in the lung during *T. muris* infection, contributing to dampening of allergic asthma, further studies are required to investigate the direct role of kynurenine on ILC2 in this disease context.

As mentioned, metabolomic profiling identified elevated levels of the xenobiotic metabolite 3-(3-hydroxyphenyl)propionic acid sulfate (3-3HPPA-SO_4) in lung tissue during chronic *T.*

muris infection. In contrast, its unsulfated precursor, 3-3HPPA and the structural isomer 3-4HPPA, were increased in the colon. Notably, as chronic *T. muris* infection is associated with alterations in gut microbial composition, including reduced overall diversity and expansion of Firmicutes, particularly Clostridia (Holm et al., 2015; Houlden et al., 2015). Clostridia are known to metabolise dietary phenolic acids into products such as 3-3HPPA (Beloborodova et al., 2012). Sulfation of 3-3HPPA likely occurs through first-pass hepatic metabolism, generating a more soluble compound capable of entering systemic circulation before reaching the lung (Feng et al., 2022; Sekura and Jakoby, 1979). While phenolic acid derivatives, including 3-3HPPA, have been reported to exhibit anti-inflammatory and antioxidant properties in various contexts, their role in allergic airway inflammation remains poorly defined. To investigate whether these metabolites contribute directly to suppression of airway type 2 responses, 3-3HPPA was administered orally during allergic airway inflammation. While treatment reduced overall lymphocyte trafficking to the lung, including eosinophils and Th2 cells, ILC2 numbers and effector function were unaffected. Moreover, administration of 3-3HPPA resulted in a broad dampening of cytokine levels in lung homogenates, including IFNγ, IL-6, IL-17, and IL-22, suggesting a general anti-inflammatory effect rather than selective modulation of ILC2. Additionally, the suppression by 3-3HPPA and its sulfated derivative in vitro and in vivo was variable, including a lack of suppressive effects against ILC2 in vitro. These findings indicate that while xenobiotic phenolic acid derivatives are a distinct feature of the metabolic landscape during chronic *T. muris* infection, they do not directly account for the selective metabolic and functional suppression of ILC2 observed in this model. The accumulation of these metabolites likely reflects the significant changes in microbiome diversity during chronic infection that support the survival of the helminth. Phenolic acids, including 3-3HPPA have been reported to possess antimicrobial properties that may contribute to reduced microbial diversity, promoting the expansion of specific bacterial species such as Clostridia (Feng et al., 2022). Such microbial reshaping has been proposed as a form of “crowd control” that limits excessive helminth colonisation during *T. muris* infection (White et al., 2018). Nevertheless, the consequences for the host include an increase in metabolites associated with dampened inflammation, potentially contributing to an overall anti-inflammatory milieu that supports chronic infection without directly targeting ILC2 in the lung.

As mentioned, an increase in IDO1 and kynurenine is consistent with elevated IFNγ signalling, and chronic *T. muris*infection is known to induce IFNγ. IFNγ suppresses type 2 immunity and directly represses ILC2s Molofsky et al. (2015); Moro et al. (2016). We therefore

hypothesised that a chronic low-grade IFNγ environment may contribute to the impaired ILC2 proliferation during allergic airway inflammation. We observed that IFNγ production by CD4 T cells peaked at day 21 and was sustained through day 27, coinciding with the initiation of papain exposure. This result coincides with previous findings defining the peripheral immune response during chronic and *T. muris*infection (Taylor et al., 2000). Defining the long-term maintenance of Th1 and IFNγ-producing T cells, including memory markers, would be informative. However, RAG1$^{-/-}$ mice, which lack T and B cells, remain susceptible to chronic infection when exposed to a high egg dose (Chenery et al., 2016). Furthermore, SCID mice, also lacking T and B cells, maintain an increase in IFNγ, suggesting an innate origin, likely NKs, ILC1s, or myeloid-derived cells (Artis et al., 1999). In line with this, we found the highest IFNγ capacity in non-CD4 and non-CD8 cells. Although beyond the scope of this study, SCID or RAG$^{-/-}$ mice may be useful to identify the innate cellular source of IFNγ that promotes chronicity. It would also be valuable to examine how nutrient changes in the colon support a type 1 environment and prime NK cells and CD4 T cells to produce IFNγ.

Given the overlap between elevated IFNγ and initial allergen exposure, the impact of such an environment on ILC2 was examined both at steady-state and during activation. At steady-state, lung ILC2 from day 21 *T. muris*-infected mice displayed no major changes in number or effector function, consistent with previous reports that naive ILC2 are relatively resistant to IFNγ mediated suppression in the absence of activation signals (Cautivo et al., 2022). However, there was significant evidence of IFNγ signalling within ILC2 during allergic activation. ILC2 from *T. muris*-infected mice exhibited increased expression of interferon-stimulated genes, including *Irf1* and *Cxcl10*, indicating direct exposure to IFNγ signalling. Additionally, expression of Sca-1, a marker associated with IFNγ signalling as well as restricted extravasation and proliferation in ILC2, was increased on ILC2 during chronic *T. muris* infection and papain. Although ex vivo phospho-STAT1 staining is not possible as it is obscured by tissue digestion, the transcriptional and phenotypic changes observed provide indirect but consistent evidence for IFNγ-STAT1 pathway engagement in ILC2. The functional relevance of IFNγ signalling was further supported by in vitro whole lung culture experiments. When lung cells from *T. muris*-infected mice mice were activated with IL-33, ILC2 proliferation and cytokine production were impaired compared with controls. Importantly, blockade of IFNγ during activation partially restored ILC2 proliferation and fully rescued effector cytokine production. As IFNγ was not added exogenously to these cultures, this finding implies the possibility of IFNγ producing cells within the lung environment as active suppressors of ILC2 during allergen exposure. IL-33 is a potent activator of ILC2 but can also coordinate with

type 1 cytokines to enhance CD8 T cells in certain disease contexts (Liang et al., 2022). In a lung environment already skewed toward type 1 immunity, IL-33 release following allergen exposure may therefore reinforce an IFNγ driven suppression rather than support type 2 inflammation.

We investigated directly if IFNγ contributes to the metabolic phenotype observed in ILC2 by local IFNγ blockade in vivo. Neutralisation of IFNγ during chronic *T. muris* infection and papain exposure restored key metabolic features of ILC2, including lipid uptake and lipid droplet formation, reduced cellular ROS, and increased mitochondrial membrane potential. In addition, there was increased AHA transport through *Slc1a5* following IFNγ blockade, suggesting that IFNγ signalling may limit amino acid transport pathways required for redox balance and metabolic support in ILC2. Additionally, we observed that Sca-1 expression on ILC2 was reduced following IFNγ blockade, further supporting a link between IFNγ signalling on ILC2, restricted proliferative behaviour, and metabolic constraint. Although additional validation, including assessment of phospho-STAT1 or IFNγ receptor-deficient ILC2 would strengthen this conclusion that IFNγ signalling during chronic *T. muris* infection and papain is driving the metabolic and proliferative restraint on ILC2. Nevertheless, these findings position IFNγ as a central mediator during chronic helminth infection and allergic asthma.

Given the redox imbalance we observed in ILC2 during chronic *T. muris* infection and allergic airway inflammation, we investigated whether disruption of the thioredoxin system contributes mechanistically to IFNγ mediated ILC2 suppression. Other redox systems were investigated, such as the GPX and Peroxiredoxins system, however, there were no significant changes detected transcriptionally in these redox pathways. The thioredoxin system is a critical regulator of cellular redox homeostasis, and its activity is tightly controlled by thioredoxin-interacting protein (TXNIP), which inhibits thioredoxin and promotes oxidative stress. Wientjens et al. (2025) elegantly demonstrated that ILC2 are highly sensitive to perturbations in the thioredoxin system, as pharmacological inhibition of thioredoxin activity is sufficient to reduce ILC2 numbers and function. Reanalysis of publicly available RNA-sequencing data revealed that *Txnip* expression is increased in ILC2 following combined IFNγ and IL-33 exposure compared with IL-33 alone (Cautivo et al., 2022; Moro et al., 2016). Importantly, the induction of *Txnip* was absent in IFNγ receptor-deficient ILC2, suggesting IFNγ signalling can directly regulate TXNIP. Consistent with these findings, increased *Txnip* expression was observed in ILC2 isolated from mice infected with chronic *T. muris* and papain challenge, as well as in the IFNγ and IL-33 in vivo model used in this study. In parallel, expression of *Gsr*,

which encodes glutathione reductase and supports regeneration of reduced glutathione, was increased, whereas expression of *Gclc* (glutamate-cysteine ligase), the rate-limiting enzyme for de novo glutathione synthesis, remained unchanged. This suggests an attempt to increase recycling of GSH in response to elevated oxidative stress. To test whether TXNIP is required for IFNγ mediated suppression of ILC2, TXNIP deficient ILC2 and wild type controls were examined in vivo during chronic *T. muris* and acute papain challenges. However, TXNIP deficiency did not rescue ILC2 numbers, eosinophil accumulation, or function in ILC2. Cellular ROS levels remained elevated in TXNIP-deficient ILC2, comparable to wild type controls, indicating that loss of TXNIP is insufficient to restore redox balance or function. To further investigate the role of TXNIP under more controlled conditions, naive ILC2 were activated in vitro with IFNγ and IL-33. TXNIP deficient ILC2 were also not protected from IFNγ mediated suppression in vitro, and their proliferative and functional responses were comparable to wild-type control ILC2. At the same time, in wild-type ILC2, IFNγ and IL-33 stimulation increased *Txnip* expression in vitro, as well as reduced expression of *Slc1a5*, and increased cellular ROS. This could suggest that altered amino acid transport and redox stress occur upstream and/or independently of TXNIP function. Additionally, these data support the idea that TXNIP induction reflects an IFNγ driven stress response rather than a primary driver of ILC2 suppression. Pharmacological modulation of TXNIP using the small molecule SRI-3770 produced slight increases in ILC2 proliferation and type 2 cytokine production in vitro. However, the function of SRI-3770 in ILC2 has not yet been characterised. In addition, as it modulates translation of TXNIP, it is important to interpret the data cautiously, as it could reflect off-target effects. Collectively this data shows that although TXNIP expression is induced in ILC2 following IFNγ signalling, genetic and pharmacological evidence does not support a direct role for TXNIP in mediating ILC2 suppression in this setting.

Despite TXNIP reflecting a downstream rather than causal link of suppression, it remained evident that elevated cellular ROS was a consequence of IFNγ signalling in ILC2. We asked whether ROS scavenging during culture with IFNγ could rescue ILC2 numbers and function. As discussed, it was previously demonstrated by Wientjens et al. (2025) that GSH and NAC could restore ILC2 viability during redox imbalance. In vitro, the addition of NAC or GSH to cultures of activated ILC2 exposed to IFNγ resulted in the reduction of intracellular ROS levels. Importantly, reducing ROS restored ILC2 numbers as well as partially restoring function. These findings indicate that increased ROS contributes to impaired ILC2 expansion and that redox balance is a limiting factor for ILC2 proliferation in a mixed type 1/type 2 cytokine environment. However, antioxidant treatment did not fully restore all aspects of ILC2.

Despite improved proliferation and function, mitochondrial membrane potential remained significantly reduced. Furthermore, *Nampt* expression remained high, and while NAD^+/NADH levels should be measured, it may suggest an additional pathway of IFNγ mediated suppression that targets the mitochondria and redox-balancing cofactors. IFNγ is known to induce a highly oxidative environment and induce *Nampt* in monocytes to support respiratory burst (McCann et al., 2022). Additionally, an increase in *Nampt* is important for IFNγ production in CD4 T cells in a model of lupus nephritis (Li et al., 2023). Although in this context, it is for the functional support of monocytes and Th1 cells, it may be a double-edged sword as a method for controlling type 2 immunity. While, IFNγ mediated suppression of ILC2 has been demonstrated by Moro et al. (2016), the effect of IFNγ on ILC2 metabolism, including reduced mTOR signalling has not been reported until now. In addition, we observed that IFNγ reduced *c-Myc* expression in ILC2. Ramana et al. (2000) showed that IFNγ can suppress *c-Myc* in fibroblasts, which was partially dependent on STAT1. This could suggest a link between STAT1, c-MYC, and mTOR regulation in ILC2. Importantly, balancing ROS was not sufficient to restore mTOR or *c-Myc* expression in ILC2 in our in vitro assay, indicating that redox balancing alone may be insufficient to overcome all aspects of IFNγ-driven transcriptional and metabolic repression. These findings may suggest that IFNγ suppresses ILC2 through at least two mechanisms. The first is that IFNγ induces redox stress that limits ILC2 proliferation, which can be alleviated by antioxidant treatment. Second, IFNγ imposes a redox-independent brake on cellular metabolism and effector function, mediated through STAT1-dependent transcriptional programmes that suppress mTOR activity and metabolic remodelling. While the sustained IFNγ during chronic *T. muris* does not put as harsh a brake on ILC2 metabolism, these data reveal that redox imbalances contribute to reduced proliferation and function during chronic *T. muris* and allergic asthma.

A limitation of this study is the biological variability observed in the chronic papain model compared with the acute model. As evidence suggests that ILC2 populations are heterogeneous and may exhibit differential sensitivity to IFNγ (Moro et al., 2016). The extent to which distinct ILC2 subsets, such as the IL-25-activated inflammatory ILC2, contribute to variability in protection during *T. muris* and allergic asthma warrants further investigation. Nevertheless, the suppressive effects of chronic *T. muris* infection on airway inflammation were reproducible across independent experiments, and key phenotypes such as reduced ILC2 and eosinophilia, impaired lipid metabolism, and elevated cellular ROS were observed. However, several questions remain unanswered. While IFNγ was identified as a major player in suppressing ILC2, the precise cellular sources producing IFNγ during chronic infection were not

defined, nor was their potential role in protecting against allergic airway inflammation. While metabolic and transcriptional changes in ILC2 were characterised, RNA sequencing was not performed, which would enable a much more in-depth investigation of the mechanisms of suppression. Importantly, however, transcript data cannot give information regarding nutrient availability or enzymatic activity within a cell, and measurements such as specific nutrient tracing or untargeted metabolomics would be a valuable addition to the story. Furthermore, targeted nutrient depletion or add-back assays, as well as manipulation of IFNγ signalling pathways, would further refine the relative contribution of specific metabolic pathways to ILC2 suppression. Importantly, the direct source of ROS was not identified, and determining this pathway could be an alternative targetable strategy in ILC2 suppression during allergic asthma. Collectively we demonstrated that chronic *T. muris* infection can mediate protection against allergic airway inflammation by imposing metabolic restraint on ILC2. The presence of IFNγ within the lung impairs lipid metabolism and induces a redox imbalance in activated ILC2, limiting their proliferation and function despite preserved basal metabolic function. Overall, this highlights that *T. muris* have intelligently hijacked an immunological paradigm to support their perseverance in the tissue niche and prevent expulsion.

5. Abstract

Chronic diseases such as asthma have increased dramatically over the last century, coinciding with a decline in parasitic helminth infections. Allergic asthma is characterised by the expansion of type 2 immune cells, including the activation of group 2 innate lymphoid cells (ILC2). While helminth infections have been linked to lower incidence of allergic airway inflammation, the mechanisms underlying this protection remain incompletely understood. This thesis investigated whether chronic infection with the intestinal helminth *Trichuris muris* protects against allergic airway inflammation by inducing a metabolic restraint in lung ILC2s. Chronic *T. muris* infection significantly reduced ILC2 numbers, proliferation, and cytokine production in a model of murine asthma. ILC2s from *T. muris*-infected mice displayed impaired lipid metabolism, increased cellular ROS, reduced mitochondrial membrane potential, and a decreased NAD^+/NADH ratio, corresponding with disrupted mitochondrial function and redox imbalance. Despite these metabolic impairments, the protein translation was preserved, suggesting metabolic dysfunction rather than complete metabolic shutdown. Protection from airway inflammation was associated with a type 1 skewed immune environment and elevated IFNγ levels. In vitro, IFNγ promoted an enhanced oxidative intracellular environment in ILC2s, leading to impaired lipid metabolism and reduced mTOR signaling, effects that could be partially rescued by buffering reactive oxygen species using antioxidants NAC and GSH in vitro. Importantly, blocking local IFNγ in vivo during *T. muris* and papain rescued the function and metabolic impairments in ILC2. Together, these findings demonstrate that chronic *T. muris* infection enforces a redox-linked metabolic restraint on pathogenic ILC2 through an IFNγ dependent pathway.

6. List of Figures

7. List of Tables

8. References

Adolph TE and Tilg H. Western diets and chronic diseases. *Nat Med*, 30:2133–2147, 2024.

Amores-Sánchez MI and Medina MÁ. Glutamine, as a Precursor of Glutathione, and Oxidative Stress. *Molecular Genetics and Metabolism*, 67(2):100–105, 1999.

Angela M, Endo Y, and Asou H. Fatty acid metabolic reprogramming via mTOR-mediated inductions of PPARγ directs early activation of T cells. *Nat Commun*, 7:13683, 2016.

Antignano F, Mullaly SC, Burrows K, and Zaph C. Trichuris muris Infection: A Model of Type 2 Immunity and Inflammation in the Gut. *J Vis Exp*, 51(e2774), 2011.

Argüello RJ, Combes AJ, Char R, Gigan JP, Baaziz AI, Bousiquot E, Camosseto V, Samad B, Tsui J, Yan P, Boissonneau S, Figarella-Branger D, Gatti E, Tabouret E, Krummel MF, and Pierre P. Targeted deletion of thioredoxin-interacting protein regulates cardiac dysfunction in response to pressure overload. *Cell Metab*, 32(6):1063–1075, 2020.

Artis D, Potten CS, Else KJ, Finkelman FD, and Grencis RK. Trichuris muris: host intestinal epithelial cell hyperproliferation during chronic infection is regulated by interferon-gamma. *Exp Parasitol*, 92(2):144–153, 1999.

Atakkatan A, Magesh A, Yong HM, Murray E, Gour N, and Lajoie S. Complement-producing adventitial fibroblasts form an IL-33 alarmin hub that maintains ILC2s during airway allergy. *Cell Reports*, 44(12), 2025.

Aviner R. The science of puromycin: From studies of ribosome function to applications in biotechnology. *Comput Struct Biotechnol J*, 18:1074–1083, 2020.

Bager P, Arnved J, Rønborg S, Wohlfahrt J, Poulsen LK, and Westergaard T. Trichuris suis ova therapy for allergic rhinitis: A randomized, double-blind, placebo-controlled clinical trial. *Journal of Allergy and Clinical Immunology*, 125(1):123–130, 2010.

Baker EH and Baines DL. Airway Glucose Homeostasis: A New Target in the Prevention and Treatment of Pulmonary Infection. *Chest*, 153(2):507–514, 2018.

Bancroft AJ and Grencis RK. Immunoregulatory molecules secreted by Trichuris muris. *Parasitology*, 148(14):1–7, 2021.

Bancroft AJ, Else KJ, Sypek JP, and Grencis RK. Interleukin-12 promotes a chronic intestinal nematode infection. *Eur J Immunol*, 27(4):866–870, 1997.

Banerjee RR, Rangwala SM, Shapiro JS, Rich AS, Rhoades B, Qi Y, Wang J, Rajala MW, Pocai A, Scherer PE, Steppan CM, Ahima RS, Obici S, Rossetti L, and Lazar MA. Regulation of fasted blood glucose by resistin. *Science*, 303(5661):1195–1198, 2004.

Banno A, Reddy AT, Lakshmi SP, and Reddy RC. PPARs: Key Regulators of Airway Inflammation and Potential Therapeutic Targets in Asthma. *Nucl Receptor Res*, 16:101306, 2018.

Bar-Peled L and Sabatini DM. Regulation of mTORC1 by amino acids. Trends Cell Biol. *Trends Cell Biol*, 24(7):400–406, 2014.

Bassoy EY, Walch M, and Martinvalet D. Reactive Oxygen Species: Do They Play a Role in Adaptive Immunity? *Front Immunol*, 12(755856), 2021.

Bayeva M, Khechaduri A, Puig S, Chang HC, Patial S, Blackshear PJ, and Ardehali H. mTOR regulates cellular iron homeostasis through tristetraprolin. *Cell Metab*, 16(5):645–657, 2012.

Belkaid Y and Artis D. Immunity at the barriers. *Eur J Immunol*, 43(12):3096–3097, 2013.

Bell LV and Else KJ. Regulation of colonic epithelial cell turnover by IDO contributes to the innate susceptibility of SCID mice to Trichuris muris infection. *Parasite Immunol*, 33(4): 244–249, 2011.

Beloborodova N, Bairamov I, Olenin A, Shubina V, Teplova V, and Fedotcheva N. Effect of phenolic acids of microbial origin on production of reactive oxygen species in mitochondria and neutrophils. *J Biomed Sci*, 19(1):89, 2012.

Bick F, Brenis Gómez CM, Lammens I, Moorleghem J Van, De Wolf C, Dupont S, Dumoutier L, Smith NP, Villani AC, Browaeys R, Alladina J, Haring AM, Medoff BD, Cho JL, Bigirimana R, Vieira J, Hammad H, Blanchetot C, Schuijs MJ, and Lambrecht BN. IL-2 family cytokines IL-9 and IL-21 differentially regulate innate and adaptive type 2 immunity in asthma. *Journal of Allergy and Clinical Immunology*, 154(5):1129–1145, 2024.

Billiau A and Matthys P. Interferon-gamma: a historical perspective. *Cytokine Growth Factor Rev*, 20(2):97–113, 2009.

Bizjak DA, Stangl M, Börner N, Bösch F, Durner J, and Drunin G. Kynurenine serves as useful biomarker in acute, Long- and Post-COVID-19 diagnostics. *Front Immunol*, 13(6), 2024.

Blackwell NM and KJ Else. B cells and antibodies are required for resistance to the parasitic gastrointestinal nematode Trichuris muris. *Infect Immun*, 69:3860–3868, 2001.

Bohnacker S, Troisi F, De Los Reyes Jiménez M, and Esser-von Bieren J. What Can Parasites Tell Us About the Pathogenesis and Treatment of Asthma and Allergic Diseases. *Front Immul*, 11:2106, 2020.

Bujoreanu I and Gupta V. Anatomy, Lymph Nodes. *StatPearls Publishing*, 2025.

Carlberg I and Mannervik B. Glutathione reductase. *Methods Enzymol*, 113:484–490, 1985.

Cautivo KM, Matatia PR, Lizama CO, Mroz NM, Dahlgren MW, and Yu X. Interferon gamma constrains type 2 lymphocyte niche boundaries during mixed inflammation. *Immunity*, 55(2): 254–271.e7, 2022.

Chassaing B, Miles-Brown J, Pellizzon M, Ulman E, Ricci M, Zhang L, Patterson AD, Vijay-Kumar M, and Gewirtz AT. Lack of soluble fiber drives diet-induced adiposity in mice. *Am J Physiol Gastrointest Liver Physiol*, 309(7):G528–41, 2015.

Chen J, Yang J, Ma L, Li J, Shahzad N, and Kim CK. Structure-antioxidant activity relationship of methoxy, phenolic hydroxyl, and carboxylic acid groups of phenolic acids. *Sci Rep*, 10(1): 2611, 2020.

Chen T, Tibbitt CA, Feng X, Stark JM, Rohrbeck L, and Rausch L. PPAR-γ promotes type 2 immune responses in allergy and nematode infection. *Science Immunology*, 2(9):eaal5196, 2017.

Chenery AL, Antignano F, Burrows K, Scheer S, Perona-Wright G, and Zaph C. Low-Dose Intestinal Trichuris muris Infection Alters the Lung Immune Microenvironment and Can Suppress Allergic Airway Inflammation. *Infection and Immunity*, 84(2):491–501, 2016.

Choi EH and Park SJ. TXNIP: A key protein in the cellular stress response pathway and a potential therapeutic target. *Exp Mol Med*, 55(7):1348–1356, 2023.

Choi G, Ju HY, Bok J, Choi J, Shin JW, and Oh H. NRF2 is a spatiotemporal metabolic hub essential for the polyfunctionality of Th2 cells. *Proceedings of the National Academy of Sciences*, 121(28):e2319994121, 2024.

Circu ML and Aw TY. Reactive oxygen species, cellular redox systems, and apoptosis. *Free Radic Biol Med*, 48(6):749–762, 2010.

Cohn L, Homer RJ, Niu N, and Bottomly K. T helper 1 cells and interferon gamma regulate allergic airway inflammation and mucus production. *J Exp Med*, 190(9):1309–1318, 1999.

Colaço Gaspar M, Hofer P, Oberer M, and Zechner R. PNPLA-mediated lipid hydrolysis and transacylation – At the intersection of catabolism and anabolism. *Molecular and Cell Biology of Lipids*, 1869(2):159410, 2024.

Colonna M. Innate Lymphoid Cells: Diversity, Plasticity, and Unique Functions in Immunity. *Immunity*, 48(6):1104–1117, 2018.

Dahlgren MW, Jones SW, Cautivo KM, Dubinin A, Ortiz-Carpena JF, Farhat S, Yu KS, Lee K, Wang C, Molofsky AV, Tward AD, Krummel MF, Peng T, and Molofsky AB. Adventitial Stromal Cells Define Group 2 Innate Lymphoid Cell Tissue Niches. *Immunity*, 50(3):707–722, 2019.

Daynes RA and Jones DC. Emerging roles of PPARS in inflammation and immunity. *Nat Rev Immunol*, 2(10):748–759, 2002.

De Federicis D, Capuano C, Ciuti D, Molfetta R, Galandrini R, and Palmieri G. Nutrient transporter pattern in CD56dim NK cells: CD16 (FcγRIIIA)-dependent modulation and association with memory NK cell functional profile. *Front Immunol*, 15:1477776, 2024.

D'Elia R, DeSchoolmeester ML, Zeef LAH, Wright SH, Pemberton AD, and Else KJ. Expulsion of Trichuris muris is associated with increased expression of angiogenin 4 in the gut and increased acidity of mucins within the goblet cell. *BMC Genomics*, 10:492, 2009.

Egbujor MC, Olaniyan OT, Emeruwa CN, S Saha, L Saso, and Tucci P. An insight into role of amino acids as antioxidants via NRF2 activation. *Amino Acids*, 56(1):23, 2024.

Else KJ and Grencis RK. Cellular immune responses to the murine nematode parasite Trichuris muris. I. Differential cytokine production during acute or chronic infection. *Immunology*, 74(4):508–513, 1991.

Endale HT, Tesfaye W, and Mengstie TA. ROS induced lipid peroxidation and their role in ferroptosis. *Front Cell Dev Biol*, 11(1226044), 2023.

Everaere L, Ait-Yahia S, Molendi-Coste O, Vorng H, Quemener S, and LeVu P. Innate lymphoid cells contribute to allergic airway disease exacerbation by obesity. *Journal of Allergy and Clinical Immunology*, 138(5):1309–1318, 2016.

Fan C, Huang X, and Mei J. Epithelial cells: liaisons of immunity. *EMBO J*, 44:4772–4802, 2025.

Feng J, Ge C, Li W, and Li R. 3-(3-Hydroxyphenyl)propionic acid, a microbial metabolite of quercetin, inhibits monocyte binding to endothelial cells via modulating E-selectin expression. *Fitoterapia*, 156:105071, 2022.

Fitzsimmons CM, Falcone FH, and Dunne DW. Helminth Allergens, Parasite-Specific IgE, and Its Protective Role in Human Immunity. *Front Immunol*, 5(61), 2014.

Fox EM, Morris CP, Hübner MP, and Mitre E. Histamine 1 Receptor Blockade Enhances Eosinophil-Mediated Clearance of Adult Filarial Worms. *PLOS Neglected Tropical Diseases*, 9(7), 2015.

Frauwirth KA, Riley JL, Harris MH, Parry RV, Rathmell JC, and Plas DR. The CD28 Signaling Pathway Regulates Glucose Metabolism. *Immunity*, 16(6):769–777, 2002.

Funjika E, Colombo SAP, Hayes KS, Tozer MJ, Tyrrell KA, Cai S, Faniyi AA, Shears RK, Dooley M, Alshammari Y, Alhazmi W, Assas M, Almilaibary A, Jackson-Jones LH, Thornton DJ, Worthington JJ, and Grencis RK. High-fat diet-induced resistance to helminth infection via alternative induction of type 2 immunity. *Biochimica et Biophysica Acta (BBA)-Molecular and Cell Biology of Lipids*, 16(1):27–38, 2023.

Förster R, Schubel A, Breitfeld D, Kremmer E, Renner-Müller I, Wolf E, and Lipp M. CCR7 coordinates the primary immune response by establishing functional microenvironments in secondary lymphoid organs. *Cell*, 99(1):23–33, 1999.

Gomez G. Current Strategies to Inhibit High Affinity FcεRI-Mediated Signaling for the Treatment of Allergic Disease. *Front Immunol*, 175(10), 2019.

Grohmann U and Puccetti P. The Coevolution of IDO1 and AhR in the Emergence of Regulatory T-Cells in Mammals. *Front Immunol*, 6(58), 2015.

Haberstroh U, Pocock J, Gómez-Guerrero C, Helmchen U, Hamann A, Gutierrez-Ramos JC, Stahl RA, and Thaiss F. Expression of the chemokines MCP-1/CCL2 and RANTES/CCL5 is differentially regulated by infiltrating inflammatory cells. *Kidney Int*, 62(4):1264–1276, 2002.

Hachim MY, Elemam NM, Ramakrishnan RK, Salameh L, Olivenstein R, Hachim IY, Venkatachalam T, Mahboub B, Al Heialy S, Halwani R, Hamid Q, and Hamoudi R. Blood and Salivary Amphiregulin Levels as Biomarkers for Asthma. *Front Med (Lausanne)*, 7:561866, 2020.

Hammad H and Lambrecht BN. Barrier Epithelial Cells and the Control of Type 2 Immunity. *Immunity*, 43(1):29–40, 2015.

Hammad H and Lambrecht BN. The basic immunology of asthma. *Cell*, 184(6):1469–1485, 2021.

Hansen TV, Hansen M, Nejsum P, Mejer H, Denwood M, and Thamsborg SM. Glucose Absorption by the Bacillary Band of Trichuris muris. *PLoS Negl Trop Dis*, 10(9):e0004971, 2016.

Hayes KS and Grencis RK. Trichuris muris and comorbidities - within a mouse model context. *Parasitology*, 148(14):1–9, 2021.

Hodge SH, Krauss MZ, Kaymak I, King JI, Howden AJM, and Panic G. Amino acid availability acts as a metabolic rheostat to determine the magnitude of ILC2 responses. *Journal of Experimental Medicine*, 17(3):e20221073, 2023.

Holm JB, Sorobetea D, Kiilerich P, Ramayo-Caldas Y, Estellé J, and Ma T. Chronic Trichuris muris Infection Decreases Diversity of the Intestinal Microbiota and Concomitantly Increases the Abundance of Lactobacilli. *PLoS One*, 10(5):e0125495, 2015.

Houlden A, Hayes KS, Bancroft AJ, Worthington JJ, Wang P, and Grencis RK. Chronic Trichuris muris Infection in C57BL/6 Mice Causes Significant Changes in Host Microbiota and Metabolome: Effects Reversed by Pathogen Clearance. *PLoS One*, 10(5):e0125945, 2015.

Howell I, Howell A, and Pavord ID. Type 2 inflammation and biological therapies in asthma: Targeted medicine taking flight. *J Exp Med*, 220(7):e20221212, 2023.

Hu X and Ivashkiv LB. Cross-regulation of signaling pathways by interferon-gamma: implications for immune responses and autoimmune diseases. *Immunity*, 31(4):539–550, 2009.

Huang G, Wang Y, Vogel P, Kanneganti TD, Otsu K, and Chi H. Signaling via the kinase p38α programs dendritic cells to drive TH17 differentiation and autoimmune inflammation. *Nat Immunol*, 13(2):152–161, 2012.

Huang L, Li L, Klonowski KD, Tompkins SM, Tripp RA, and Mellor AL. Induction and Role of Indoleamine 2,3 Dioxygenase in Mouse Models of Influenza A Virus Infection. *PLOS ONE*, 8(6):e66546, 2013.

Huang Y and Paul WE. Inflammatory group 2 innate lymphoid cells. *Int Immunol*, 28(1): 23–28, 2016.

Huang Y, Guo L, Qiu J, Chen X, Hu-Li J, Siebenlist U, Williamson PR, Urban JF Jr, and Paul WE. IL-25-responsive, lineage-negative KLRG1(hi) cells are multipotential 'inflammatory' type 2 innate lymphoid cells. *Nat Immunol*, 16(2):161–169, 2015.

Humphreys NE, Xu D, Hepworth MR, Liew FY, and Grencis RK. IL-33, a potent inducer of adaptive immunity to intestinal nematodes. *J Immunol*, 180(4):2443–2449, 2008.

Hurrell BP, Sakano Y, Shen S, Helou DG, Li M, and Shafiei-Jahani P. Iron controls the development of airway hyperreactivity by regulating ILC2 metabolism and effector function. *Sci Transl Med*, 16(746):eadk4728, 2024.

Jain A and Pasare C. Innate Control of Adaptive Immunity: Beyond the Three-Signal Paradigm. *J Immunol*, 198(10):3791–3800, 2017.

Jang YH, Choi JK, Jin M, Choi YA, Ryoo ZY, Lee HS, Park PH, Kim SU, Kwon TK, Jang MH, Im SH, Moon SY, Lee WJ, Lee SJ, Kim DW, and Kim SH. House Dust Mite Increases pro-Th2 Cytokines IL-25 and IL-33 via the Activation of TLR1/6 Signaling. *J Invest Dermatol*, 137(11):2354–2361, 2017.

Jeffrey IW, Bushell M, Tilleray VJ, Morley S, and Clemens MJ. Inhibition of protein synthesis in apoptosis: differential requirements by the tumor necrosis factor alpha family and a DNA-damaging agent for caspases and the double-stranded RNA-dependent protein kinase. *Cancer Res*, 62(8):2272–2280, 2002.

Jiang L, Diaz PT, Best TM, Stimpfl JN, He F, and Zuo L. Molecular characterization of redox mechanisms in allergic asthma. *Annals of Allergy, Asthma & Immunology*, 113(2):137–142, 2014.

Kaiko GE, Horvat JC, Beagley KW, and Hansbro PM. Immunological decision-making: how does the immune system decide to mount a helper T-cell response? *Immunology*, 123: 326–338, 2008.

Karagiannis F, Masouleh SK, Wunderling K, Surendar J, Schmitt V, and Kazakov A. Lipid-Droplet Formation Drives Pathogenic Group 2 Innate Lymphoid Cells in Airway Inflammation. *Immunity*, 52(4):620–634, 2020.

Kedia Mehta N and Finlay DK. Competition for nutrients and its role in controlling immune responses. *Nat Commun*, 10(2123), 2019.

Kersten S. The impact of fasting on adipose tissue metabolism. *Biochimica et Biophysica Acta (BBA)-Molecular and Cell Biology of Lipids*, 1868(3):159262, 2023.

Kim HY, Chang YJ, Subramanian S, Lee HH, Albacker LA, Matangkasombut P, Savage PB, McKenzie AN, Smith DE, Rottman JB, DeKruyff RH, and Umetsu DT. Innate lymphoid cells responding to IL-33 mediate airway hyperreactivity independently of adaptive immunity. *J Allergy Clin Immunol*, 129(1):216–227, 2012.

Klein Wolterink RG, Kleinjan A, van Nimwegen M, Bergen I, de Bruijn M, Levani Y, and Hendriks RW. Pulmonary innate lymphoid cells are major producers of IL-5 and IL-13 in murine models of allergic asthma. *Eur J Immunol*, 42(5):1106–1116, 2012.

Klementowicz JE, Travis MA, and Grencis RK. Trichuris muris: a model of gastrointestinal parasite infection. *Semin Immunopathol*, 34:815–828, 2012.

Kobayashi T, Motomura Y, and Moro K. The discovery of group 2 innate lymphoid cells has changed the concept of type 2 immune diseases. *Int Immunol*, 33(12):705–709, 2021.

Koh CH, Lee S, and Kwak M et al. CD8 T-cell subsets: heterogeneity, functions, and therapeutic potential. *Exp Mol Med*, 55:2287–2299, 2023.

Kokubo K, Hirahara K, Kiuchi M, Tsuji K, Shimada Y, and Sonobe Y. Thioredoxin-interacting protein is essential for memory T cell formation via the regulation of the redox metabolism. *Proceedings of the National Academy of Sciences*, 120(2):e2218345120, 2023.

Kondo Y, Yoshimoto T, Yasuda K, Futatsugi-Yumikura S, Morimoto M, Hayashi N, Hoshino T, Fujimoto J, and Nakanishi K. Administration of IL-33 induces airway hyperresponsiveness and goblet cell hyperplasia in the lungs in the absence of adaptive immune system. *Int Immunol*, 20(6):791–800, 2008.

Kopp EB, Agaronyan K, Licona-Limón I, Nish SA, and Medzhitov R. Modes of type 2 immune response initiation. *Immunity*, 56(4):687–694, 2023.

Kornberg MD. The immunologic Warburg effect: Evidence and therapeutic opportunities in autoimmunity. *Wiley Interdiscip Rev Syst Biol Med*, 12(5):e1486, 2020.

Koyama K. NK1.1+ cell depletion in vivo fails to prevent protection against infection with the murine nematode parasite Trichuris muris. *Parasite Immunology*, 24(11-12):527–533, 2002.

Krishnaswamy JK, Chu T, and Eisenbarth SC. Beyond pattern recognition: NOD-like receptors in dendritic cells. *Trends Immunol*, 34(5):224–233, 2013.

Krisna SS, Deagle RC, Ismailova N, Esomojumi A, Roy-Dorval A, Roth F, Berberi G, Del, Rincon SV, and Fritz JH. Immunometabolic analysis of primary murine group 2 innate lymphoid cells: a robust step-by-step approach. *Front Immunol*, 16:1545790, 2024.

Kuruvilla ME, Vanijcharoenkarn K, Shih JA, and Lee FE. Epidemiology and risk factors for asthma. *Respir Med*, 149:16–22, 2019.

Larsen SB, Cowley CJ, and Fuchs E. Epithelial cells: liaisons of immunity. *Curr Opin Immunol*, 62:45–53, 2020.

Lee J, Walsh MC, Hoehn KL, James DE, Wherry EJ, and Choi Y. Regulator of fatty acid metabolism, acetyl coenzyme a carboxylase 1, controls T cell immunity. *J Immunol*, 192(7): 3190–3199, 2014.

Lewis G, Wang B, Shafiei Jahani P, Hurrell BP, Banie H, Aleman Muench GR, Maazi H, and Helou DG. Dietary Fiber-Induced Microbial Short Chain Fatty Acids Suppress ILC2-Dependent Airway Inflammation. *Front Immunol*, 10:2051, 2019.

Li M, Lai Y, Chen B, Guo C, Zhou M, Zhao S, Wang S, Li J, Yang N, and Zhang H. NAMPT is a metabolic checkpoint of IFNγ-producing CD4+ T cells in lupus nephritis. *Mol Ther*, 31 (1):193–210, 2023.

Li S, Bostick JW, Ye J, Qiu J, Zhang B, Urban JF Jr, Avram D, and Zhou L. Aryl Hydrocarbon Receptor Signaling Cell Intrinsically Inhibits Intestinal Group 2 Innate Lymphoid Cell Function. *Immunity*, 49(5):915–928, 2018a.

Li S, Bostick JW, and Zhou L. Regulation of Innate Lymphoid Cells by Aryl Hydrocarbon Receptor. *Front Immunol*, 8:1909, 2018b.

Li Y, Lan F, Yang Y, Xu Y, Chen Y, Qin X, Lv Z, Wang W, Ying S, and Zhang L. The absence of IL-9 reduces allergic airway inflammation by reducing ILC2, Th2 and mast cells in murine model of asthma. *BMC Pulm med*, 22(1):180, 2022.

Liang Y, Wang X, Wang H, Yang W, Yi P, Soong L, Cong Y, Cai J, Fan X, and Sun J. IL-33 activates mTORC1 and modulates glycolytic metabolism in CD8+ T cells. *Immunology*, 165 (1):61–73, 2022.

Lin YJ, Goretzki A, Rainer H, Zimmermann J, and Schülke S. Immune Metabolism in TH2 Responses: New Opportunities to Improve Allergy Treatment — Cell Type-Specific Findings (Part 2). *Curr Allergy Asthma Rep*, 23(1):41–52, 2023.

Lin Z, Chang C, Zhao S, Fang L, and Wang P. Amino acids shape the metabolic and immunologic landscape in the tumor immune microenvironment: from molecular mechanisms to therapeutic strategies. *Cancer Biol Med*, 22(7):726–746, 2025.

Liu TT, Kim S, Desai P, Kim DH, Huang X, Ferris ST, Wu R, Ou F, Egawa T, Van Dyken SJ, Diamond MS, Johnson PF, Kubo M, Murphy TL, and Murphy KM. Ablation of cDC2 development by triple mutations within the Zeb2 enhancer. *Nature*, 607(7917):142–148, 2022.

Longo VD and Mattson MP. Fasting: Molecular Mechanisms and Clinical Applications. *Cell Metabolism*, 19(2):181–192, 2014.

MacNabb BW, Tumuluru S, Chen X, Godfrey J, Kasal DN, Yu J, Jongsma MLM, Spaapen RM, Kline DE, and Kline J. Dendritic cells can prime anti-tumor CD8+ T cell responses through major histocompatibility complex cross-dressing. *Immunity*, 55(6):982–997, 2022.

Mandler R, Finkelman FD, Levine AD, and Snapper CM. IL-4 induction of IgE class switching by lipopolysaccharide-activated murine B cells occurs predominantly through sequential switching. *J Immunol*, 150(2):407–418, 1993.

Martí I, Líndez AA, and W Reith. Arginine-dependent immune responses. *Cell Mol Life Sci*, 78(13):5303–5324, 2021.

Matsuyama T, Machida K, Mizuno K, Matsuyama H, Dotake Y, Shinmura M, Takagi K, and Inoue H. The Functional Role of Group 2 Innate Lymphoid Cells in Asthma. *Biomolecules*, 13(6):893, 2023.

McCann KJ, Christensen SM, Colby DH, McGuire PJ, Myles IA, Zerbe CS, Dalgard CL, Sukumar G, Leonard WJ, McCormick BA, and Holland SM. IFNγ regulates NAD+ metabolism to promote the respiratory burst in human monocytes. *Blood Adv*, 6(12):3821–3834, 2022.

Meier C, Ristic Z, Klauser S, and Verreym F. Activation of system L heterodimeric amino acid exchangers by intracellular substrates. *EMBO J*, 21(4):580–589, 2002.

Miao Y, Zhong C, Bao S, Wei K, Wang W, Li N, Bai C, Chen W, and Tang H. Impaired tryptophan metabolism by type 2 inflammation in epithelium worsening asthma. *iScience*, 27 (6):109923, 2024.

Michalek RD, Gerriets VA, Jacobs SR, Macintyre AN, MacIver NJ, Mason EF, Sullivan SA, Nichols AG, and Rathmell JC. Cutting edge: distinct glycolytic and lipid oxidative metabolic programs are essential for effector and regulatory CD4+ T cell subsets. *J Immunol*, 186(6): 3299–3303, 2011.

Missiaen R, Lesner NP, and Simon MC. HIF: a master regulator of nutrient availability and metabolic cross-talk in the tumor microenvironment. *EMBO J*, 42(6):e112067, 2023.

Mohamed IN, Li L, Ismael S, Ishrat T, and El-Remessy AB. Thioredoxin interacting protein, a key molecular switch between oxidative stress and sterile inflammation in cellular response. *World J Diabetes*, 12(12):1970–1999, 2021.

Molofsky AB, Van Gool F, Liang HE, Van Dyken SJ, Nussbaum JC, and Lee J. Interleukin-33 and Interferon-γ Counter-Regulate Group 2 Innate Lymphoid Cell Activation during Immune Perturbation. *Immunity*, 43(1):161–174, 2015.

Monticelli LA, Sonnenberg GF, Abt MC, Alenghat T, Ziegler CG, Doering TA, Angelosanto JM, Laidlaw BJ, Yang CY, Sathaliyawala T, Kubota M, Turner D, Diamond JM, Goldrath AW, Farber DL, Collman RG, Wherry EJ, and Artis D. Innate lymphoid cells promote lung-tissue homeostasis after infection with influenza virus. *Nat Immunol*, 12(11):e20221140, 2011.

Monticelli LA, Buck MD, Flamar AL, Saenz SA, Tait Wojno ED, Yudanin NA, Osborne LC, Hepworth MR, Tran SV, Rodewald HR, Shah H, Cross JR, Diamond JM, Cantu E, Christie JD, Pearce EL, and Artis D. Arginase 1 is an innate lymphoid-cell-intrinsic metabolic checkpoint controlling type 2 inflammation. *Nat Immunol*, 17(6):656–665, 2016.

Moro K, Kabata H, Tanabe M, Koga S, Takeno N, and Mochizuki M. Interferon gamma constrains type 2 lymphocyte niche boundaries during mixed inflammation. *Nat Immunol*, 17 (1):76–86, 2016.

Munteanu C and Schwartz B. The relationship between nutrition and the immune system. *Front Nutr*, 9:1082500, 2022.

Murphy K and Weaver C. Janeway's immunobiology. 9th ed. *Science/Taylor & Francis Group*, 2017.

Murray M, Smith WD, Waddell AH, and Jarrett WFH. Nippostrongylus brasiliensis: Histamine and 5-hydroxytryptamine inhibition and worm expulsion. *Experimental Parasitology*, 30(1): 58–63, 1971.

Musiol S, Harris CP, Karlina R, Gostner JM, Rathkolb B, Schnautz B, Schneider E, Mair L, Vergara EE, Flexeder C, Koletzko S, Bauer CP, Schikowski T, Berdel D, von Berg A, Herberth G, Rozman J, Hrabe de Angelis M, Standl M, Schmidt-Weber CB, Ussar S, and Alessandrini F. Dietary digestible carbohydrates are associated with higher prevalence of asthma in humans and with aggravated lung allergic inflammation in mice. *Allergy*, 78(5): 1218–1233, 2023.

Myhill LJ, Jensen P, Arora P, Jensen AM, Zhu L, and Vedsted-Jakobsen A. Dietary fibre promotes chronic whipworm infection through direct and time-dependent modulation of innate immunity. *bioRxiv*, 10, 2025.

Mısırlıoğlu PE. Energy restriction drives adipose tissue remodeling and thermogenic adaptation. *Discov Med*, 2(1):295, 2025.

Najmanová I, Pourová J, Vopršalová M, Pilařová V, Semecký V, and Nováková L. Flavonoid metabolite 3-(3-hydroxyphenyl)propionic acid formed by human microflora decreases arterial blood pressure in rats. *Molecular Nutrition & Food Research*, 60(5):981–991, 2016.

Nakajima T, Kanno T, Yokoyama S, Sasamoto S, Asou HK, Tumes DJ, Ohara O, Nakayama T, and Endo Y. PPAR-γ promotes type 2 immune responses in allergy and nematode infection. *J Exp Med*, 218(12):e20210639, 2021.

Neill DR, Wong SH, Bellosi A, Flynn RJ, Daly M, Langford TK, Bucks C, Kane CM, Fallon PG, Pannell R, Jolin HE, and McKenzie AN. Nuocytes represent a new innate effector leukocyte that mediates type-2 immunity. *Nature*, 464(7293):1367–1370, 2010.

Newsholme EA, Crabtree B, and Ardawi MS. The role of high rates of glycolysis and glutamine utilization in rapidly dividing cells. *Biosci Rep*, 5(5):393–400, 1985.

Ngo V and Duennwald ML. Nrf2 and Oxidative Stress: A General Overview of Mechanisms and Implications in Human Disease. *Antioxidants*, 11(12):2345, 2022.

Nobs SP, Natali S, Pohlmeier L, Okreglicka K, Schneider C, Kurrer M, Sallusto F, and Kopf M. PPARγ in dendritic cells and T cells drives pathogenic type-2 effector responses in lung inflammation. *J Exp Med*, 214(10):3015–3035, 2017.

Nussbaum J, Van Dyken S, and von Moltke J. Type 2 innate lymphoid cells control eosinophil homeostasis. *Nature*, 502:245–248, 2013.

Oboki K, Ohno T, Kajiwara N, Arae K, Morita H, and Ishii A. IL-33 is a crucial amplifier of innate rather than acquired immunity. *Proceedings of the National Academy of Sciences*, 107(43):18581–18586, 2010.

O'Neill LA, Kishton RJ, and Rathmell J. A guide to immunometabolism for immunologists. *Nat Rev Immunol*, 16(9):81–82, 2016.

Ordoñez CL, Khashayar R, Wong HH, Ferrando R, Wu R, Hyde DM, Hotchkiss JA, Zhang Y, Novikov A, Dolganov G, and Fahy JV. Mild and moderate asthma is associated with airway

goblet cell hyperplasia and abnormalities in mucin gene expression. *Am J Respir Crit Care Med*, 163(2):517–523, 2001.

Osbourn M, Soares DC, Vacca F, Cohen ES, Scott IC, and Gregory WF. HpARI Protein Secreted by a Helminth Parasite Suppresses Interleukin-33. *Immunity*, 47(4):739–751, 2017.

Ozdowski L and Gupta V. Physiology, Lymphatic System. *StatPearls Publishing*, 2023.

Panda SK, Kim DH, Desai P, Rodrigues PF, Sudan R, and Gilfillan S. SLC7A8 is a key amino acids supplier for the metabolic programs that sustain homeostasis and activation of type 2 innate lymphoid cells. *Proceedings of the National Academy of Sciences*, 119(46): e2215528119, 2022.

Panda SK, Kim DH, Desai P, Wu S, Rodrigues PF, Sudan R, Liu Y, Jung H, Lee I, Gilfillan S, Cella M, Van Dyken SJ, and Colonna M. SLC7A8 is essential for metabolic fitness and function of Th2 cells. *J Exp Med*, 223(2):e20250439, 2023.

Papier K, Williams GM, Luceres-Catubig R, Ahmed F, Olved RM, and McManus DP. Childhood Malnutrition and Parasitic Helminth Interactions. *Clin Infect Dis*, 59(2):234–243, 2014.

Park J, Lee J, and Choi C. Mitochondrial Network Determines Intracellular ROS Dynamics and Sensitivity to Oxidative Stress through Switching Inter-Mitochondrial Messengers. *PLOS ONE*, 6(8):e23211, 2023.

Pearce EJ and Pearce EL. Immunometabolism in 2017: Driving immunity: all roads lead to metabolism. *Nat Rev Immunol*, 18(2):81–82, 2018.

Pearce EL and Pearce EJ. Metabolic Pathways in Immune Cell Activation and Quiescence. *Immunity*, 38(4):633–643, 2013.

Pearce EL, Walsh MC, Cejas PJ, Harms GM, Shen H, Wang LS, Jones RG, and Choi Y. Enhancing CD8 T-cell memory by modulating fatty acid metabolism. *Nature*, 460(7251): 103–107, 2008.

Pelgrom LR, Davis GM, O'Shaughnessy S, Wezenberg EJM, VanKasteren SI, Finlay DK, and Sinclair LV. QUAS-R: An SLC1A5-mediated glutamine uptake assay with single-cell resolution reveals metabolic heterogeneity with immune populations. *Cell Rep*, 42(8):112828, 2023.

Pimpão RC, Ventura MR, Ferreira RB, Williamson G, and Santos CN. Phenolic sulfates as new and highly abundant metabolites in human plasma after ingestion of a mixed berry fruit purée. *British Journal of Nutrition*, 113(3):454–463, 2015.

Pradeu T, Thomma BPHJ, Girardin SE, and Lemaitre B. The conceptual foundations of innate immunity: Taking stock 30 years later. *Immunity*, 57(4):613–631, 2024.

Pritchard DI, Falcone FH, and Mitchell PD. The evolution of IgE-mediated type I hypersensitivity and its immunological value. *Allergy*, 76(4):1024–1040, 2021.

Ramana CV, Grammatikakis N, Chernov M, Nguyen H, Goh KC, Williams BR, and Stark GR. Regulation of c-myc expression by IFN-gamma through Stat1-dependent and -independent pathways. *EMBO J*, 19(2):263–272, 2000.

Resende SD, Magalhães FC, Rodrigues-Oliveira JL, Castro VN, Souza CSA, Oliveira EJ, Carneiro M, Geiger SM, and Negrão-Corrêa DA. Modulation of Allergic Reactivity in Humans Is Dependent on Schistosoma mansoni Parasite Burden, Low Levels of IL-33 or TNF-α and High Levels of IL-10 in Serum. *Front Immunol*, 9:3158, 2019.

Rodrigues LC, Newcombe PJ, Cunha SS, Alcantara-Neves NM, Genser B, Cruz AA, Simoes SM, Fiaccone R, Amorim L, Cooper PJ, and ML Barreto. Social Change, Asthma and Allergy in Latin America. Early infection with Trichuris trichiura and allergen skin test reactivity in later childhood. *Clin Exp Allergy*, 38(11):1769–1777, 2008.

Roediger B, Kyle R, Tay SS, Mitchell AJ, Bolton HA, and Guy TV. IL-2 is a critical regulator of group 2 innate lymphoid cell function during pulmonary inflammation. *Journal of Allergy and Clinical Immunology*, 136(6):1653–1663, 2015.

Roth-Walter F, Berni Canani R, and L O'Mahony. Nutrition in chronic inflammatory conditions: Bypassing the mucosal block for micronutrients. *Allergy*, 79:353–383, 2024.

Roy-Dorval A, Deagle RC, Roth F, Raybaud M, Ismailova N, Krisna SS, Aboud DGK, Stegen C, Leconte J, Berberi G, Esomojumi A, and Fritz JH. Analysis of lipid uptake, storage, and fatty acid oxidation by group 2 innate lymphoid cells. *Front Immunol*, 15:1493848, 2024.

Salter BM, Aw M, and Sehmi R. The Functional Role of Group 2 Innate Lymphoid Cells in Asthma. *Journal of Leukocyte Biology*, 106(4):889–901, 2019.

Saluzzo S, Gorki AD, Rana BMJ, Martins R, Scanlon S, Starkl P, Lakovits K, Hladik A, Korosec A, Sharif O, Warszawska JM, Jolin H, Mesteri I, McKenzie ANJ, and Knapp S. First-Breath-Induced Type 2 Pathways Shape the Lung Immune Environment. *Cell Rep*, 18(8): 1893–1905, 2017.

Sappington DR, Siegel ER, Hiatt G, Desai A, Penney RB, Jamshidi-Parsian A, Griffin RJ, and Boysen G. Glutamine drives glutathione synthesis and contributes to radiation sensitivity of A549 and H460 lung cancer cell lines. *Biochim Biophys Acta*, 1860(4):836–843, 2016.

Scalise M, Pochini L, Console L, Losso MA, and Indiveri C. The Human SLC1A5 (ASCT2) Amino Acid Transporter: From Function to Structure and Role in Cell Biology. *Front Cell Dev Biol*, 6, 2018.

Schmitz J, Owyang A, Oldham E, Song Y, Murphy E, McClanahan TK, Zurawski G, Moshrefi M, Qin J, Li X, Gorman DM, Bazan JF, and Kastelein RA. IL-33, an interleukin-1-like cytokine that signals via the IL-1 receptor-related protein ST2 and induces T helper type 2-associated cytokines. *Immunity*, 23(5):479–490, 2005.

Sekura RD and Jakoby WB. Phenol sulfotransferases. *J Biol Chem*, 254(13):5658–5663, 1979.

Shao F, Yu D, Xia P, and Wang S. Dynamic regulation of innate lymphoid cells in the mucosal immune system. *Cell Mol Immunol*, 18(6):1387–1394, 2021.

Sheikh A, Lu J, Melese E, Seo JH, and Abraham N. IL-7 induces type 2 cytokine response in lung ILC2s and regulates GATA3 and CD25 expression. *J Leukoc Biol*, 112:1105–1113, 2022.

Sherwood ER, Burelbach KR, McBride MA, Stothers CL, Owen AM, Hernandez A, Patil NK, Williams DL, and Bohannon JK. Innate Immune Memory and the Host Response to Infection. *J Immunol*, 208(4):785–792, 2022.

Singh LP. Thioredoxin Interacting Protein (TXNIP) and Pathogenesis of Diabetic Retinopathy. *J Clin Exp Ophthalmol*, 4:2155–9570, 2013.

Smits HH, Hammad H, van Nimwegen M, Soullie T, Willart MA, Lievers E, Kadouch J, Kool M, Kos-van Oosterhoud J, Deelder AM, Lambrecht BN, and Yazdanbakhsh M. Protective effect of Schistosoma mansoni infection on allergic airway inflammation depends on the intensity and chronicity of infection. *J Allergy Clin Immunol*, 120(4):932–940, 2007.

Steinman RA and Cohn ZA. IDENTIFICATION OF A NOVEL CELL TYPE IN PERIPHERAL LYMPHOID ORGANS OF MICE : I. MORPHOLOGY, QUANTITATION, TISSUE DISTRIBUTION. *J Exp Med*, 137(5):1142–1162, 1973.

Stiemsma LT, Reynolds LA, Turvey SE, and Finlay BB. The hygiene hypothesis: current perspectives and future therapies. *Immunotargets Ther*, 4:143–157, 2015.

Surace L, Doisne JM, Croft CA, Thaller A, Escoll P, and Marie S. Dichotomous metabolic networks govern human ILC2 proliferation and function. *Nat Immunol*, 22(11):1367–1374, 2021.

Suzuki Y, Hayashi T, Yokoyama R, Nakagawa F, Inoue J, Higashi T, Onodera R, and Motoyama K. Fasting impairs type 2 helper T cell infiltration in the lung of an eosinophilic asthma mouse model. *FEBS Open Bio*, 11(9):2619–2630, 2021.

Taylor MD, Betts CJ, and Else KJ. Peripheral cytokine responses to Trichuris muris reflect those occurring locally at the site of infection. *Infect Immun*, 68(4):1815–1819, 2000.

Taylor MW and Feng GS. Relationship between interferon-gamma, indoleamine 2,3-dioxygenase, and tryptophan catabolism. *FASEB J*, 5(11):2516–2522, 1991.

Thery C and Amigorena S. The cell biology of antigen presentation in dendritic cells. *Current Opinion in Immunology*, 13(1):45–51, 2001.

Thielen LA, Chen J, Jing G, Moukha Chafiq O, Xu G, Jo S, Grayson TB, Lu B, Li P, Augelli Szafran CE, Suto MJ, Kanke M, Sethupathy P, Kim JK, and A Shalev. Identification of an Anti-diabetic, Orally Available Small Molecule that Regulates TXNIP Expression and Glucagon Action. *Cell Metab*, 32(3):1970–1999, 2020.

Thio CLP, Lai ACY, Ting YT, Chi PY, and Chang YJ. The ketone body β-hydroxybutyrate mitigates ILC2-driven airway inflammation by regulating mast cell function. *Cell Reports*, 40 (13):1147–1151, 2022.

Tian Q, Dan G, and Wang X. IDO1 inhibits ferroptosis by regulating FTO-mediated m6A methylation and SLC7A11 mRNA stability during glioblastoma progression. *Cell Death Discov*, 11(1):22, 2025.

Turner JE, Morrison PJ, Wilhelm C, Wilson M, Ahlfors H, Renauld JC, Panzer U, Helmby H, and Stockinger B. IL-9-mediated survival of type 2 innate lymphoid cells promotes damage control in helminth-induced lung inflammation. *J Exp Med*, 210(13):2951–2965, 2013.

van der Ploeg EK, Golebski K, van Nimwegen M, Fergusson JR, Heesters BA, Martinez-Gonzalez I, Kradolfer CMA, van Tol S, Scicluna BP, de Bruijn MJW, de Boer GM, Tramper-Stranders GA, Braunstahl GJ, van IJcken WFJ, Nagtegaal AP, van Drunen CM, Fokkens WJ, Huylebroeck D, Spits H, Hendriks RW, Stadhouders R, and Bal SM. Steroid-resistant human inflammatory ILC2s are marked by CD45RO and elevated in type 2 respiratory diseases. *Sci Immunol*, 6(55):eabd3489, 2021.

Van Gool F, Molofsky AB, Morar MM, Rosenzwajg M, Liang HE, Klatzmann D, Locksley RM, and Bluestone JA. Interleukin-5-producing group 2 innate lymphoid cells control eosinophilia induced by interleukin-2 therapy. *Blood*, 124(24):705–709, 2014.

von Moltke J, Ji M, Liang HE, and Locksley RM. Tuft-cell-derived IL-25 regulates an intestinal ILC2-epithelial response circuit. *Nature*, 529(7585):221–225, 2016.

Wang R, Lan C, Benlagha K, Camara NOS, Miller H, and Kubo M. The interaction of innate immune and adaptive immune system. *MedComm*, 5(10):e714, 2024.

Warburg O. The Metabolism of Carcinoma Cells. *The Journal of Cancer Research*, 9(1): 148–163, 1925.

White EC, Houlden A, Bancroft AJ, Hayes KS, Goldrick M, Grencis RK, and Roberts IS. Manipulation of host and parasite microbiotas: Survival strategies during chronic nematode infection. *Sci Adv*, 4(3):eaap7399, 2018.

White MV. The role of histamine in allergic diseases. *Journal of Allergy and Clinical Immunology*, 86(4):599–605, 1990.

Whitmire JK, Eam B, and Whitton JL. Tentative T cells: memory cells are quick to respond, but slow to divide. *PLoS Pathog*, 4(4):e1000041, 2008.

Wientjens C, Doverman M, Zurkovic J, More T, Surendar J, and Nesic S. Tolerance to ferroptosis facilitates lipid metabolism and pathogenic type 2 immunity in allergic airway inflammation. *Immunity*, 2025.

Wilhelm C, Hirota K, Stieglitz B, Van Snick J, Tolaini M, Lahl K, Sparwasser T, Helmby H, and Stockinger B. An IL-9 fate reporter demonstrates the induction of an innate IL-9 response in lung inflammation. *Nat Immunol*, 12(11):1071–1077, 2011.

Wilhelm C, Harrison OJ, Schmitt V, Pelletier M, Spencer SP, Urban JF Jr, Ploch M, Ramalingam TR, Siegel RM, and Belkaid Y. Critical role of fatty acid metabolism in ILC2-mediated barrier protection during malnutrition and helminth infection. *J Exp Med*, 213(8):1409–1418, 2016.

Wolfson RL and Sabatini DM. The Dawn of the Age of Amino Acid Sensors for the mTORC1 Pathway. *Cell Metab*, 26(2):301–309, 2017.

Yamamoto S and Hayaishi O. Tryptophan pyrrolase of rabbit intestine. D- and L-tryptophan-cleaving enzyme or enzymes. *J Biol Chem*, 242(22):5260–5266, 1967.

Yamane H and Paul WE. Early signaling events that underlie fate decisions of naive CD4(+) T cells toward distinct T-helper cell subsets. *Immunol Rev*, 252(1):275, 1999.

Yang K, Shrestha S, Zeng H, Karmaus PW, Neale G, Vogel P, Guertin DA, Lamb RF, and Chi H. T cell exit from quiescence and differentiation into Th2 cells depend on Raptor-mTORC1-mediated metabolic reprogramming. *Immunity*, 39(6):1043–1056, 2013.

Ye L, Pan J, Liang M, Pasha MA, Shen X, D'Souza SS, Fung ITH, Wang Y, Patel G, Tang DD, and Yang Q. A critical role for c-Myc in group 2 innate lymphoid cell activation. *Allergy*, 75(4):841–852, 2020.

Yoshioka J, Imahashi K, Gabel SA, Chutkow WA, Burds AA, Gannon J, Schulze PC, MacGillivray C, London RE, Murphy E, and Lee RT. Targeted deletion of thioredoxin-interacting protein regulates cardiac dysfunction in response to pressure overload. *Circ Res*, 101(12):1328–1338, 2007.

Yu H, Jacquelot N, and Belz GTM. Metabolic features of innate lymphoid cells. *J Exp Med*, 219(11):e20221140, 2022.

Yu HS, Angkasekwinai P, Chang SH, Chung Y, and Dong C. Protease Allergens Induce the Expression of IL-25 via Erk and p38 MAPK Pathway. *J Korean Med Sci*, 25(6):829–834, 2010.

Zheng C, Wu H, Lu Z, Bi J, and Wan X. IL-33-induced reactive oxygen species are required for optimal metabolic programming in group 2 innate lymphoid cells. *Cell Mol Immunol*, 17 (12):1266–1268, 2020.

Zhu H, Bi D, and Zhang Y. Ketogenic diet for human diseases: the underlying mechanisms and potential for clinical implementations. *Sig Transduct Target Ther*, 7(11):645–657, 2022.

9. Statement On Own Contributions

The work presented in this study was carried out at the Institute of Clinical Chemistry and Clinical Pharmacology under the supervision of Prof. Dr. Christoph Wilhelm. The initial study design was provided by Prof. Dr. Christoph Wilhelm, while I further developed and executed the work. Experiments included in this thesis were performed by me unless indicated otherwise below or with the support indicated below.

RNA extractions and qPCRs were performed by myself, Patricia Weiss, Carola Sarici, and Roman Rombo. All LEGENDplex assays were performed by me. Patricia Weiss, Carola Sarici, Roman Rombo, Chantal Wientjens, and Dhruvi Shah have all provided experimental help on sacrifice days of animal experiments throughout this study.

The data used for the evaluation of metabolites in lung and colon tissue was generated by Alexander Kasakov and Jayagopi Surendar and reanalyzed and visualised by myself and the UKB Bioinformatics Facility by Dr. Svetozar Nesic.

The reanalysis of RNA sequencing data from Cautivo et al. (2022); Moro et al. (2016) was accessed by the following accession codes GSE73272 and GSE190208 and visualised by me.

The sorting of immune cells was performed by the Flow Cytometry Core Facility of the Medical Faculty at the University of Bonn by Peter Wurst funded by the Deutsche Forschungsgemeinschaft (DFG, German Research Foundation) – DFG project number 216372545.

Flow Cytometry was performed by me with instrumentation provided by the Flow Cytometry Core Facility of the Medical Faculty at the University of Bonn funded by the Deutsche Forschungsgemeinschaft (DFG, German Research Foundation) – DFG project number 387335189.

The Red5 mice for crossing were provided by Dr. Richard Locksley.

All animal experiments were carried out by me with the support of Chantal Wientjens. The general animal care was provided by staff from the animal facility at the UKB (HET and iFET). In consultation with me, breedings were set up and maintained by Patricia Weiss and Carola

Sarici.

In preparing this work, I used ChatGPT in some parts of the thesis to improve readability and language. After using this tool, I reviewed and fully edited the relevant passages and take full responsibility for the content of the published dissertation.

I confirm that I have written this thesis independently and have not used any sources or aids other than those specified by me.

I hereby confirm that my thesis complies with the Statement by the Executive Committee of the Deutsche Forschungsgemeinschaft (DFG, German Research Foundation) on the Influence of Generative Models of Text and Image Creation on Science and the Humanities and on the DFG's Funding Activities.

10. Acknowledgements

I would like to thank Prof. Dr. Christoph Wilhelm for giving me the opportunity to carry out research in your lab and supporting the completion of this thesis. I really respect that you often hire people with diverse backgrounds, both academically and culturally. I wasn't a biologist by training, and this enabled me to continue my passion for immunological research in a diverse environment with a bunch of really amazing people. Thank you also for your valuable feedback on my thesis. I would also like to thank Prof. Dr. Natalio Garbi, Prof. Dr. Zeinab Abdullah, and Prof. Dr. Irmgard Forster for agreeing to be a part of my dissertation committee.

Special thanks has to go to the members of AG Wilhelm, who I am ever grateful for the support, coffee breaks, sun breaks, and discussions about data. In particular I want to thank Chantal for your friendship and collegial support over the last four years. Doing experiments together was such a breeze, and your ambition and drive always inspired me. You have truly been a pillar of support throughout the difficult times and the good times. I can't quite believe we won't be colleagues anymore, and I will really miss that, but I am grateful to always have you as a friend. A huge thank you to Patricia for your friendship and scientific support—you are truly the backbone of our lab, working tirelessly and providing such amazing experimental support (you will roll your eyes at that part). I will miss all our chats. I also want to give a massive thanks to Dhruvi, Rafa, Laetitia, and Carola for your friendship as well as scientific and experimental support. Dhruvi, I have loved being neighbors. That security of knowing if one of us forgets a key, the other has got our back. Kind of symbolic. You have been an amazing colleague and friend. This PhD would not be possible without all of your help. Also hashtag womeninstem, am I right? It has been so inspiring to be surrounded by creative and intelligent women in science. All the trips to Frau Kramer and our crafting evenings will be missed. Shoutout to a past member of AG Wilhelm, Tim Wellinghof, you have always encouraged me and helped me believe in my abilities. You're a great friend. I wish you the best for your own PhD journey.

Thank you to the postdocs of the group- Fotis and Tim. You both have provided valuable scientific input when I had doubts, and I appreciate that. Zizi, I didn't get to work with you for long enough, but from the moment you joined as a postdoc, you have been supporting all of us, and I wish you the best for your career in science. You got this. Thanks to Roman, who

really made the animal license stuff smoother and helped with experiments during difficult times.

Thank you also to members of AG Surace including Dr. Laura Surace, Susanna, Philip, Alina and Lina. It has been great to have such close collaboration with another lab as well as getting to know great people in the process. Thank you to Svetosar from the bioinformatics core facility for tackling the metabolomics data set with me. Thank you to Peter Wurst from the flow core facility for sorting my samples. I also want to thank members of Immei, especially Amina. I am thankful for your friendship and company in those early days in the mouse house on the weekends and for generally being incredibly supportive of me.

Thanks to my family, who have no idea what I am doing or why I am doing it but support me despite it. Thanks to my friends scattered across the world who have offered their support to me throughout this experience. Thanks to my two cats, Ru and Lua, for emotional support, which they will never realise. Lastly, I cannot even begin to express my thanks to Cian, Mo chuid den tsaol. You're my biggest support system. You also have no clue what I am talking about in my PhD but you offer support in so many other ways. From being my proofreader, format checker, code troubleshooter, and personal chef. My everything, actually. You are my biggest cheerleader and are always pushing and encouraging me. Thank you.